EMF of cardiac implants at low frequencies 50 Hz in a normative context

Mengxi Zhou

UNIVERSITÉ DE LORRAINE

École Doctorale IAEM
Institut Jean Lamour

Thèse

Présentée et soutenue publiquement pour l'obtention du titre de

DOCTEUR DE l'UNIVERSITE DE LORRAINE

Mention : **Systèmes électroniques**

par **Mengxi ZHOU**

Sous la direction de **Djilali KOURTICHE, Julien CLAUDEL**

CEM des implants cardiaques aux basses fréquences 50 Hz dans un contexte normatif

Juin 5, 2023

Membres du jury :

Directeur de thèse :	Pr. KOURTICHE Djilali	Université de Lorraine
Co-Directeur de thèse :	Dr. CLAUDEL Julien	Université de Lorraine
Rapporteurs :	Pr. BERQUEZ Laurent	Université Paul Sabatier Toulouse III
	Pr GADOT Frédérique	Université Paris Nanterre
Président :	Pr. NADI Mustapha	Université de Lorraine
Examinatrice :	Dr MAGNE Isabelle	EDF, Service des Études Médicales
Membres invités :	DESCHAMPS François	RTE, Direction Développement Ingénierie
	Dr. SOUQUES Martine	EDF, Service des Études Médicales

Acknowledgements

This thesis work was conducted within the team *Measurement and Electronic Architectures* of department *Nanomatériaux, Électronique Et Vivant* of *Institut Jean Lamour* (*Université de Lorraine – CNRS UMR 7198*). I'd like to express my gratitude for offering me with the opportunities and resources to pursue my PhD study.

First and foremost, my profound appreciation to Professor Djilali KOURTICHE, my primary supervisor, who provided me precious opportunities and constant support for three years. I would like to thank Dr. Julien CLAUDEL, my secondary supervisor, who offered me numerous invaluable feedbacks, inspiration, and encouragement. The completion of this study would not have been possible without their guidance, effort, and understanding.

Special thanks to Professor Laurent BERQUEZ and Professor Frédérique GADOT for being on my committee, evaluating my work and attending my defense.

This thesis was co-financed by RTE R&D in the framework of a partnership with the University of Lorraine. A great thanks to Mr. François DESCHAMPS. I greatly appreciated his constructive criticism and scientific rigor, and professionalism.

I'm extremely grateful to Dr. Isabelle MAGNE from EDF SEM (EDF-Service des études médicales) for her numerous comments during our discussions. Dr. Martine SOUQUES (EDF SEM) has also contributed a great deal to this thesis through her advice and remarks, for which I thank her.

I'd like to thank my colleagues in the team Mr. Mustapha NADI, professor at *Université de Lorraine*, Mr. Patrice ROTH, design engineer at *Institut Jean Lamour*, and Mr. Pierre SCHMITT, research engineer at *Institut Jean Lamour*. I benefited greatly from their assistance, dedication, motivation, humor, and friendship.

In addition, many thanks to Medtronic® and *Département de Cardiologie* of *CHU de Nancy Brabois* for providing help, services, and information during the journey.

Furthermore, I'd like to express my love and gratitude to my father Shaowei ZHOU and my mother Liping XUE, for bringing me into the world and enabling me to embrace the scientific research domain. Many thanks to my families and friends, for their concern and encouragement. My deepest love and appreciation to my fiancé Dr. Quan YUE, for offering me unwavering support and understanding throughout my life.

At last, thanks science and art, for allowing us to gaze at infinity and persistence beyond the universe above our heads

Content

List of Figures

List of Tables

Résumé en Français

- **Problématique**

Le risque de maladies cardiovasculaires est en augmentation dans la société moderne, avec l'accélération de l'industrialisation, l'urbanisation, les changements de mode de vie et le vieillissement de la population. Les dispositifs médicaux implantables actifs (DMIA) ont été développés depuis une cinquantaine d'années et largement appliqués pour le traitement des pathologies cardiaques avec des technologies constamment mises à jour au cours des dernières décennies [1][2][3]. La recherche scientifique ne cesse ainsi de progresser avec des retombées bénéfiques pour les patients.

Les stimulateurs cardiaques (SC), utilisés pour le traitement des bradycardies, et les défibrillateurs automatiques implantables (DAI), destinés à pallier les tachycardies ventriculaires graves grâce à des chocs électriques au tissu myocardique, sont des dispositifs médicaux implantables actifs. Ils sont en général implantés sous la clavicule chez les patients.

Par ailleurs, sont présents dans notre environnement des rayonnements électromagnétiques (EM) qui suscitent de multiples questions quant à leurs effets éventuels notamment pour les porteurs de DMIA. Le nombre croissant de porteurs d'implants médicaux, y compris dans la population active, a entraîné un questionnement quant au comportement des implants en présence d'un champ EM. Ainsi, la question des risques potentiels pouvant résulter d'interférences avec les environnements électromagnétiques se pose particulièrement pour les implants cardiaques (SC ou DAI), qui sont devenus les implants médicaux actifs les plus répandus dans le monde. Ces interrogations ont, dès les années 60, concerné les possibles interférences liées au réseau de transport de l'énergie. En effet, les fréquences allouées à l'énergie électrique (50 Hz et 60 Hz) entrent dans la bande fréquentielle d'analyse des signaux utiles de l'activité cardiaque, dont le spectre s'étend de 0,05 Hz à 150 Hz environ chez l'adulte. Pour cette raison, bien que les implants cardiaques actifs soient équipés de filtres sélectifs, permettant de réduire considérablement ou d'éliminer les interférences au-delà de 150 Hz, il apparaît que les fréquences de 50 Hz et 60 Hz ne sont pas filtrées, afin de garantir une détection correcte et une analyse complète des ondes cardiaques.

Les études sur l'immunité des DMIA portent principalement sur les expositions aux champs magnétiques à haute fréquence, en particulier dans le contexte de l'Imagerie par Résonance Magnétique (IRM) [4][5][6]. Les expositions aux champs électriques à basse fréquence ont toujours reçu moins d'attention, malgré leur omniprésence sur les lieux de travail des industries électriques, par exemple à proximité des lignes et des sous-stations électriques.

Sur les lieux de travail donc, certains postes pouvant être soumis à des rayonnements électromagnétiques, la présence de travailleurs portant des DMIA est à considérer comme cas spécifiques. En d'autres termes, il convient d'accorder une attention particulière aux porteurs de DMIA exposés à des champs électromagnétiques, et de mettre en place un processus d'évaluation des risques correspondant. La directive européenne 2013/35/UE établit l'obligation pour les employeurs "d'évaluer tous les risques pour les travailleurs découlant des champs électromagnétiques sur le lieu de travail" [7]. Dans le cas particulier des travailleurs portant des DMIA, la procédure d'évaluation des expositions aux champs EM est standardisée par la norme EN 50527. Cependant, établir une procédure d'évaluation des risques nécessite une méthode d'essai simple, reproductible et sans risque pour l'employé. Ainsi, les tests *in vitro*, qui permettent également d'étudier le comportement des DMIA dans des situations similaires, semblent être une meilleure approche pour répondre à ces trois critères.

Le but de ce travail de thèse est donc de déterminer des facteurs d'équivalence permettant d'établir les correspondances ad hoc entre des tests *in vitro* et des expositions réelles, dans le cas de porteurs d'implants cardiaques actifs soumis à des champs électriques de 50 Hz, fréquence propre au réseau de distribution électrique européen. À cet effet, une étude théorique et expérimentale a été réalisée sur un implant cardiaque placé dans un fantôme simulant les tissus humains, afin de déterminer la tension induite aux bornes de la sonde de l'implant lorsque l'ensemble est soumis à un champ électrique 50 Hz. Le fantôme se compose de deux zones ayant des caractéristiques électriques similaires à celles du cœur humain et de la cage thoracique, lieux où la sonde cardiaque et le boîtier sont respectivement implantés. Les mesures expérimentales et la simulation numérique concordent, ce qui valide les facteurs d'équivalence que nous avons trouvés pour notre système. Ainsi le fantôme *in vitro* peut être appliqué comme système équivalent dans les travaux sur la susceptibilité électromagnétique des implants cardiaques. En corollaire, nous avons également établi une relation d'équivalence entre un système d'exposition au champ électrique et un système par injection de courant. Ce résultat nous permet alors de ramener une étude sous champ électrique, dont la mise en œuvre est complexe et contraignante (haute tension, installation et protocoles de sécurité), à une étude en perturbations conduites, beaucoup plus simple à réaliser.

- **Contenu de thèse**

Ce mémoire comprend quatre chapitres complétés par une conclusion générale, une bibliographie et plusieurs annexes.

Chapitre 1, intitulé ***Implants cardiaques et champs électriques : entre soins de santé et profession***, présente le contexte et la conduite pour l'établissement d'une procédure d'évaluation des risques. L'histoire et le développement des DMIA (en particulier les SC et les DAI) sont brièvement présentés, ainsi que leur intérêt et les défis à relever. Les expositions aux champs électriques dans l'environnement public et professionnel et les risques d'interférences dans les DMIA sont discutées. Le contenu des normes et des directives est également inclus dans ce chapitre, ainsi qu'une bibliographie des études précédentes sur ce sujet. Compte tenu des préoccupations concernant la sécurité et la santé des travailleurs portant des implants cardiaques, il est nécessaire d'adopter une approche simple accessible à toute entreprise pour réaliser des tests d'immunité sur les DMIA afin d'élaborer une procédure d'évaluation des risques pour ces employés porteurs de DMIA et susceptibles d'être soumis à des interférences électromagnétiques sur leur lieu de travail.

Chapitre 2, intitulé ***Validation théorique et numérique d'une procédure d'évaluation des risques***, présente une description de trois approches (modèle numérique, modèle d'exposition et modèle par injection) permettant d'obtenir l'estimation de la tension induite à l'entrée des implants cardiaques dans le cas d'exposition à un champ électrique. Après une description du modèle virtuel humain ANSOFT utilisé pour étudier l'exposition en situation réelle, nous présentons ensuite le système d'exposition au champ électrique pour reproduire l'interférence dans le cadre d'une exposition équivalente et le système équivalent par injection de tension. La simulation numérique réalisée par le logiciel CST EM® valide notre approche et fournit des marqueurs utiles pour les mesures expérimentales. Les résultats de la simulation ont permis de valider l'association des trois systèmes numériquement afin d'élaborer la procédure d'évaluation des risques pour les implants cardiaques soumis à des expositions de champ électrique. Pour effectuer une évaluation des risques dans le cas d'un patient porteur d'un implant cardiaque supposé exposé à un champ électrique de 10 kV/m, il faut :

A- Système d'exposition :

- un champ électrique de 4,35 kV/m pour le mode de détection unipolaire;
- un champ électrique de 3,55 kV/m pour le mode de détection bipolaire;

B- Système par injection :

- une tension de 2,74 mV pour le mode de détection unipolaire;
- une tension de 1,88 mV pour le mode de détection bipolaire.

Chapitre 3, intitulé ***Validation expérimental : conception et mise en œuvre.*** Il montre l'approche expérimentale et la procédure d'évaluation des risques. Les montages expérimentaux pour la génération d'interférences, la configuration du fantôme et la réalisation d'un système de mesure "*in vitro*" basé sur la transmission des signaux par fibre optique sont décrits. Des optimisations du système de mesure en matière d'isolation, de conditionnement et transmission des signaux, et d'installation ont été réalisées afin d'améliorer ses performances. Les mesures sont effectuées dans les deux systèmes équivalents (système d'exposition et système d'injection). Elles concordent avec les résultats de la simulation et valident ainsi notre approche dans ce contexte. Selon les résultats expérimentaux, pour effectuer une évaluation des risques dans le cas d'un patient porteur d'un implant cardiaque exposé à un champ électrique de 10 kV/m, il faut :

A- Système d'exposition :

- un champ électrique de 4,18 kV/m pour le mode de détection unipolaire ;
- un champ électrique de 2,75 kV/m pour le mode de détection bipolaire ;

B- Système par injection :

- une injection de 2,37 mV de tension pour le mode de détection unipolaire ;
- une injection de 1,82 mV de tension pour le mode de détection bipolaire.

Chapitre 4, intitulé ***Procédure d'évaluation des risques pour les DMIAs : Applications.*** Dans ce dernier chapitre, nous avons effectué des tests d'immunité sur quatre implants cardiaques (deux SC : Advisa SR et Adapta, deux DAI : Secura DR et Evera XT VR). Les mesures ont été effectuées dans les deux systèmes afin de vérifier l'équivalence entre le système d'exposition au champ électrique et le système par injection. Les implants cardiaques détectent les signaux cardiaques anormaux et réagissent aux événements cardiaques. Pour simuler l'environnement d'implantation réel et observer les événements cardiaques générés par l'interférence du champ électrique, des signaux cardiaques à 1 Hz ont été envoyés aux implants cardiaques pendant le test d'immunité. Les seuils d'interférence ont été étudiés dans les quatre implants sous test et une analyse correspondante de la tension induite a été réalisée. L'estimation et l'analyse de la tension induite qui provoque le dysfonctionnement de l'appareil ont été effectuées sur la base de la méthode introduite dans cette étude en tenant compte de la distance inter-électrodes de la sonde de stimulation. Compte tenu des résultats obtenus et en tenant compte de l'analyse du

seuil d'interférence pour les employés porteurs de DMIA, le système par injection équivalent est introduit sur la base des normes et directives.

En plus des chapitres principaux, une table des matières, les abréviations et les unités, la conclusion générale, l'annexe et la liste des références complètent le manuscrit de la thèse.

- **Résumé des principaux résultats obtenus**

Les tensions induites à l'entrée des implants cardiaques exposés ont été mesurées dans les systèmes équivalents grâce au dispositif expérimental conçu dans le cadre de cette étude. Le *Tableau.1* présente les résultats des mesures expérimentales obtenues avec les deux systèmes équivalents et comparés avec ceux du modèle ANSOFT.

Tableau.1 Tensions induites dans les trois systèmes avec une dose d'exposition unitaire

Tension induite	**Système standard** (Pour une exposition de 1 kV/m)	**Système équivalent A** (Pour une exposition de 1 kV/m)	**Système équivalent B** (Pour une injection de 1 mV)
	Modèle ANSOFT	Système d'exposition	Système d'injection de tension
Unité	µV	µV	µV
Unipolaire	183	438	772
Bipolaire	22	80	121

L'association des trois systèmes d'exposition a été étudiée et les résultats sont regroupés dans les figures ci-dessous pour la détection unipolaire (*Figure.1*) et la détection bipolaire (*Figure.2*). Pour une valeur d'exposition sur le modèle ANSOFT (axe horizontal), le niveau de champ électrique requis pour mener des tests équivalents dans le système d'exposition se trouve sur l'axe gauche, la tension injectée requise dans le système par injection se trouve sur l'axe droit.

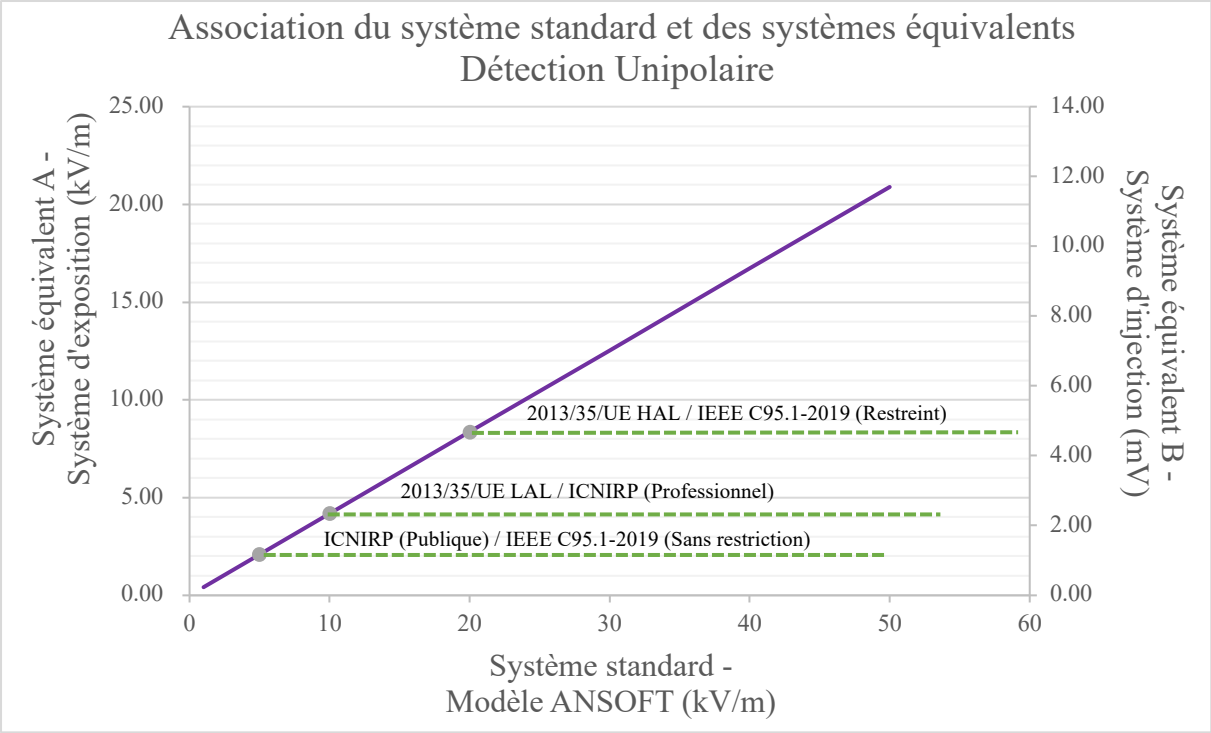

Figure.1 Association du système standard et des systèmes équivalents pour la détection unipolaire

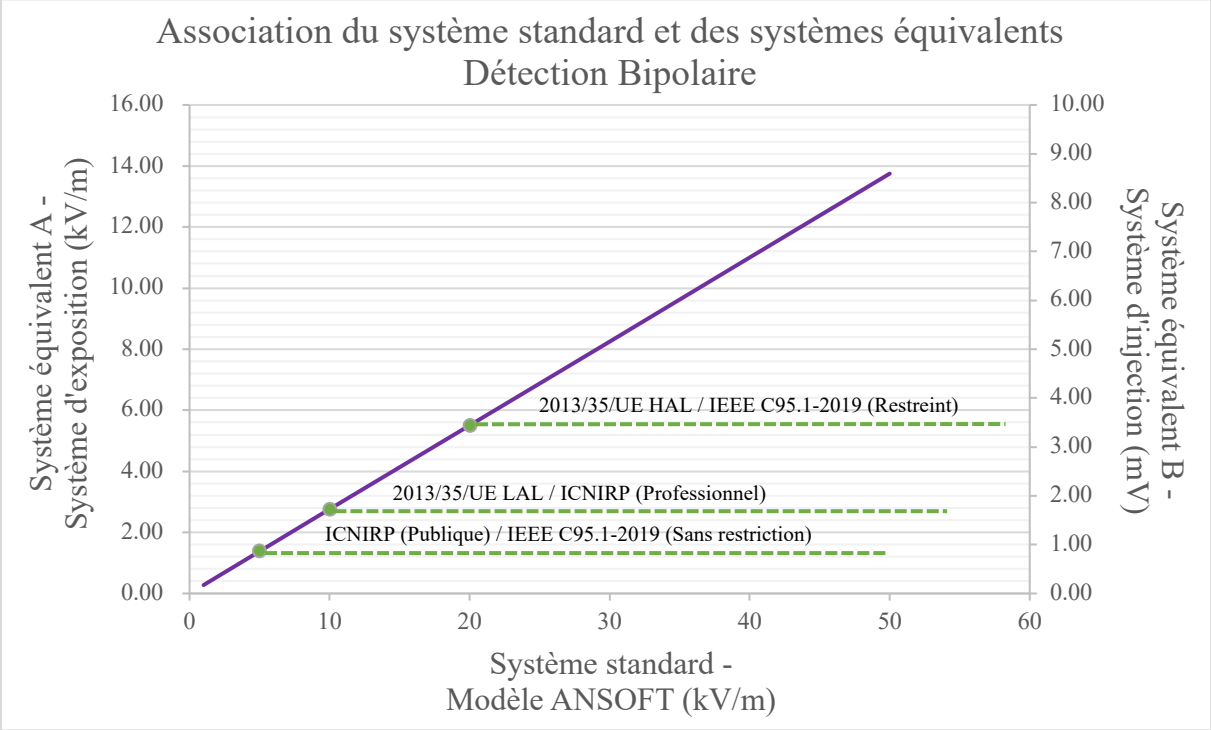

Figure.2 Association du système standard et des systèmes équivalents pour la détection bipolaire

Quatre implants cardiaques ont été étudiés dans le cadre du test d'immunité. Les tensions induites qui ont provoqué un dysfonctionnement du dispositif (seuils d'interférence) ont été obtenues selon la méthode proposée dans cette étude et sont présentées dans le *Tableau.2*.

Tableau.2 Tensions induites au niveau des implants avec une dose d'exposition unitaire

Modèle	**Écartement inter-électrodes**	**Polarité**	**Sensibilité**	**Tension induite** Système d'exposition	**Tension induite** Système d'injection
	mm		mV	mV	mV
Advisa SR	23	Unipolaire	0.45	6.38	6.58
			2.8	6.21	6.58
			4	6.21	6.58
		Bipolaire	0.45	4.02	2.80
			0.9	3.97	2.77
			4	3.66	2.74
Adapta	10	Unipolaire	1	2.19	1.82
			2.8	5.48	5.91
			4	7.94	8.64
		Bipolaire	1	2.96	3.92
			2.8	3.33+	10.78
			4	3.33+	15.70
Secura DR	28	Bipolaire	0.15	0.13	0.12
			0.3	0.28	0.27
			0.6	0.56	0.54
Evera XT VR	10	Bipolaire	0.15	0.12	0.11
			0.3	0.27	0.25
			0.6	0.56	0.50

▪ Conclusion et perspectives

Nous avons dans ce travail de thèse analysé les seuils d'interférence pour les employés porteurs de DMIA exposés à un champ électrique de haute intensité à 50 Hz. Trois systèmes d'exposition ont été proposés basé sur l'estimation de la tension induite à l'entrée des implants cardiaques en cas d'exposition à un champ électrique :

1) le modèle virtuel ANSOFT comme système standard pour étudier l'exposition réelle ;

2) le système d'exposition au champ électrique (système équivalent A) ;

3) le système par injection de tension (système équivalent B).

L’étude des trois systèmes a permis de valider notre démarche ; Le système par injection proposé sur la base des résultats obtenus permet l'évaluation des risques d’interférences sur les lieux de travail.

En ce qui concerne l'approche expérimentale et compte tenu des faibles niveaux des tensions induites à mesurer, certains paramètres peuvent être affinés pour mieux simuler les situations d’expositions réelles. L'eau salée, en tant que matériau liquide du fantôme, ne permet pas de maintenir l'homogénéité du fantôme de manière constante. Un fantôme en gélatine peut donc être utiliser pour maintenir à la fois la position de l'objet sous test et garantir une homogénéité de la distribution de la conductivité.

Bien que la configuration du trajet de détection ait été contrôlée avec précision pour mesurer la tension induite sur les implants cardiaques, la taille du système de mesure est encore quatre fois plus grande que celle d'un boîtier d'implant cardiaque. Un système de mesure de taille réduite peut avoir moins d'influence sur la distribution du champ à proximité et moins d'impact sur la mesure du mode de détection unipolaire.

Dans le test d'immunité sur les implants cardiaques, un dispositif expérimental a été utilisé pour délivrer des signaux cardiaques standard au fantôme. Or, dans la réalité, les signaux cardiaques varient en amplitude, en fréquence et en forme, en particulier pour les patients souffrant de maladies cardiaques.

De plus, les travailleurs sont généralement exposés à des champs électriques, à des champs magnétiques ou à une combinaison des deux. Cette thèse s'est concentrée sur l'exposition professionnelle aux champs électriques à très basse fréquence (50 Hz). La fréquence du réseau électrique public en Amérique et dans certaines parties de l'Asie est de 60 Hz. La configuration du dispositif expérimental utilisé peut être légèrement ajustée pour effectuer les tests à 60 Hz, ce qui permet d'adapter la procédure d'évaluation des risques pour ces régions. Les travaux de recherche peuvent être aussi menés sur les champs magnétiques seuls ou une combinaison entre champs électriques et magnétiques suivant la même procédure.

General Introduction

The risk of cardiovascular diseases for humans continues to increase in modern society with the acceleration of industrialization, urbanization, lifestyle changes, and an aging population. Targeting cardiology diagnosis and treatment, active implantable medical devices (AIMDs) have been rapidly developed and widely applied with constantly updated technologies in recent decades [1][2][3]. Meanwhile, it is vital for scientific research to catch up with the speed of the information era in terms of the side effects on human beings and the environment.

Pacemakers (PMs), used for the treatment of bradycardia, and implantable cardioverter defibrillator (ICDs), for palliating serious ventricular tachycardia by electric shocks to the myocardial tissue are important AIMDs implanted in the human chest. Electromagnetic radiation is inevitably present in our surroundings and raised many questions concerning the potential effects on the AIMD-wearers. The increasing number of medical implant wearers, including those in active professional activities, has led to questions regarding their performance in the presence of an occupational electromagnetic field (EMF) exposure.

Cardiac implants are the most widespread active medical implants in the world. With their development and upgrading, the subjects regarding the potential risks caused by electromagnetic interference are highlighted. Since the 1960s, these questions have concerned possible interference linked to the energy transport network. The frequencies allocated to electrical energy (50 Hz and 60 Hz) are in the analysis bandwidth of the cardiac signals, of which spectrum extends from a few Hertz to approximately 150 Hz.

The AIMDs are usually equipped with selective filters enabling to significantly reduce or eliminate the interference. However, considering the nature formation of the heart signals, the power frequency 50 Hz or 60 Hz may not be filtered in order to ensure the cardiac signal waves are correctly and completely sensed.

In the workplaces, it is inevitable to have the existence of workers who are susceptible to the electromagnetic field (EMF)-related impact. The presence of workers wearing AIMDs is then to be considered as specific cases. In other words, particular attention should be given to AIMD carriers who are subject to higher risks and corresponding risk evaluation process should be established. European Directive 2013/35/EU laid down the obligation that employers are obliged to “assess all risks for workers arising from electromagnetic fields at the workplace” [7]. Organizational preventive measures are widely recognized and adopted for the purpose of protecting employees from over-exposure.

The procedure for assessing the EMF exposures for workers bearing AIMDs was proposed in EN 50527 to determine the risk arising from the exposures in the workplaces. Immunity tests on AIMDs is critical in the risk assessment procedure. *In vitro* testing allows the behaviors of AIMDs to be investigated in a similar situation to *in vivo* testing but without risk. The establishment of the risk assessment procedure requires a simple, feasible, and risk-free test method. The studies on the immunity of AIMDs were carried out mostly for magnetic field exposures at high frequencies, especially in the context of Magnetic Resonance Imaging (MRI) [4][5][6]. To date, the electric field exposure at low frequency has received little attention yet they commonly exist in the workplaces in electrical industries, for example, area near power

lines and substations. To ensure the safety of workers implanted with a cardiac implant, here we define them as the AIMD-employees, it is necessary to assess the EMI that they are subjected to. Thus, in this study, high-intensity electric field exposures are mainly concerned. The frequency band was limited to extremely low frequency at 50 Hz to focus on the occupational exposures caused by power sources.

EMI affects the sensing capability of a cardiac implant when it cannot be filtered but its level exceeds the sensitivity setting in the sensing system of the cardiac implant. The interference can be evaluated by the estimation of the induced voltage at its input. Equivalent systems can be built up by adopting this conception to reproduce the exposures and the implantation conditions in order to generate the same effects at the input of cardiac implants (same induced voltage).

In this work, a theoretical and experimental study was performed on an *in vitro* phantom that allowed to determine the voltage induced at the input of a cardiac implant subjected to a high-intensity electric field at 50 Hz. The phantom is composed of two parts with electrical characteristics similar to those of the human heart and the chest, where the cardiac lead and the housing are implanted. Experimental measurements and numerical simulations are coherent which validates the equivalence factors we found for our systems. Thus, the *in vitro* phantom can be applied as an equivalent system in the workplace for the immunity test on cardiac implants. Another result we established in this study is the equivalence between an electric field exposure system and an injection system. This equivalence allows us to reduce the complexity of the study and conduct simpler tests with reproduced perturbations.

This thesis contains four chapters and finished by a general conclusion, annexes and references:

Chapter 1, entitled ***Cardiac implants and electric fields: between healthcare and profession***, presents the background and the scope of the establishment of a risk assessment procedure. The history and development of AIMDs (especially PMs and ICDs) are briefly introduced, as well as their future and challenges. Electric field exposures in public and professional environment, and the underlying reasons of interference to AIMDs are discussed. The related contents of standards and guidelines are also included in this chapter, as well as a review of the previous studies on this subject.

Chapter 2, entitled ***Theoretical and numerical validation of a risk assessment procedure***, presents theoretical approach and numerical approach of the establishment of a risk assessment procedure. An association of three exposure systems is proposed on the basis of the estimation of the induced voltage at the input of cardiac implants under electric field exposure. ANSOFT virtual human body is introduced to study the real-case exposure. Controlled EF exposure system is introduced to reproduce the interference under an equivalent exposure. Voltage injection system is introduced to reproduce the interference with a manageable parameter in the system. Numerical simulations in the software CST EM® validates the association of the three exposure systems and provides reference and evidence for experimental measurement.

Chapter 3, entitled ***Design and implementation of experimental validation***, presents the experimental approach of the establishment of a risk assessment procedure. The *in vitro* experimental set-ups of the equivalent systems are introduced in this chapter as well as a measuring system based on optical transmission in real time. The optimizations on the measuring system in the aspect of isolation, transmission, and installations are made to improve its performance. The measurements are conducted in the two equivalent systems. The results are coherent to those in numerical simulation and validate the proposed method.

Chapter 4, entitled ***Risk assessment procedure for AIMD: establishment and application***, presents the employment of the immunity test proposed in this study in the establishment of the risk assessment procedure. Immunity tests were conducted on four cardiac implants (two SCs and two ICDs). The measurements were performed in both equivalent systems to verify the relation between the controlled EF exposure system and the injection system. Based on the results obtained and taking into account the analysis of the interference threshold for the AIMDs, the voltage injection system in the workplace is introduced on the basis of the exposure limitation or reference indicated by the standards and guidelines.

In addition to the main chapters, content tables, abbreviations and units, general conclusion, annex, and reference list serve to the construction and organization of the thesis.

1

Cardiac implants and electric fields: between healthcare and professions

I. Introduction

Cardiovascular disease is one of the leading causes of death all over the world, responsible for 3.8 million deaths each year in Europe, accounting for 45% of all deaths [8]. It causes approximately 659,000 deaths per year in the United States, accounting for 25% of all deaths [9]. With the rapid development of modern medicine and technology, active implantable medical devices (AIMDs) are extensively used in the treatment and diagnosis of various diseases and are constantly being upgraded and iterated. Approximately 500,000 pacemakers (PMs) implantation were performed in 2016, and 100,000 implantable cardioverter defibrillators (ICDs) were implanted in Europe [10]. On the other hand, with the continuous upgrading of global electrification and wireless technologies, humans are confronting unprecedented and inevitable electromagnetic fields (EMFs) in their surroundings. From medical radiography using X-ray to every power socket associated with low-frequency EMFs, EMF sources play an important role in human daily life. Thus, the fact of AIMD carriers submitted to EMFs is a subject of great concern, especially the case for patients bearing cardiac implants.

The first chapter introduces the background of cardiac implantable devices and the potential impacts from EMFs on the cardiac implants: PM and ICD, as well as the future and challenges confronting AIMD. The underlying reasons of electromagnetic interference (EMI) between EMF sources and implantable medical devices are discussed with current solutions. This chapter also includes contents from related standards and guidelines, and a brief review of studies on different frequencies, applications, aspects.

II. Heart Disease and Implantable Medical Devices

1. Heart disease

With rapid socio-economic development, lifestyle changes, coupled with an aging population and accelerated urbanization, unhealthy lifestyles of humans are highlighted and their impact on cardiovascular disease risk factors, such as diabetes mellitus (DM), hypertension, dyslipidemia, and obesity, is increasing, as is their impact on global human health. The incidence of cardiovascular disease continues to increase. About 19 million deaths were attributed to cardiovascular disease globally in 2020, which amounted to an increase of 18.7% from 2010. The European Heart Network has estimated that the expenditure associated with cardiovascular disease costs the EU economy more than 200 billion euros a year [11]. According to the report of the American Heart Association (AHA) [9], the estimated direct and indirect cost of coronary heart disease in the U.S. was 378 billion dollars from 2017 to 2018. There are findings indicating cardiovascular disease prevalence and costs will increase substantially. Effective prevention strategies are necessary.

Cardiovascular disease (CVD) is a general term for diseases affecting the heart or blood vessels, including coronary heart disease (CHD) that a disease of the blood vessels supplying the heart

muscle. The heart is a fist-sized muscular pump with four chambers, two on the left and two on the right. The upper chambers are the atrium (left and right atria) and the lower chambers are the right and left ventricles. In order for the heart to work properly, the chambers of the heart must work in harmony at the proper rate, 60 to 100 times per minute when not exercising in adults. The heart's circuit system controls the pumping action of the chambers. A normal heart rhythm begins in the right atrium, the sinus node which is the original pacemaker producing regular electrical impulses that are transmitted through specific muscle fibers. When the electrical impulses reach the right and left atria, they contract and pump blood into the ventricle chambers. After a minuscule delay, the ventricles refill with blood and the electrical impulses reach the ventricles, causing them to contract and expel blood to the rest of the body. Typically, the sinus node creates a steady pace of electrical impulses. The pace changes depending on activity, emotions, and other factors. If the heart beats abnormally (tachycardia or bradycardia), which is considered as a sick sinus syndrome, blood will not be able to circulate adequately through the body, so it will result in fatigue, fainting, shortness of breath, confusion, and even serious complications: atrial fibrillation (a type of irregular heartbeat, arrhythmia), heart failure, stroke, cardiac arrest.

2. Cardiac implantable medical devices

Targeting cardiology diagnosis and treatment, many different types of medical devices, partially or fully implanted in the human body, were produced. Automated external defibrillators (AEDs) are portable electronic devices that can automatically diagnose heart arrest and can help rescuers determine whether a shock is needed to restore a normal heartbeat. AEDs are often found in public places and are not difficult to manipulate, but training in the use of AEDs is always highly recommended. In cardiac resynchronization therapy (CRT), a small electronic device is used to treat heart failure. It sends tiny electrical pulses to the heart, causing the two ventricles to pump together in a coordinated way. There are two types of devices: CRT pacemakers (CRT-P) and CRT defibrillators (CRT-D). Both of them send electrical impulses to the heart to trigger a heartbeat when needed. However, it is well known that about half of the deaths of cardiac patients are sudden deaths. The most common causes of sudden death are severe ventricular arrhythmia, such as ventricular fibrillation and ventricular tachycardia. These severe arrhythmias often occur without warning and cannot be completely prevented by drugs. This arrhythmia must be terminated immediately when it occurs.

Therefore, PMs and ICDs are widely applied for cardiac disease treatment which allow patients to obtain proper therapies whenever they need them. PM and ICD are implantable medical devices for cardiac rhythm control. Patients who suffer from irregular heart rhythm benefit significantly from the development of pacing technologies, especially in the quality of life. In European countries, more than 1000 pacemaker implantation has been performed per million people in France, Italy, and Sweden while implantable cardioverter-defibrillator implantation peaked at more than 300 per million people in the Czech Republic and Germany [11]. Moreover, 86,181 cardiac pacemakers were implanted in China in 2020 during the COVID-19 pandemic [2].

PM and ICD represent the system composed of a generator and one or multiple leads. The generator contains a chip programmed with function algorithms, a capacitor, and a battery, implanted under the skin in the chest or abdomen (*Figure 1-1*). The lead contains an electrode wire or wires, and its isolator. The lead, connected to the generator at one extremity, passes through a vein to the targeted heart chamber and is inserted into the heart muscle at the other extremity. The processes of implantation of an ICD system and a PM are similar. Pathologies are diverse and the device must be able to distinguish each pathology to provide appropriate therapy. The sensitivity threshold is set by the doctor according to the voltage level delivered by the patient's heart. If the implant is configured with a lower sensitivity value, it will detect lower amplitude signals, and be at the same time more sensitive to electromagnetic disturbances.

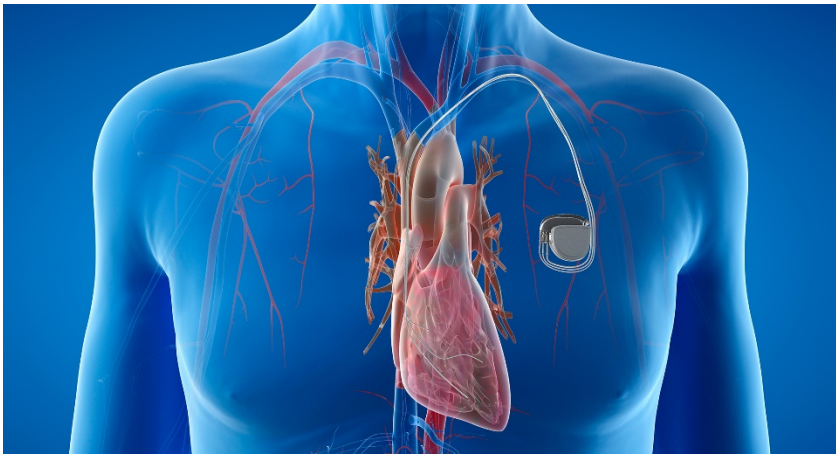

Figure 1-1 AICD implantation (UCSF Health)

After the PM or ICD system is implanted, an external computer, called a programmer, can be used to program the device, and retrieve information from it. This information will assist the doctor in the treatment. In the patients' daily activities, the implanted device continuously monitors the heart and automatically delivers therapies to correct abnormal rhythms when necessary.

3. Development of Pacemakers

Pacemaker (PM) is a device implanted in the chest or abdomen to control a low heart rhythm, providing electrical impulses to stimulate the heart muscles and set the heart back to a normal rhythm. When an arrhythmia occurs caused by faulty electrical conduction, PM uses low-energy electrical pulses to rectify this dysfunction. Pacemakers are able to monitor and record electrical activities and give proper stimulation when the heart is not able to pump enough blood for the body. The PM can relieve some symptoms of arrhythmia, such as fatigue and fainting, and help people with abnormal heart rhythms return to a relatively active life.

The invention of cardiac pacing was in the 1950s [3] then put to therapeutic use in the following decades. In 1950, Dr. John Hopps designed and built the first pacemaker prototype [12], which was 30 cm in length, used vacuum tubes to generate pulses, and was powered by 60 Hz household current (*Figure 1-2*). The transvenous catheter electrodes developed by Hopps are still being used in today's implantable devices. In 1958, Åke Senning, a thoracic surgeon at the

Karolinska Hospital in Stockholm, and Rune Elmqvist, an engineer from the Swedish firm Elema Schönander have first implanted a definitive electronic pacemaker in a 40-year-old patient. Yet the pacemaker failed within a few hours and the patient received another pacemaker in 1960. The impressive progress of electro-diagnosis and electrotherapy has provided a promising quality of life for patients suffering from heart failure. In 1960, Dr. William Chardack of the Buffalo VA Hospital (now the Buffalo VA Medical Center), engineer Wilson Greatbatch and Dr. Andrew Gage implanted a pacemaker into a 77-year-old man, who lived 10 months after the implantation surgery. Their design was the first commercially produced implanted pacemaker. Incremental improvements in hardware and procedures of cardiac pacing have taken place in the 1960s.

Figure 1-2 The original pacemaker designed by Hopps (Photo courtesy of the National Research Council of Canada)

The lithium iodide cell battery for powering pacemakers was developed by Wilson Greatbatch in 1971. Since then, lithium iodide or lithium anode cells became the standard for future pacemaker designs. Microprocessor-driven pacemakers appeared in the 1990s with the complex capability of detecting and storing. In recent years, leadless pacemakers have emerged as novel alternatives to traditional devices. Nowadays, pacemakers are produced with different functions, for different applications, and for different groups of people. *Figure 1-3* shows some models from the family of pacemakers from Medtronic. Micra™ is completely self-contained within the heart and provides therapy needed without a visible or physical reminder of a medical device. The Azure™ pacemaker is equipped with BlueSync™ technology and the latest innovation from Medtronic in remote monitoring, MyCareLink Heart mobile app. The Advisa™ MRI SureScan™ pacemaker is designed for safe use in the MRI environment. Adapta™ works completely automatically, constantly adjusting its settings and adapting to meet the heart's needs in order to avoid unnecessary pacing.

Figure 1-3 Medtronic pacemakers (left to right): Micra, Azure, Advisa, Adapta

4. Development of implantable cardioverter defibrillator

The implantable cardioverter defibrillator (ICD) is designed to help control or monitor irregular (rapid) heartbeats in people with certain heart rhythm disorders and heart failure as well. It can be considered as the combination of PM and defibrillator. The ICD is inserted just under the collar bone. The outlook feature looks similar to a pacemaker but with a bigger housing. If the patient has already had a life-threatening abnormal heart rhythm and is at risk of having it again, he/she might be suggested to have an ICD implantation by the doctor instead of a pacemaker. ICD has all the functionalities of a pacemaker, but also the ability to act as an external automatic defibrillator for patients at risk for sudden cardiac death due to ventricular fibrillation and ventricular tachycardia.

The research on the ICD started in 1969 and the first implantation was conducted in 1980. In 1972, Bernard Lown, the inventor of the external defibrillator, and Paul Axelrod stated in the journal Circulation – "The very rare patient who has frequent bouts of ventricular fibrillation is best treated in a coronary care unit and is better served by an effective anti-arrhythmic program or surgical correction of inadequate coronary blood flow or ventricular malfunction. In fact, the implanted defibrillator system represents an imperfect solution in search of a plausible and practical application" [13]. A system that allows detection of ventricular fibrillation or ventricular tachycardia was designed for the first implanted ICD, which weighed 289 g, had the volume of 150 cm^3 and a thickness of 22 mm [14]. This innovation represents a modern medical achievement dedicated to patients at risk of life-threatening arrhythmias. The technology of the ICD was developed in generations and specific challenges have emerged constantly. The future will hold expanding indications for ICD implantation, while further meeting patients' medical and psychosocial adjustment needs [15]. A cardiac resynchronization therapy with defibrillators (CRT-D) is an implantable cardiac resynchronization therapy (CRT) defibrillator for patients with heart failure. The device, like an ICD, monitors the heart's rhythm, detects irregularities, and corrects them with electrical impulses, stops life-threatening ventricular tachycardia and fibrillation with relatively weak and painless stimulation therapy or electrical shocks [16]. CRT-Ds differ from ICDs is that have three leads that deliver energy to the heart rather than one or two to help the heart’s lower chambers – the ventricles – work in tandem and minimizes inappropriate ICD shocks [17]. *Figure 1-4* shows some models from this heart devices family from Medtronic.

Figure 1-4 Medtronic Cobalt™ and Crome™ cardiac medical devices

5. Future and challenges of implantable medical devices

Instead of conventional pacemakers that consist of transvenous intracardiac lead and a subcutaneous device as an impulse generator, the leadless pacemaker is implanted into the heart through a vein in the leg and does not require a lead (*Figure 1-5*). The implantation process doesn't involve a chest incision so potential medical complications can be significantly reduced. The Food and Drug Administration (FDA) approved Micra™ AV, Medtronic in 2020 for use in the single-chamber application. Micra AV can be a pacing solution for patients who suffer from AV block, a condition that electrical signals between the chambers of the heart are impaired [18]. The leadless pacemaker is a promising innovation that provides possibilities for the next generation pacing method.

Figure 1-5 Pacemakers a) Traditional single-chamber pacemaker and lead; b) Leadless pacemaker, Micra Medtronics

The performance of implantable electronic devices is also subject to the life span of their battery. The development of battery-free technologies will be an important step toward a revolution of implantable medical devices. Especially access to leadless devices for battery replacement is more difficult. A symbiotic cardiac pacemaker, which harvests biomechanical energy from cardiac motion based on an implantable triboelectric nanogenerator, was successfully tested in living pigs in 2019 [19]. The energy harvested from each cardiac motion cycle is higher than the required endocardial pacing threshold of pigs and humans. However, human testing is still

unlikely in the near future considering the hurdles on fixation (minimally invasive implantation) and long-term biosafety.

III. Electromagnetic Fields and Implantable Medical Devices

1. Electromagnetic field

The electromagnetic field (EMF) is caused by the motion of an electric charge. A stationary charge produces an electric field in the surrounding space. If the charge is moving, a magnetic field is produced. A changing magnetic field also produces an electric field. The mutual interaction of electric and magnetic fields produces an electromagnetic field. The way in which charges and currents interact with the electromagnetic field is described by Maxwell's equations and the Lorentz force law.

EMFs are invisible areas of energy, often referred to as radiation, that are associated with the use of electrical power and various forms of natural and man-made lighting. EMFs are typically categorized by their frequency (*Figure 1-6*) into

- non-ionizing EMFs, which are generally perceived as harmless to humans, e.g., wireless networks, home electrical appliances, MRIs, etc.
- ionizing EMFs, which have the potential for cellular and DNA damage, e.g., X-rays, sunlight, gamma rays, etc.

The classical perspective in the history of electromagnetism takes the electromagnetic field as a smooth, continuous field, propagated in a wavelike manner. With the development of the perspective of quantum field theory, this field is seen as quantized, meaning that the free quantum field can be expressed as the Fourier sum of creation and annihilation operators in energy-momentum space while the effects of the interacting quantum field may be analyzed in perturbation theory via the S-matrix with the aid of a whole host of mathematical techniques [20].

The electromagnetic force is responsible for many of the chemical and physical phenomena observed in daily life. Scientific research was conducted constantly about EMFs. Electromagnetic interference (EMI) is a disturbance generated by an external source that affects an electrical circuit by electromagnetic induction, electrostatic coupling, or conduction. Thanks to Maxwell’s equations, the effects caused by EMI can be studied and analyzed. Many of the computational software for the analysis of EMFs are designed on the basis of Maxwell’s equations.

Frequency is an important characteristic of electromagnetic fields. The utility frequency is the standardized frequency of the oscillation of alternative current (AC) for power transmission between power stations and users, providing possibilities of international trade in electrical equipment. Two utility frequencies exist nowadays thanks to standardization: 50 Hz is applied

by the eastern hemisphere and 60 Hz mostly in the western hemisphere (not all). High-voltage alternating current (HVAC) is used for energy transmission world widely thanks to its efficiency for short and medium distances.

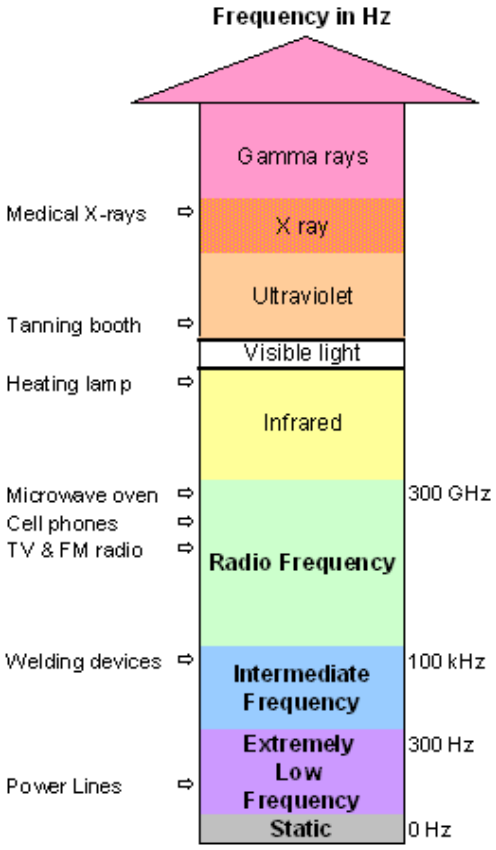

Figure 1-6 Frequency ranges of electromagnetic fields [21]

2. EMF exposures in public environment

In daily life everybody is, to a greater or lesser degree, exposed to electromagnetic fields (*Table 1-1*). In addition, with the radical evolution of electrification and computerization in modern life, exposures to EMF are inevitable and cannot be ignored. The power lines, sockets, cellphones, microwaves, computers, and other appliances send out a stream of invisible energy waves constantly. Where electricity is used, where electric and magnetic fields are produced. More than 90 % of the world's population has access to electricity nowadays [22]. Human beings are facing unprecedented degree of EMF exposures and increasing trend.

Table 1-1 Typical sources of electromagnetic fields [21]

Frequency range	Frequencies	Some examples of exposure sources
Static	0 Hz	video display units; MRI (medical imaging) and other diagnostic or scientific instrumentation; industrial electrolysis; welding devices
ELF (Extremely Low Frequencies)	0-300 Hz	power lines; domestic distribution lines; domestic appliances; electric engines in cars, trains and tramways; welding devices
IF (Intermediate Frequencies)	300 Hz – 100 kHz	video display units; anti-theft devices in shops; hands-free access control systems, card readers and metal detectors; MRI; welding devices

RF (Radio Frequencies)	100 kHz – 300 GHz	mobile telephones; broadcasting and TV; microwave ovens; radar and radio transceivers; portable radios; MRI

3. EMF exposures in professional environment

Workplaces generally have power nominally supplied at 230 volts (single phase) and 400 volts (3 phases). Some larger workplaces receive electricity at a higher supply voltage. The electrical facilities generate EMFs in the workplaces. The prevalence of the exposure to low frequency electric and magnetic fields in many workplaces can reach almost the 100% of the workers in the modern urban areas [23]. Workers may be exposed to high electric and magnetic fields if they work near electrical systems that use large amounts of electric power, such as large electric motors, powerful generators power supplies, electric cables of a building, etc. Magnetic fields are also found near power saws, drills, copy machines, electric pencil sharpeners, and other small electric appliances. The strength of the electromagnetic field depends on equipment design and current flow but not specifically on equipment size, complexity, or voltage. Electric power lines and indoor lighting spread across the world in the 20th century. Scientists realized that the power lines supplying all that energy to the world's population were sending off EMFs, just like the sun does naturally.

A job-exposure matrix (JEM) was developed recently, retrieving from 35,000 different occupations. The results showed that 62.4% of the occupations were exposed to radiofrequency (RF) (>10 MHz), thermal intermediate frequency (IFRF) (100 kHz – 10 MHz), and/or non-thermal intermediate frequency (ELF) (3 Hz -100 kHz) electromagnetic fields [24]. Especially in the electric power industry, a large number of workers are likely exposed to EMFs at the workplace. The fact has heightened concerns about the possible health effects during occupational exposures. In the European Union, health surveillance of EMF-exposed workers is mandatory according to the Directive 2013/35/EU, aimed at the prevention of known direct biophysical effects and indirect EMF's effects.

4. EMF interference on implantable medical devices

First reports of EMI with cardiac implants were published in the early 1960s [25]. Since then, a vast number of studies targeting EMI have been carried out. AIMD technologies have been developed radically over 50 years. AIMD manufacturers, such as Medtronic, Biotronik, Boston Scientific, and Microport, seizing the majority of the market, continuously update the technologies and applications.

Many of cardiac implant devices, especially ICDs, were implanted in relatively young patients who are expected to have active working activities, and some of them may be still working with the risk of high-intensity field exposure in specific occupational environments. EMI on the cardiac implant devices may cause risk of malfunction and other safety threats. Inappropriate therapy from ICD, e.g., shock delivery, may give rise to an increased risk for overall survival and psychological distress [26].

Considering the nature formation of the cardiac signals, in order to ensure that the waves are correctly sensed, 50 Hz and 60 Hz may not be filtered by the cardiac medical device. *Figure 1-7* shows the approximate characteristics of the P and R waves that cardiac implants are intended to sense. The detection amplifier's filters are designed to sense signals above the U-shaped which represents the amplifier threshold. 50 Hz and 60 Hz may be included in the frequency range of the detection of R waves. Thus, for EMFs at 50/60 Hz, the investigation for EMI on AIMDs is necessary for the safety of AIMD-carriers.

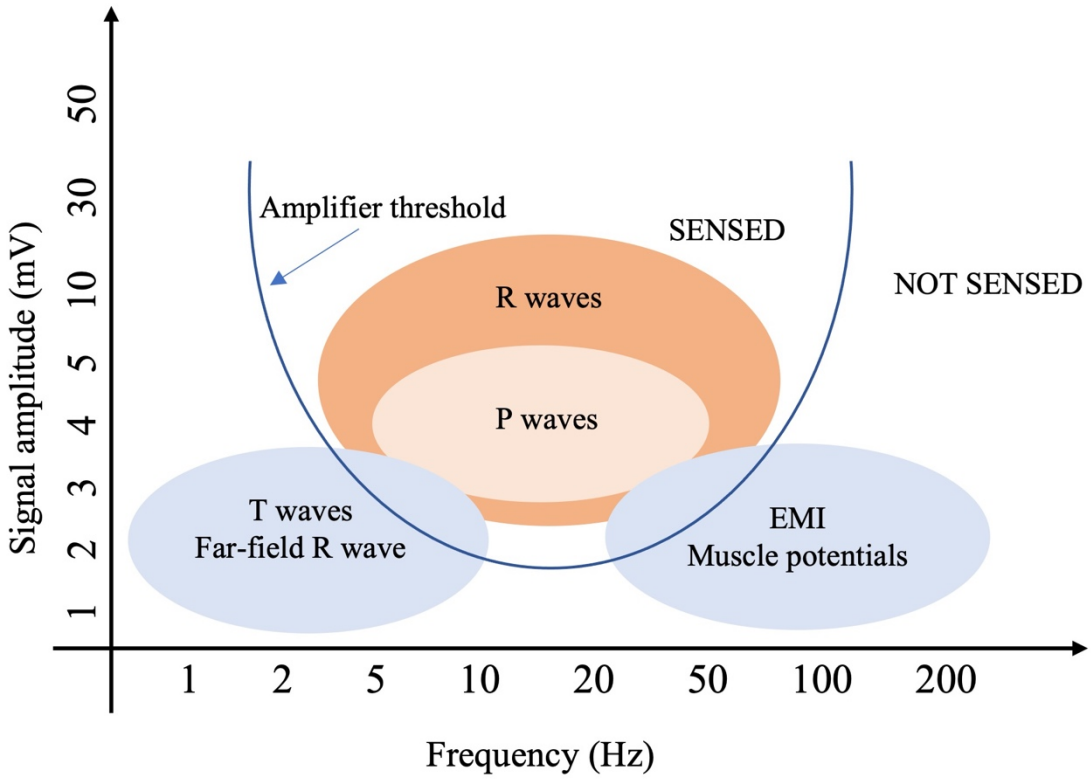

Figure 1-7 Cardiac signal detection frequency and amplitude

IV. Standards, Guidelines, and Related Research

Standards and guidelines were published and constantly updated for electromagnetic exposure in public and professional area. Abundant studies were carried out upon this subject. European Directive 2013/35/UE laid down the action level (AL), which represents the exposure level for protection or prevention from interference with AIMDs. For the purpose of demonstrating compliance, the magnetic field and electric field are always considered separately instead of additively in the standards and norms. All the values in this section are given in RMS quantities (even it's in peak value in the original document).

1. Directive 2013/35/UE

Directive 2013/35/EU is a legislative act issued by the European parliament and the Council of the European Union, which states the minimum health and safety requirements regarding the

exposure of workers to the risks arising from physical agents, as static magnetic and time-varying electric, magnetic and electromagnetic fields with frequencies up to 300 GHz. The directive laid down the obligations of the employer, who shall assess all risks for workers arising from electromagnetic fields in the workplace as well as the action levels (ALs) which were given as the operation levels established for the compliance with relevant exposure limit values (ELVs) (*Table 1-2*). 'Health effects ELVs' means those ELVs above which workers might be subject to adverse health effects, such as thermal heating while 'sensory effects ELVs' means those ELVs above which workers might be subject to transient disturbed sensory perceptions and minor changes in brain functions.

Table 1-2 ELVs for internal electric field strength (50/60 Hz)

Frequency (Hz)	Health effects ELVs (V/m)	Sensory effects ELVs (V/m)
50	0.198	1.56
60	0.238	1.56

The AL terminology is used in terms of 'low ALs' and 'high ALs' of which the magnitudes are laid down to ensure the compliance with relevant ELVs or at which relevant protection or prevention measures must be taken (*Table 1-3*). The AL for exposure to static magnetic field that causes interference with active implanted devices, was given as 0.5 mT.

Table 1-3 ALs for exposure to electric field and magnetic field (50/60 Hz)

Exposure	Frequency (Hz)	Low ALs	High Als
EF	50	10 kV/m	20 kV/m
	60	8.33 kV/m	16.7 kV/m
MF	50	1 mT	6 mT
	60	1 mT	5 mT

2. European standards

The European Committee for Electrotechnical Standardization (CENELEC) approved the European standard EN50527 in 2018 regarding the procedure for assessment of the exposure to electromagnetic fields of workers bearing AIMDs. The purpose of the assessment is to determine the risk for workers with implanted medical devices arising from exposure to electromagnetic fields in the workplaces. Only devices equipped with transvenous lead implanted are considered. It proposes investigation by *in vitro* testing, clinical study and by comparative study. *Figure 1-8* shows an example of *in vitro* procedure given in EN50527. The international organization for standardization (ISO) published ISO 14117:2019 to specify test methodologies of electromagnetic compatibility (EMC) for implantable cardiac pacemakers, implantable cardioverter defibrillators and cardiac re-synchronization devices. The tests are proposed using direct injection without reproducing the real-case phenomenon.

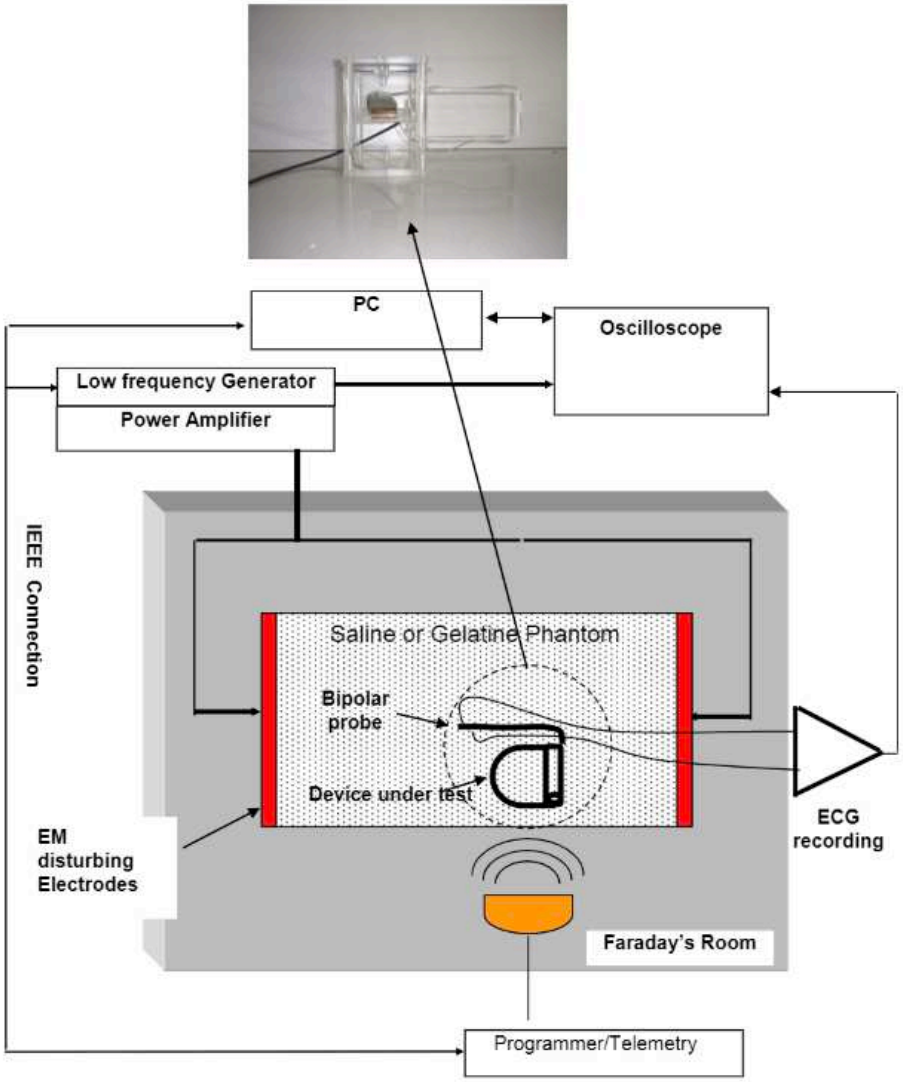

Figure 1-8 Example of in vitro procedure for EM interference at low frequency

3. C95.1-2019-IEEE standard

Developed by the IEEE international committee on electromagnetic safety, as a revision and merging of IEEE Std C95.1-2005 and IEEE Std C95.6-2002, the standard C95.1-2019 is for the safety levels with respect to human exposure to electric, magnetic, electromagnetic fields, 0 Hz to 300 GHz. Given levels are expressed in terms of dosimetric reference limits (DRL) and exposure reference levels (ERL). Adverse health effects associated with electrostimulation may occur in the human body when the DRLs are exceeded. ERLs are limits on external field strengths, induced and contact currents, contact voltages and incident power density to prevent such levels exceeding the DRLs.

Table 1-4 DRLs for electrostimulation mechanisms (50/60 Hz)

Exposed tissue	Frequency (Hz)	Persons in unrestricted environments (V/m)	Persons in restricted environments (V/m)
Brain	50	1.47×10^{-2}	4.43×10^{-2}
	60	1.77×10^{-2}	5.31×10^{-2}
Heart	50/60	0.943	0.943
Limb	50/60	2.10	2.10
Other tissues	50/60	0.701	0.701

Table 1-4 lists DRLs for particular body areas in terms of *in situ* electric field which depends on the exposure situation: persons in unrestricted environments and persons in restricted environments. These exposure situations can be considered as public exposure and occupational exposure. ERLs derived from DRLs are given for electric field exposure and magnetic field exposure. *Table 1-5* lists ERLs in terms of unperturbed external sinusoidal electric field at frequency 50/60 Hz, in which the exposed individual is within reach of a grounded conductive object. *Table 1-6* lists the ERLs for the sinusoidal magnetic field in terms of magnetic flux density *B* for exposure of the head and torso and the limbs. *Table 1-5* and *Table 1-6* apply to against possible adverse health effects. Refer to them helps ensure compliance with *Table 1-4*. Safety programs to prevent the exceeding of DRLs and ERLs, are provided in IEEE C95.7-2014 in the frequency range of 3 kHz to 300 GHz, which may be used in lower frequency cases. However, patients under the care of medical professionals, for example with medical device implementations, are not considered in this standard. The exposure limits do not guarantee for the prevention of electromagnetic interference.

Table 1-5 Electric field ERLs – whole body exposure (50/60 Hz)

Frequency (Hz)	Persons in unrestricted environments (kV/m)	Persons in restricted environments (kV/m)
50/60	5	20

Table 1-6 Magnetic field ERLs – head, torso, and limbs (50/60 Hz)

Exposed tissue	Frequency (Hz)	Persons in unrestricted environments (mT)	Persons in restricted environments (mT)
Heart and torso	50/60	0.904	2.71
Limb	50	75.8	75.8
	60	63.2	63.2

4. ICNIRP guidelines

For the protection of humans exposed to electric and magnetic fields in the low-frequency range of the electromagnetic spectrum, international commission on non-ionizing radiation protection (ICNIRP) published the guidelines for limiting exposure to time-varying electric and magnetic fields. The ICNIRP 2010 covers the low frequency part of the 1998 guidelines (ICNIRP 1998). Reference values of exposure are given (*Table 1-7*), as well as internal restriction for human

exposures. As it has been summarized, authoritative exposure limit values for people implanted with AIMDs are still vacant in standards.

Table 1-7 Reference levels for general public exposure (50/60 Hz)

Exposure resource	Frequency (Hz)	General public exposure	Occupational exposure
EF	50	5 kV/m	10 kV/m
	60	4.17 kV/m	8.33 kV/m
MF	50	200 μT	1000 μT
	60	200 μT	1000 μT

5. Related research

Regarding the electromagnetic interference for cardiac implants, research was developed in frequency, scenarios, applications, etc. Both clinical and non-clinical studies were carried out on this subject.

In vivo provocation studies were conducted in Research Center for Bioelectromagnetic Interaction (FEMU) in Aachen Germany, regarding patients carrying cardiac implants exposed to every day electric and magnetic fields, static electric and magnetic fields, direct current (DC), alternating current (AC), and hybrid electric fields (various DC; constant AC) [27][28][29][30]. Interference thresholds of 110 ICD patients (1-, 2-, and 3-chambers ICDs) were evaluated in a specifically developed site in an *in vivo* study. It was concluded that extremely low-frequency daily-life electromagnetic fields do not disturb sensing capabilities of ICDs. However, high-intensity electromagnetic fields at 50 Hz, present in certain occupational environments, may cause inappropriate sensing, potentially leading to false detection of atrial/ventricular arrhythmic events [31].

EM environments may give rise to possible interferences for implantable cardiac devices in hospital and real working scenes (under power lines or near substation). *In vitro* experiments were conducted by using a watertight human-shaped phantom. It is pointed out that the impact of the varying conductivity of body tissues could be significant since the location of PM electrodes might change the threshold of PMs up to 40% [32][33][34].

In vitro studies on the electromagnetic interference for AIMDs normally include the interference source, a model to simulate the implantation, and a method to observe the interference and relevant effects. U.S. Food and Drug Administration (FDA) has published *in vitro* studies of electromagnetic interference to pacemakers and implantable cardioverter-defibrillators in radiofrequency range [35] and in static magnetic field [36], in addition to numerical analysis at low frequency [37]. The interference between implantable cardiac devices and ophthalmic laser systems was studies by placing the devices in a simulated thoracic chamber and exposing to three ophthalmic laser systems [38]. Transient electromagnetic fields can as well induce electromagnetic noise in the pacing loop and inhibit the release of pacing

pulses according to an *in vitro* study on a swine torso model with skin and rib cage to simulate the clinical condition of dual-chamber pacemaker implantation [39].

As the investigation of the susceptibility of AIMDs was normally based on the estimation of the induced electrical levels on the device input, the measurements of induced current density are significant in the experimental approach. The Italian national institute of health proposed an optically coupled sensor for the measurement of induced currents while the target subjects to MRI gradient fields [40]. The present research works mainly focus on the study of whether the interference from an electromagnetic source disturbs the functions of AIMDs. However, certain quantities are necessary to be determined and analyzed via experiments in order to obtain a scientific confirmed exposure dose for the sake of the safety of AIMD carriers.

V. Conclusion

According to the related standards, guidelines, and scientific research, the risks to AIMDs in the presence of strong EMFs must be assessed. They cannot be neglected, considering that cardiac implants are vital and life-saving devices.

In this chapter, implantable medical devices were introduced from the perspective of heart disease and electromagnetic fields. History and development on AIMDs were retrospected, especially for PM and ICD that were investigated in this study. As a common solution for heart disease treatment now, AIMDs are still facing many challenges. With the development of the technologies on AIMDs, scientific research needs to keep up to ensure its compatibility with the modern society.

Electrification and computerization are important features of modern society. Human beings are facing unprecedent degree of exposure to electromagnetic fields. It is significant to verify the immunity of AIMDs to ensure the safety and life quality of the patients, as they may be subjected to high-intensity electromagnetic fields in the workplace. The risk for employees wearing an AIMD should be assessed. A large number of studies on this subjected were carried out on the basis of the standards and guideline. However, the studies focus mostly on high frequency range and magnetic fields. The occupational EF exposure at extremely low frequency lacks attention but possesses great significance, which will be the object of this study.

2

Theoretical and numerical validation of a risk assessment procedure

I. Introduction

In this chapter, the theoretical and numerical studies are presented on a risk assessment process for cardiac implants. We limited the frequency band of the occupational exposures to the low frequency EFs (50 Hz); thus, the studies of exposures to the EFs and MFs can be carried out separately. In this study, we have focused on the EF exposures. Evaluation of the induced voltage on the unipolar and bipolar cardiac implants under high intensity EF exposures was carried out by numerical approach. CST EM® software, based on the finite integration technique (FIT), was used for the simulations with the electro/magneto-quasi-static equations.

Based on Maxwell's equations, analytical calculations on homogeneous human models can be derived which allows obtaining an order of magnitude of the currents induced inside the human body. According to the induced EF estimation, a risk assessment process, based on phantoms with different conception, was introduced by applying an equivalence factor *F*. Induced voltage on the input of the cardiac implants were investigated by numerical approach in this chapter. An association between the real case and experimental reproductions was established based on the induced voltages. This association validates the risk assessment procedure that we proposed in this study.

The numerical anatomical models provide a digital representation of human bodies. They are valuable tools for the investigations in the bio-electromagnetism field. Analysis on the anatomical models ensures the accurate results on the body's response to the EMF without exposing any biological objects to any risks. For the purpose of establishing risk assessment approaches for cardiac implantable devices at low frequency (50 Hz), a virtual human body - ANSOFT model was taken as real-case study which was taken as a reference to the other systems.

To investigate the performance of cardiac implants under electric fields (EFs), the controlled exposure system was proposed as an equivalent exposure system in the laboratory for *in vitro* studies. The equivalent exposure system generates the same electrical conditions as the reference system by applying the equivalence factor. Homogenous EFs were generated and applied on an *in vitro* phantom which reproduces the induction diversity of different tissues under electric field exposures. This system contains set up delivering high-intensity EFs which was also used in the tests of the interference threshold for cardiac implants. To facilitate the process of risk assessment, the voltage injection system was proposed as a further equivalent exposure system to conduct such tests without harsh experimental set up. This system can be considered as a simplified, portable version of the controlled exposure system which allows tests on the devices with the same effects. Both equivalent exposure systems were studied numerically to provide reference values for experimental measurements.

II. Theoretical background and conception

1. Evaluation of EF interference on cardiac implants

To study the electromagnetic interference on cardiac implants, the physical characteristics should be observed and analyzed. Displacement of electric charges in conductive objects may be triggered by exposure to time-varying electric fields. The electric charges move back and forth while the fields are alternating, which results in an induced alternating current inside the conductive object. For a human body exposed to an EF, the induced current may occur in the body. For the investigation of the induced current in the human body under electric field exposure, the international norm IEC 62226 defined a shape factor K_E, representing the capacitive coupling between the field source and the conductive object exposed to the field. This shape factor K_E depends on the size, conductivity, form, and the position of the object. From Maxwell's equations, fundamental basis of electromagnetism, an analytical method can be deduced for calculating the induced currents in conductors in electro-quasi-static fields:

$$\boldsymbol{J_{in}} = K_E \times f \times \boldsymbol{E_{ex}} \quad [1]$$

where J_{in} is the induced current density within the conductive body, E_{ex} is the vertical external electric field, and f is the frequency. In other words, for a human body exposed to an EF at a certain frequency, the induced current depends on its geometry, mainly the ratio of length to the radius (L/R) of the body, and the location within the body where J_{in} is calculated. From the value of the induced current density J_{in}, the induced electric field E_{in} can be easily derived according to Ohm's law:

$$\boldsymbol{J_{in}} = \sigma \times \boldsymbol{E_{in}} \quad [2]$$

where σ is the electrical conductivity. In other words, the internal electric fields are induced in the body tissues when exposed to an EF.

For a cardiac implant carrier exposed to an electric field, electric fields are induced in the body tissues as well as on the surfaces of sensing electrodes of the device. The difference of electrical potentials between the electrodes, in other words, the induced voltage at the device input, may cause interference which can result in transient or permanent malfunction. Therefore, the investigation of induced voltage has been taken as an approach to assess the immunity of cardiac implants to electromagnetic interference. The evaluation of the induced voltage on the cardiac implant can be obtained by the line integral of the scalar product between the vector of the electric field inside the body and the path vector along the sensing path [41]. Unipolar sensing and bipolar sensing are the two common sensing modes. A unipolar lead is a single conductor lead with an electrode located at the tip. A bipolar lead has two separate and isolated conductors within a single lead; the distal electrode is located at the tip of the lead and the other one is usually about 20 mm more proximal, i.e., tip and ring [42]. The sensing path of a cardiac implant is: between tip and housing for unipolar sensing mode; tip-ring spacing for bipolar sensing mode (see *Figure 2-1*).

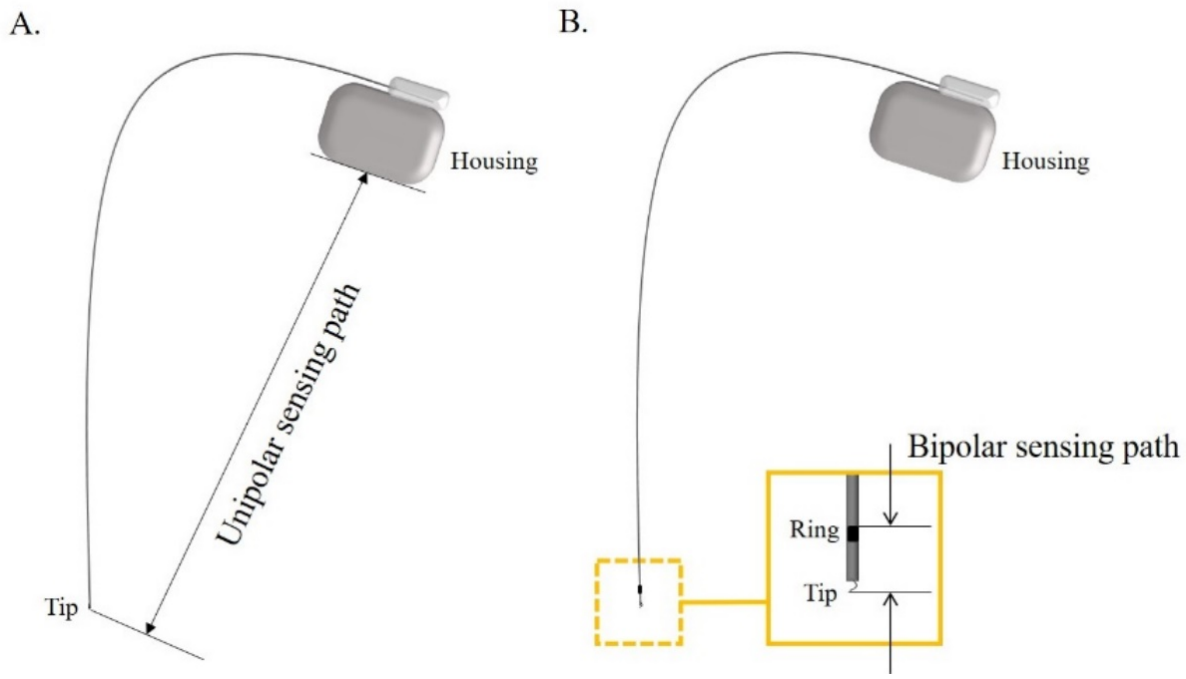

Figure 2-1 Unipolar and bipolar sensing path

For a cardiac implant carrier exposed to a low frequency electric field E_{ex}, the induced voltage U that the cardiac implant is subjected to can be obtained by evaluating the line integral of the scalar product between E_{in} and the path vector $\boldsymbol{dl}$ along the sensing path according to the following classical *Equation [3]*:

$$U = \int_{Tip}^{Generator\ /\ Ring} \boldsymbol{E_{in}} d\boldsymbol{l} \quad [3].$$

To sum up *Equations [1][2][3]*, the estimation of the induced voltage U that the cardiac implant is subjected to, calculated by integration along the sensing path D, is demonstrated in *Equation [4]*:

$$U = \int_D \ p \times f \times \boldsymbol{E_{ex}} d\boldsymbol{l} \qquad [4]$$

where p is a characteristic factor that represents the quantity K_E/σ along the integration path, depending on the size, conductivity, form, and position of the integration point. Accordingly, the voltage induced on the cardiac implant depends on the geometry of the model that the device is implanted to and its conductivity. As the induced voltages on the input of the cardiac implants are evaluated to assess the immunity of cardiac implants to electromagnetic interference, a risk assessment process was proposed based on the conception introduced above.

2. Establishment of risk assessment procedure

Considering the difficulties due to the complexity of the human body, the investigations on the susceptibility of AIMDs were mostly carried out on virtual phantoms and *in vitro* phantoms. The virtual human body allows thorough studies for the real-case exposition. It is possible to observe more detailed electromagnetic effects on different organs and body tissues. In the meantime, *in vitro* studies reproduce the researched phenomenon with certain preset conditions.

Instead of mimicking heterogeneous systems composed of muscles, bones, and air forming complex shaped boundaries, homogeneous *in vitro* phantoms can be easily fabricated and observed as equivalent models. As long as the association between the equivalent phantom and the human body can be determined, the *in vitro* testing allows the behaviors of AIMDs in the electromagnetic induction level to be investigated in a similar situation to *in vivo* tests but without risk.

As introduced in the previous section, the risk assessment for electromagnetic interference on cardiac implants is carried out by estimating the induced voltage on the input of the cardiac implants according to *Equation [4]*. Thus, in an equivalent phantom, the configuration of implantation should be the same as in the human body, in other words, it should be fixed 2 things: 1) sensing mode and 2) sensing path. An equivalence factor can be found to demonstrate the correlation between the human body, as the standard model, and the *in vitro* phantom, as the equivalent model. Thus, the effects on real-case human body can be derived from the effects obtained in the equivalent phantom by applying the equivalence factor. The equivalence factor F is demonstrated by the following equation:

$$F = \frac{U_{equivalent}}{U_{standard}} = \frac{\int_D p_{equivalent} \times f \times \boldsymbol{E_{ex}} d\boldsymbol{l}}{\int_D p_{standard} \times f \times \boldsymbol{E_{ex}} d\boldsymbol{l}} \qquad [5]$$

where $p_{equivalent}$ represents the quantity K_E/σ along the integration path in the equivalent model and $p_{standard}$ represents the quantity K_E/σ along the integration path in the human body. In addition, the equivalent factor F applies to the relationship between the electric field exposures to which models are subjected when the same effects are reproduced in the standard model and equivalent model. Thus, when the same amount of induced voltage on the cardiac implants are obtained, the equivalence factor indicates the relationship between standard exposure and equivalent exposure as presented in *Equation [6]*:

$$\boldsymbol{E_{standard}} = F \times \boldsymbol{E_{equivalent}} \qquad [6]$$

where $E_{equivalent}$ is the electric field E_{ex} that equivalent phantom subjected to, and $E_{standard}$ is the electric field E_{ex} that the human body is subjected to.

According to above, it is demonstrated that the induced voltages on the cardiac implants under electric field exposures depend on the size, conductivity, form, and position of the model. In simple terms, the induced voltage depends on the conditions where electric fields are induced in the model. This conception leads us to search for easy, feasible, efficient, and risk-free ways to study the impact on the AIMDs from electromagnetic interference. If the equivalence factor between the standard system and the equivalent system is validated, the exposure tests on cardiac implants can be carried out in the laboratories to conduct experimental measurements.

III. Numerical study on virtual human body

In the studies of bio-electromagnetism, the numerical studies are usually processed in prime considering the visualization, the analyzability and the security issues. In the meantime, significant growth in computing power has enabled the complex numerical analysis. Computational modeling with virtual human bodies apply mathematical analysis and computer science to study the behaviors and reactions of complex biological individuals. Experiments can be easily and safely conducted on the virtual human bodies in order to identify the theoretical effects and to research the corresponding solutions. Thus, the virtual human bodies, also known as the anatomical models, are indispensable in the modern bio-research. These models are typically derived from 3D scan data (computed tomography CT or MRI) or serial sectioning images providing valuable insight in the scientific research and industrial developments and the applications have rapidly increased in recent decades [43].

1. Full-body models for computational electromagnetics

In computational electromagnetics research, the virtual human models have irreplaceable significance. Various applications were carried out, such as the Body Area Networks (BANs), On-body and In-body Antenna Design, and MRI Safety of passive or active implants at high-frequency; Neurostimulation, Magnetoencephalography/Electroencephalography (MEG/EEG) Source Localization, Tumor Treating Fields at low-frequency [44]. In the studies of electromagnetic field dosimetry, numerous anatomical realistic voxel models were developed (Dawson et al. 1997, Dimbylow 1996, Furse and Gandhi 1998, Mason et al. 1999) to calculate the induced current densities as well as the electric fields according to the EMF source. A female 2 mm resolution voxel model named NAOMI was developed by the National Radiological Protection Board of the UK in 2004. This model was derived from a high-resolution magnetic resonance image (MRI) scans of a 23-year-old female subject, including 41 tissue types in the model [45]. The calculations using NAOMI were conducted from 50 Hz up to 10 MHz and provided valuable responses to the restrictions at that time (ICNIRP 1998).

The most comprehensive model family is the virtual population (ViP) from IT'IS Foundation (Switzerland), created from MRI data of volunteers [46][47]. The newest generation of models is the ViP3.1, including both sexes, with ages spanning from fetus to 84 years old and adult body mass index (BMI) ranging from 21.7 to 36.2, providing a resolution of $0.5 \times 0.5 \times 0.5$ mm^3 throughout the entire body, containing more than 300 tissues and organs per model. The Virtual Population models are compatible with the platform Sim4Life allowing postures to be modified for simulating various exposure configurations. The ViP models have also been used as a tool to investigate the interference of EMFs on cardiovascular implanted devices [48]. Zygote Media Group, Inc. has developed 3D full-body models dedicated to broadcast television, films, computer games, educational software, medical illustrations, and animations. The platform Zygote Body 3D Anatomy Online Visualizer (https://www.zygotebody.com/) has enabled immersive 3D interactive virtual anatomy. However, since these models are not based on real subjects, their application for regulatory purposes might be limited.

2. ANSOFT model

Considering that the staircase effects on the voxel models may amplify the numerical errors in the ELF, a surface-based model was chosen for the numerical study which allows better geometry construction compared to the voxel models. This anatomical model was developed by the company ANSOFT for the software MAXWELL. The ANSOFT model represents a male adult of 183.6 cm tall in a standing position, with arms on the sides and feet grounded, constructed with 272 organs and 32 tissues (ANSOFT, ANSYS, Canonsburg, PA, USA). An illustration of the ANSOFT model is shown on *Figure 2-2*.

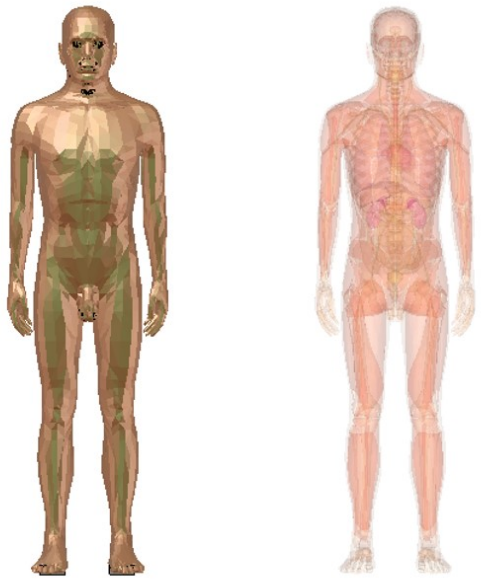

Figure 2-2 ANSOFT model: (1) With visible skin; (2) Transparent view

The electrical conductivity of tissue plays an important role in the dosimetry of the induced electric field. Most studies follow Herman Schwan dispersion relations, and use Gabriel's dielectric properties data of biological tissues. The permittivities and conductivities applied on the ANSOFT model are based on the IT'IS database version 4.1 [49] of low-frequency range which also follows the study of Gabriel (1996) [50]. See *Table 2-1* for the dielectric properties assigned to the ANSOFT model at 50 Hz.

Table 2-1 Dielectric properties of IT'IS database V4.0 low frequency at 50 Hz

Tissue	Source	Relative permittivity ε_r	Electrical conductivity σ (S/m)
Bile	Bile	1.20E+1	1.40E+0
Bladder	Urinary Bladder Wall	4.82E+5	2.05E-1
Blood Vessels	Blood Vessel Wall	8.10E+06	2.61E-01
Bone	Bone	8.87E+03	2.01E-02
Bone Marrow (red)	Bone Marrow (red)	1.70E+05	1.01E-01
Bone Marrow (yellow)	Bone Marrow (yellow)	1.67E+05	2.15E-03
Brain	Cerebellum	1.21E+07	9.53E-02
Cartilage	Cartilage	1.64E+06	1.71E-01
Cerebellum	Cerebellum	1.21E+07	9.53E-02
Skin	Skin (Dry)	1.14E+03	2.00E-04
Epididymis	Testis	1.64E+06	4.21E-01
Esophagus	Stomach	1.64E+06	5.21E-01
Eye	Eye (Vitreous Humor)	9.90E+01	1.50E+00
Heart Muscle	Heart Muscle	8.66E+06	8.27E-02
Heart Lumen	Blood	5.26E+03	7.00E-01
Kidney	Kidney	1.01E+07	8.92E-02
Large Intestine	Large Intestine	3.21E+07	5.45E-02
Larynx	Cartilage	1.64E+06	1.71E-01
Ligament	Ligament	1.71E+07	2.70E-01
Liver	Liver	1.83E+06	3.67E-02
Lung	Lung	5.76E+06	6.84E-02
Muscle	Muscle	1.77E+07	2.33E-01
Optic Nerve	Nerve	1.61E+06	2.74E-02
Pancreas	Thyroid Gland	1.64E+06	5.21E-01
Prostate	Testis	1.64E+06	4.21E-01
Small Intestine	Small Intestine	2.03E+06	5.22E-01
Spleen	Spleen	1.02E+07	8.57E-02
Stomach	Stomach	1.64E+06	5.21E-01
Tongue	Tongue	1.64E+06	2.71E-01
Tooth	Bone	8.87E+03	2.01E-02
Trachea	Trachea	8.87E+04	3.01E-01
Trachea Lumen	Trachea Lumen	1.00E+00	0.00E+00
Urethra	Blood Vessel Wall	8.10E+06	2.61E-01

The electrical conductivity of skin should be used with caution considering that its variations may significantly impact the electric field dosimetry assessment. The human skin structure is composed of multiple layers: stratum corneum, cellular epidermis, dermis, hypodermis. Due to their compositions, the conductivities of each layer are different. For a single-layer skin model, an equivalent conductivity of skin is generally adopted. However, it is unclear that whether several skin layers can be treated as a single composite tissue without impacting the estimation of the induced electric field. According to Gabriel (1996), the conductivity of tissues is almost constant in the low-frequency range and the conductivity of dry skin is 0.0002 S/m (0.00042 for wet skin) at 50 Hz [50]. A skin conductivity value of 0.1 S/m was proposed in Dimbylow (2005) by treating 'skin' as a composite tissue consisting of skin and subcutaneous fat. An equivalent skin model was proposed and suggested using a conductivity of 0.2 S/m for low frequency magnetic field dosimetry [51]. In addition, it has been proved that using very low conductivity value affect significantly in the regions where the E-field is orthogonal to the skin layers. The values are obviously not representative for peripheral nerve tissues (PNS) [52]. Thus, considering the composition of the 'contact layer' of the ANSOFT model, a skin conductivity value of 0.1 S/m was applied to it instead of 0.0002 S/m given in the IT'IS database.

3. Virtual human body exposed to EF

In this study, the ANSOFT virtual human body with grounded feet was taken as the standard system. The induced electric field in the heart and over the chest in the ANSOFT model were taken as a reference for the design of the equivalent system.

In the IEC 62226-3-1 standard, the semi-spheroidal and the axisymmetric models were proposed as representative of the human body. The simulations on these models were conducted in COMSOL based on finite element method (FEM) analysis at first for an initial study on the effects on the human body under electric fields. The dimensions of the semi-ellipsoidal model were reduced by a factor of 5 (L: 352 mm and R: 35.6 mm) of those of the reference human body defined in the standard. A material with characteristics of human body tissue is considered in the semi-ellipsoid model (ε_r: 10^5; σ: 0.2 S/m). This material was also applied to an axisymmetric model which develops some complexities of shape to approach real human body. According to the simulations conducted on these two models (*Figure 2-3*):

- Semi-ellipsoid model: the induced current density is uniform in the model;
- The axisymmetric model: the induced current density varies along the body while the value is maximum at the ankle area then the neck.

This finding confirms the fact that the EF induction occurred on the model depends on its geometry and conductivity but also on the analysis approach used for simulations. These two models were thoroughly used in the IEC 62226-3-1 for theoretical analysis and numerical simulations. In this study, they will not be described in detail.

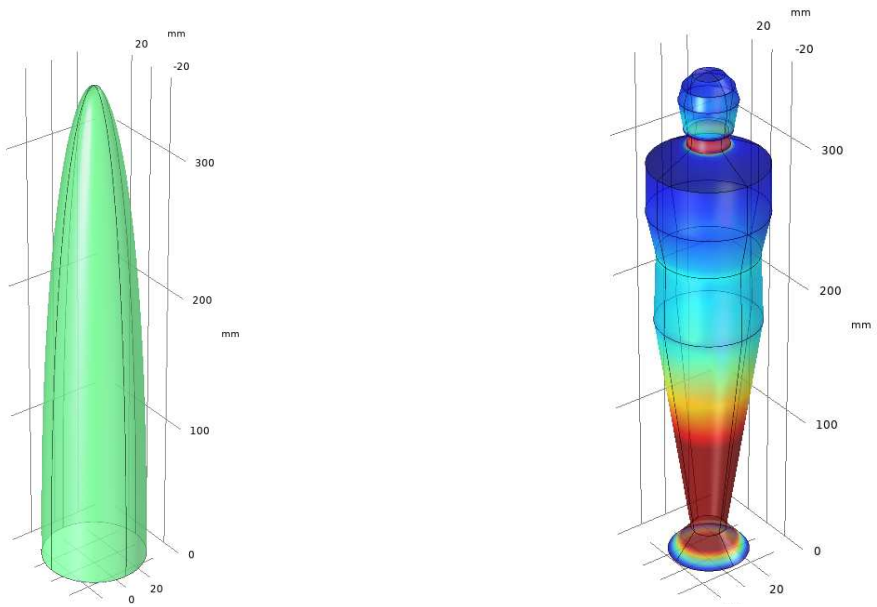

Figure 2-3 Semi-spheroid model and axisymmetric model under homogeneous EF exposure

The numerical study on ANSOFT virtual human body was carried out in the software CST EM®, based on the finite integration technique (FIT), due to its powerful visualization engine and solvers for electromagnetic simulations. FIT, similar to FDTD grids, is a consistent discretization scheme for Maxwell's equations in their integral form which allows the calculation of the elements on each grid. The resulting matrix equations of the discretized fields can be used for efficient numerical simulations [53]. According to the comparison conducted between the performance of COMSOL and CST, targeting an application of the electromagnetic interference study for cardiac implants, COMSOL may induce more errors when the geometry of the model becomes complex. COMSOL is a software for multiphysic problems and not dedicated to EM issues. CST is more efficient in terms of computation time and memory consumption [54]. Considering the heterogeneity of the EM properties of the organs, factor against limits of power and computation time, and the difficulties related to the fineness of the mesh, CST EM® was selected as the simulating environment in this study.

Since the levels of induced EF have compliance with linearity when adjusting the external exposures, the numerical studies were always conducted for an EF of 1 kV/m at 50 Hz. Under such exposure, the induced EF on the ANSOFT model varies in different organs and tissues, among those values reach relatively high in the neck, liver, stomach, and legs (*Figure 2-4*). Compared to the voxel model using hexahedral mesh, the tetrahedral mesh of ANSOFT model respects the rounded geometries of organs and avoids the step effect. The induced EFs on the organs are given in *Table 2-2*.

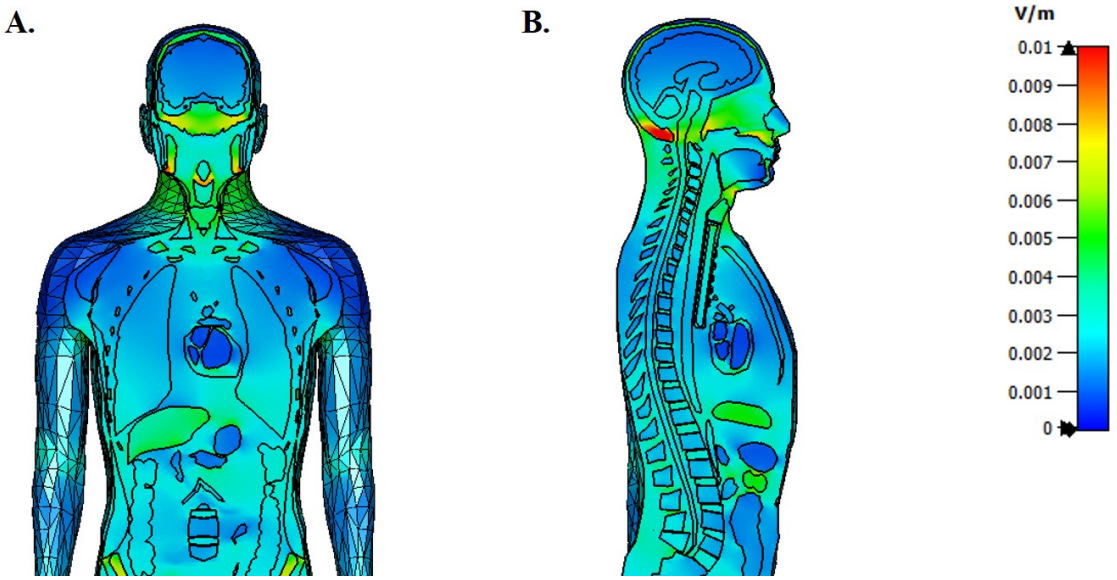

Figure 2-4 Induced electric field on ANSOFT anatomical model under 1 kV/m 50 Hz exposure: A) Front view; B) Side view

Table 2-2 ANSOFT body model exposed to a 50 Hz uniform EF, average and maximum induced EF on the organs in the body per 1 kV/m EF exposure

Organ Name	Isotropic σ [9]	E_{avg}	E_{max}
	S/m	$mV \cdot m^{-1}$	$mV \cdot m^{-1}$
Brain	0.08	0.9	1.7
Heart muscle	0.08	1.14	4
Heart lumen	0.70	0.545	2.44
Muscle	0.35	1.25	29.4
Skin	0.10	1.43	77.3

The maximum induced electric field was found 4 mV/m in the heart of ANSOFT virtual human body where the probe of cardiac implant is contained. Our finding is coherent with the other studies on virtual human bodies exposed to low frequency electric field at 50 Hz (*Table 2-3*). The value of the induced electric field in the heart will be considered as a reference for the establishment of the equivalent system. The application will be introduced in the following section.

Table 2-3 Induced electric field in the heart in mV/m under unit EF exposure (1 kV/m)

Per 1 kV/m EF	Potter 2000, [55]		Kavet 2001, [56]		Tarao 2012, [57]	Findlay 2013, [58]		Our work [59]	
	E_{avg}	E_{max}	E_{avg}	E_{max}	E_{avg}	E_{avg}	E_{max}	E_{avg}	E_{max}
Induced EF in heart	1.07	2.19	0.98	2.4	1.12	0.955	3.54	1.1	4

4. ANSOFT model implanted with an AIMD exposed to EF

To investigate the impact of external EF exposures on the AIMD, a cardiac implant was modeled in the simulation conforming to the dimensions and materials of a real implantable cardiac device. The specifications of the pacemaker (PM) and the implantable cardioverter defibrillator (ICD) were taken into consideration. The cardiac implant model contains an impulse generator (housing) and a sensing lead. The modeling of PM took the dimensions of a model of Advisa from Medtronic: 50 mm × 30 mm × 7 mm; the modeling of ICD took the dimensions of a model of Evera from Medtronic: 60 mm × 60 mm × 15 mm. As introduced in the previous section, the induction under EF exposure depends on the sensing mode and the sensing path as long as the specifications of cardiac implant stay the same. Thus, in the numerical study, the dimensions of the PM were applied for the investigation. The container of the impulse generator is made of titanium (σ: 2.38×10^{6} S/m). The length of the sensing lead was 30 mm which took the reference of a real bipolar sensing lead. The modeling of the sensing lead was composed of the isolator made of silicone (σ: 1×10^{-15} S/m), the lead made of nickel (σ: 1.44×10^{7} S/m), and the electrodes made of platinum (σ: 9.52×10^{6} S/m). The impulse generator was inserted under the collarbone on the right-side front of the chest while the probe was inserted at the left ventricle; the tip of the sensing lead was inserted in the heart muscle of the left ventricle. Two sensing modes were investigated: unipolar and bipolar. The sensing path for unipolar sensing mode, between the impulse generator and the lead tip, is 220 mm, which is determined by the configuration of implantation; the sensing path for bipolar sensing mode, between tip and ring, is 12 mm, which is determined by the feature of the considered sensing lead (See *Figure 2-5*).

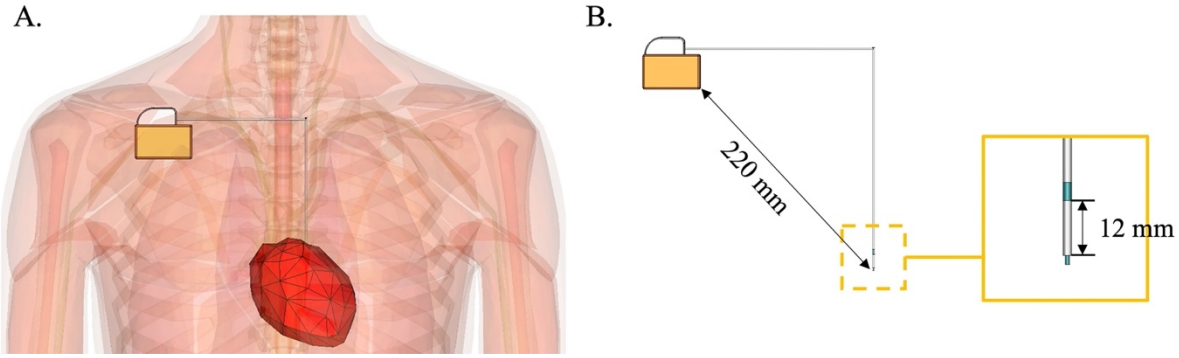

Figure 2-5 ANSOFT model and cardiac implant model: A) Right pectoral implantation of a pacemaker; B) Sensing path configuration

The induced voltage on the cardiac implant can be affected by several factors. Our team performed studies on the influence of the sensing mode, the lead dimensions, the tip position, the chamber impact, and the sensitivity settings of the cardiac implant [60]. In this study, most of the factors are fixed in order to obtained comparable and reproducible results. The influence of the sensing path will be introduced and analyzed in the chapter of experimental measurements.

To determine the electromagnetic disturbance incurred by the implant, it is necessary to specify the approach used for the simulation results, the voltage induced on the electrodes of the cardiac implant was determined as follows:

- For unipolar sensing mode, the induced disturbance voltage is the integral of the electric field along the line between the housing and the tip electrode of the probe;
- For bipolar sensing mode, the induced disturbance voltage is the integral of the electric field along the line between the tip and ring of the probe.

Figure 2.6 and *Figure 2.7* show the plots of induced EF on the sensing path. Several parameters may govern the results: 1) the choice of the numerical method; 2) the simulating environment; 3) the type and number of meshes; 4) the implantation configuration (sensing path); 5) the database of body tissue conductivity. It is well known that the finesse of meshes has a big impact on the calculation of the induced EF on the path of integration. Thus, the electrical potentials on the electrodes of cardiac implant were taken for the calculation of induced voltages in order to ensure the accuracy. Consequently, for the ANSOFT model under EF exposures of 1 kV/m at 50 Hz, the induced voltage between the tip of the probe and the housing in unipolar sensing mode was found to be 183 μV; the induced voltage between the tip and ring of the probe in bipolar sensing mode was found to be 22 μV.

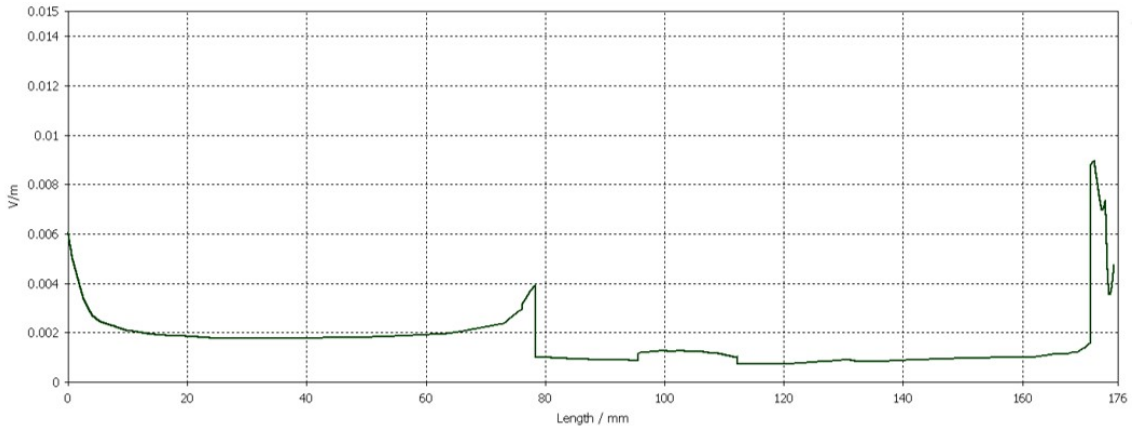

Figure 2-6 Induced EF plot between unipolar sensing path (from housing to tip)

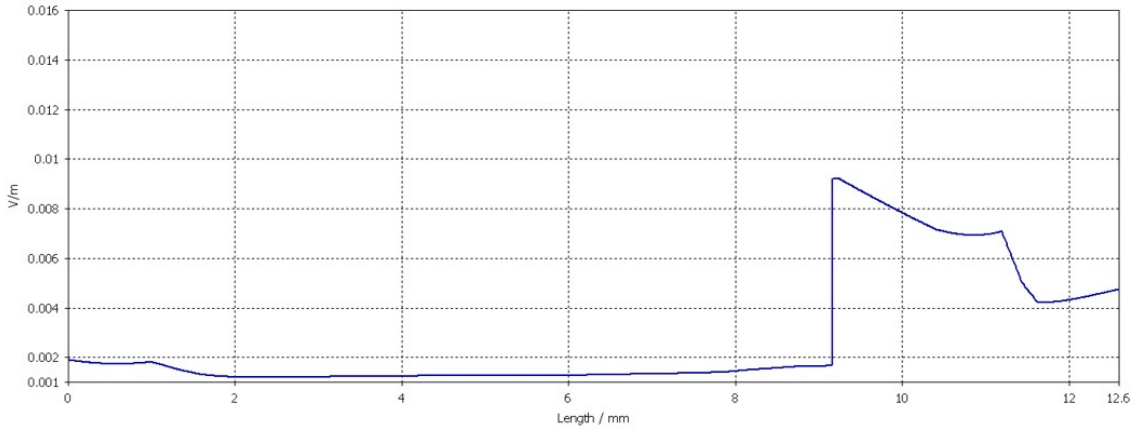

Figure 2-7 Induced EF plot between bipolar sensing path (from the ring to tip)

IV. Controlled EF exposure system

Aiming at reproducing the high-intensity EFs in the laboratory for *in vitro* tests on cardiac implants, controlled EF exposure system was designed. The *in vitro* testing reproduces the real *in vivo* situation as close as possible, which allows investigating the behavior of the implanted device in a situation close to the workplace without risk for the patient. To conduct such tests for the implanted device and the electromagnetic source, an *in vitro* phantom that represents the electrical characteristics of the implantation location is necessary. A funnel-shaped *in vitro* phantom was introduced by our team [59]. The ANSOFT virtual human body was taken as the standard system. The conception of the controlled EF exposure system was based on the equivalence factor *F* defined in *Equation [5]*. Under the same conditions of EF exposure, the equivalence factor *F* can be found from the voltages on the cardiac implants induced in the controlled exposure system and in the virtual human body (ANSOFT model):

$$F = \frac{U_{controlled\ exposure}}{U_{ANSOFT}} \qquad [7]$$

To maintain the equivalence between the standard system and the equivalent system in the experiments under EF exposures, it should be fixed 2 things: 1) sensing mode and 2) sensing path.

1. *In vitro* phantom

Rectangular phantoms and human-shape phantoms are commonly used in *in vitro* experiments simulating body tissues. Due to the complexity of the human body, these phantoms cannot present the shape influence of the human body or the diversity of different tissues for EF exposure. An *in vitro* phantom was designed to reproduce the implantation conditions in the human body and the electrical characteristics under electric field exposures in order to carry out the establishment of an equivalent system according to *Equation [7]*. Taking the ANSOFT virtual human body as the reference model, we proposed a funnel-shaped phantom as an equivalent model with a maximum circumference as the same of the human thorax (C_{Thorax}), so that the cardiac implants can be properly placed (*Figure 2-8*).

The scale of the phantom is homothetically reduced compared to the human body for facilitating the experiments in the laboratory. As we keep the same circumference of the human thorax but a smaller height, the circumference of the upper part of the phantom decreases downward into a funnel shape to prevent a decrease in induction, which is related to the ratio of height and circumference. The upper part of the phantom imitates the induction in the human chest cavity by adjusting C_{upper}, where the cardiac implant is installed. The lower part of the phantom was designed cylindrical of which the circumference (C_{lower}) was determined for the imitation of induction in the heart, where the probe of the cardiac implant is located (*Figure 2-8*). The phantom is filled with a saline solution with the conductivity of 0.2 S/m as used in IEC 62226. According to the findings on the virtual human body, to reproduce the induction environment for cardiac implants under an electric field exposure of 1 kV/m at 50 Hz, an induced electric field of 0.8 mV/m is expected in the upper part of the phantom which mimics the thorax, and

an induced electric field of 4 mV/m is expected in the lower part of phantom which mimics the heart (*Figure 2-9*).

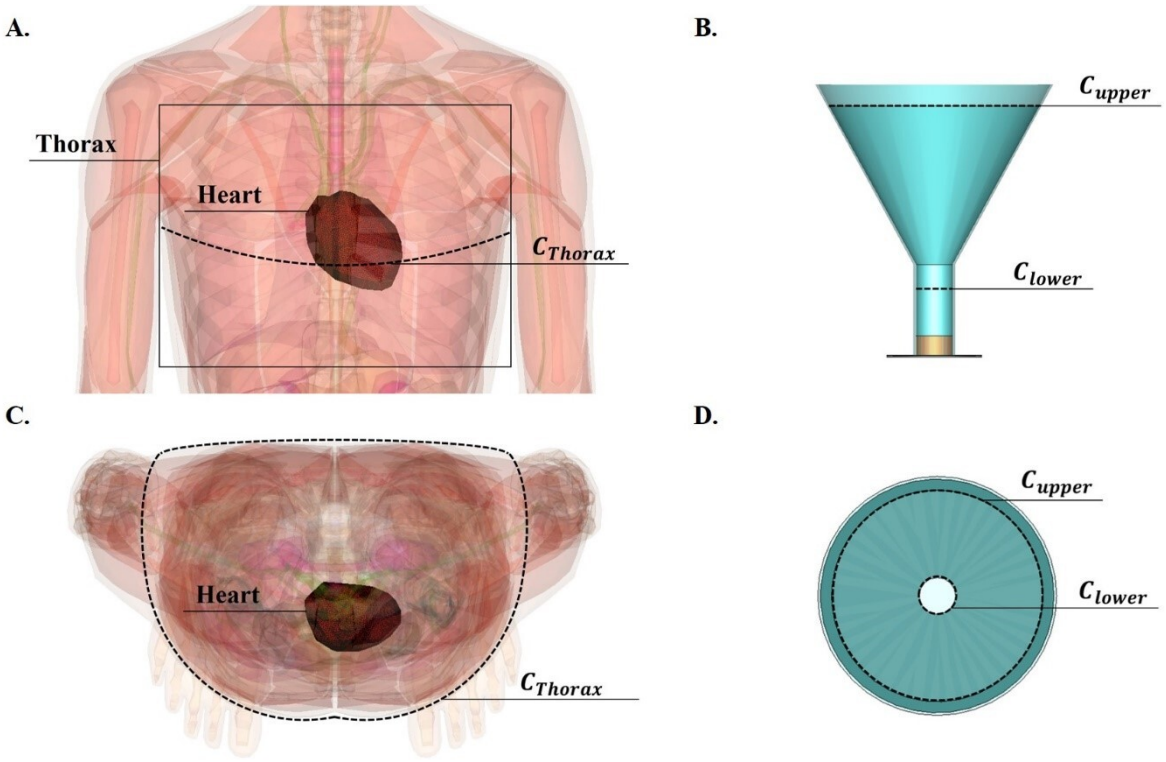

Figure 2-8 Conception demonstration of the in vitro phantom - structure

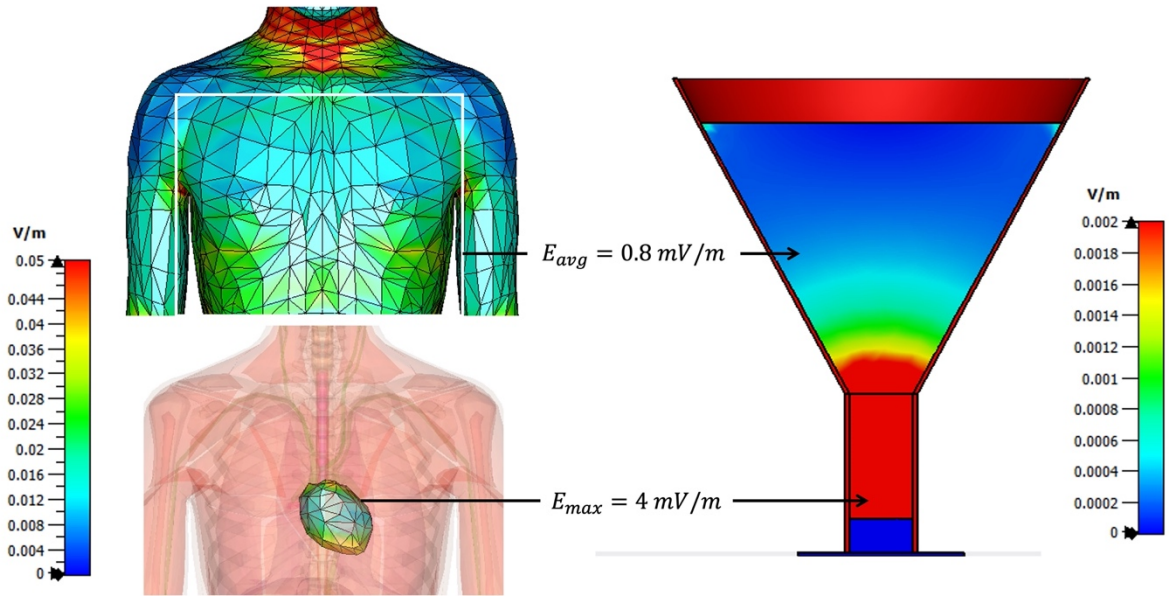

Figure 2-9 Conception demonstration of the in vitro phantom – electrical characteristics

A recipient made of 3.3 mm thickness glass was fabricated (*Figure 2-10*), providing mechanical rigidity and safety, easy fabrication, and electrically insulating and grounded base. The induced voltage on the cardiac implant decreases significantly with the thorax circumference of the

human body. In the *in vivo* study in 2009 [61], the thorax circumference of 750 mm (the smaller one from 15 volunteers) was considered the worst-case scenario among the patients, which indicates a diameter of 239 mm for the case of a cylinder. This phantom possesses a top diameter of 300 mm (D3), which allows us to perform tests with different C_{upper} (D2), i.e., different L2, and a total height of 352 mm (L3), equivalent to 1/5 of ICRP's reference values [62]. C_{lower}, i.e., the diameter of the lower part (D1) and the height of the lower part (L1), were determined to reproduce the electric field induction in the heart of the human body. A metallic pedestal is plugged into the bottom of the phantom to keep the phantom in the vertical position and grounded. As the dimensions are determined, the level of the induced electric field can be adjusted by controlling the height of the phantom solution (L2).

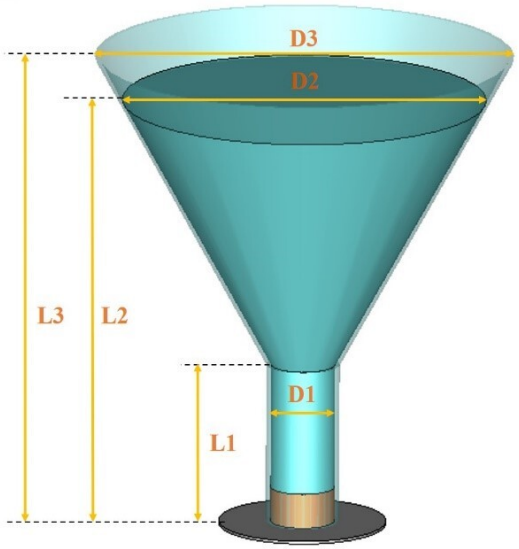

Figure 2-10 Funnel-shaped in vitro phantom

2. *In vitro* phantom exposed to EF

The induction in the phantom was studied with the software CST EM®, under unit EF exposure (1kV/m) at 50 Hz, in the same conditions as with the ANSOFT model as the bottom of the phantom is grounded. As the top diameter of the phantom (D2) determines the EF induction, we defined the distance between the surface of the phantom solution and the phantom top as $D_{liquid-to-top}$. Different values from $D_{liquid-to-top} = 0$ (full) to $D_{liquid-to-top} = 50\,mm$ were simulated (*Table 2-4*). *Figure 2-11* shows the induced electric field plotted on the central line of the phantom when $D_{liquid-to-top} = 50\,mm$. Constant EF induction occurs in the lower part of the phantom and the induced electric field decreases gradually upwards until the surface of the phantom solution. With $D_{liquid-to-top} = 30\,mm$, an electric field of 4 mV/m was induced in the lower part of the phantom which reproduces the induction in the heart of the human body where the probe of the cardiac implant is contained; an average of 0.8 mV/m was induced in the upper part which reproduces the induction over the chest of the human body where the impulse generator is contained. Thus, the $D_{liquid-to-top}$ was fixed at 30 mm to reproduce the same induced electric fields in the heart and in the chest.

Table 2-4 Induced electric field in the phantom under 1 kV/m EF exposure at 50 Hz

$D_{liquid-to-top}$	0 mm	10 mm	20 mm	30 mm	40 mm	50 mm
E *in lower part* (mV/m)	4.9	4.6	4.3	4.0	3.7	3.4
E_{avg} *in upper part* (mV/m)	0.3	0.4	1	0.8	1.5	2.5

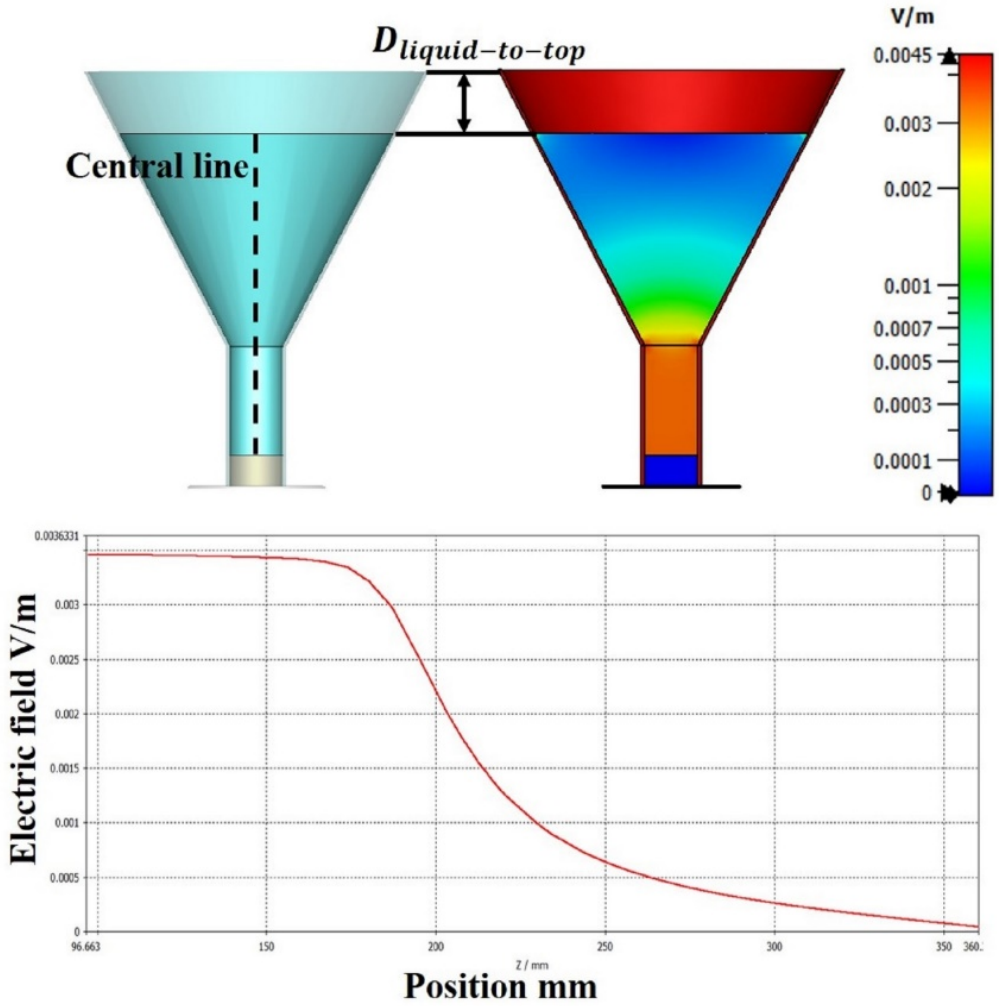

Figure 2-11 A) Induced electric field in the phantom under 1kV/m EF exposure with $D_{liquid-to-top}$=50 mm; B) Induced electric field in the central vertical line of the phantom under 1 kV/m EF exposure with $D_{liquid-to-top}$=50 mm

3. *In vitro* phantom "implanted" with an AIMD exposed to EF

A cardiac implant was inserted in this phantom, the housing placed in the upper part and the lead placed towards the lower part in parallel with the direction of external electric fields to subject to maximum exposure. The induced voltages at the input of cardiac implants were investigated by applying EF exposures on the phantom. The sensing paths were set similarly to the ANSOFT virtual human body (*Figure 2-12*) to obtain the coherence between the standard system and the equivalent system:

- Unipolar sensing path: 220 mm between the housing and the lead tip;
- Bipolar sensing path: 12 mm between the ring and tip at the end of the lead.

The induced voltages on the input of the cardiac implant were calculated with the same approach applied on the ANSOFT model: integration of the induced electric fields on the sensing path; difference of the electrodes' potentials.

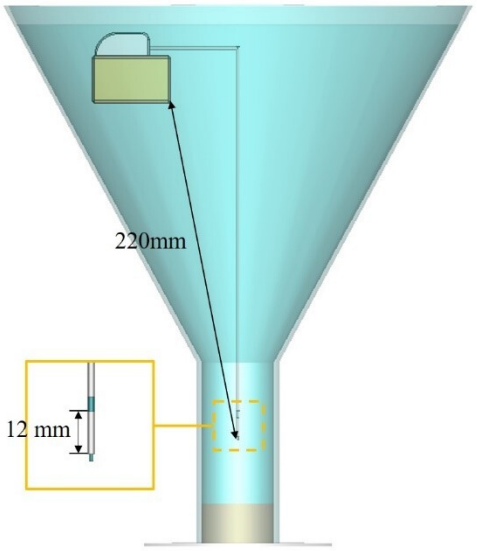

Figure 2-12 In vitro phantom implanted with an AIMD

In the simulation of the *in vitro* phantom under 1 kV/m 50 Hz homogeneous EF, the induced voltage on the probe of the cardiac implant was found 62 µV in the bipolar sensing mode and 421 µV in the unipolar sensing mode. The establishment of the relation between the standard system and the equivalent system is based on these findings and will be presented in the *Chapter 4*.

4. Exposure bench

For the purpose of further experimental investigation, the exposure source was brought to the controlled EF exposure system to provide level- and frequency-controllable electric field exposures. To ensure the reproducibility and reliability, an exposure bench was designed (*Figure 2-13*) to generate high-intensity homogeneous electric fields as the source of EF disturbance.

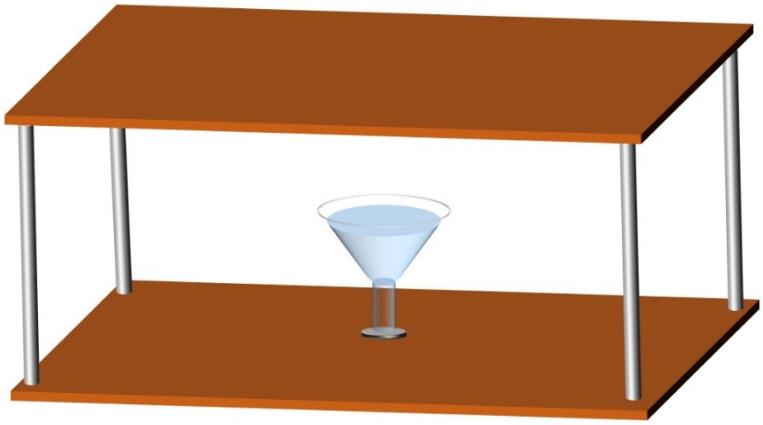

Figure 2-13 Geometry of the exposure bench and in vitro phantom in the controlled EF exposure system

The set-up was built with size to be inserted in a secure laboratory room. Two square plate conductors in aluminum (σ: 3.56×10^{7} S/m), each with a side length of 2 m, were placed in parallel, separated by a distance of 0.75 m. Four PVC insulators (ε: 6; σ: 10^{-15} S/m) as support poles between the plates were placed at the four corners. High voltages were applied on the upper plate; the lower plate was grounded. The phantom was placed in the center of the lower plate to create the condition of grounded feet to obtain the worst-case scenario. As we controlled the voltage applied to the upper plate, the level of the EF generated between the two plates could change accordingly.

An investigation of the exposure set-up was conducted to verify its performance. A voltage of 750 V was applied on the upper plate. According to the calculation of the electrical potential difference, an EF of 1 kV/m was expected between the two plates. *Figure 2-14* shows the EF plots of the exposure set-up. The generated EF varies in the areas near the edges of the plates, however, in a small level; the EF stays homogeneous in the center of the volume between the two plates. For the support poles, we barely found any influence of the insulators on the EF, except in a zone close to them (r: 5 cm). The dimensions and construction of the exposure bench are preserved in the experimental approach.

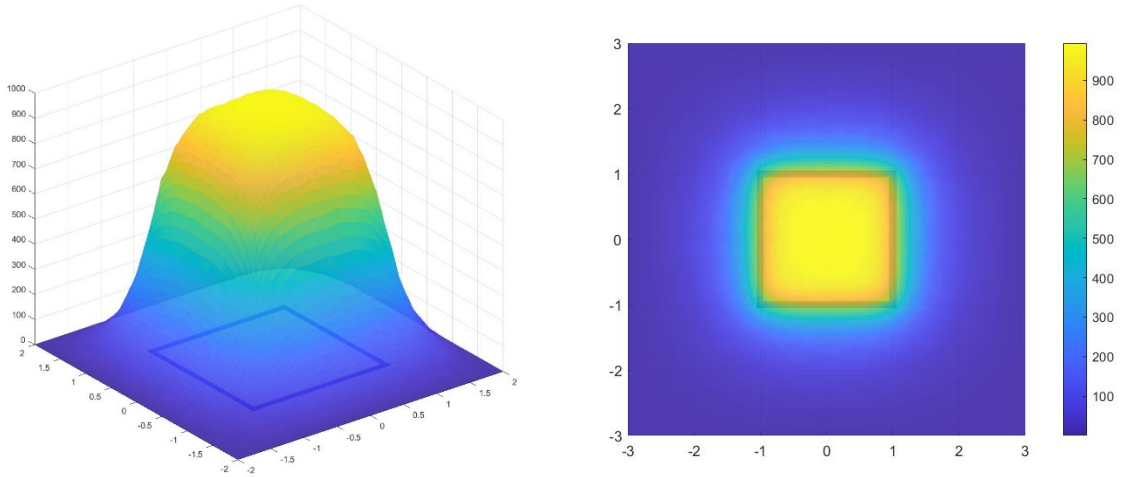

Figure 2-14 EF plots of the exposure bench: horizontal cut plane in the middle

To determine the homogeneity of the generated electric field, the error rate was introduced as an indicator, compared to the theoretical EF 1 kV/m.

$$Error\ rate = \frac{|E_{simu} - E_{theo}|}{E_{theo}} \times 100\% \qquad [8]$$

The horizontal middle line was investigated using MATLAB for error rate calculations. The region with an error rate less than 1% is about 60% at the center of the entire plot (*Figure 2-15*). Thus, the center area that takes 60% surface of the plate has good performance for generating homogeneous EF for the study, which is largely sufficient given the dimensions of the phantom. The finding validated the design of this set-up in terms of concept, size, and material. The phantoms could be placed in the center of this area, exposed to high-intensity homogeneous EFs. This set-up was fabricated and installed in a secure room in the laboratory for experimental measurements.

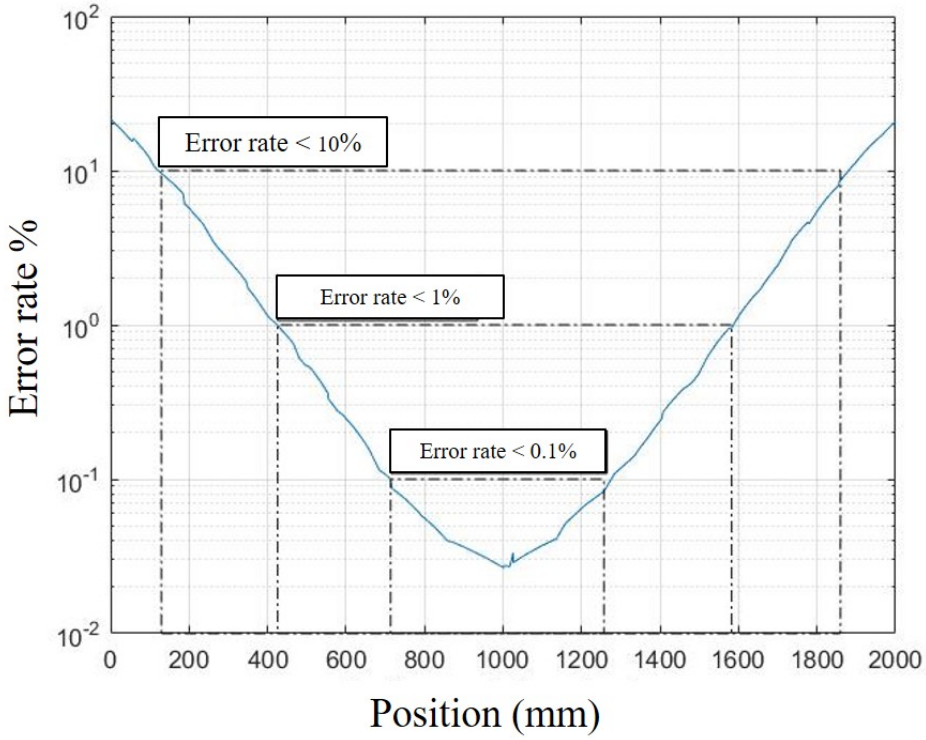

Figure 2-15 Error rate of the generated EF on the horizontal central line

V. Voltage injection system

The controlled EF exposure system provides a non-risk approach to the *in vitro* test of the susceptibility of cardiac implants under high-intensity electric fields. High voltages are applied using the exposure set-up to generate high-intensity electric fields, so it requires strict experimental environment and security protections. Electrical safety is ensured by a device which cuts off the source if a person passes through the door. For the purpose of facilitating the *in vitro* test, basic procedure for device *in vitro* testing was proposed in the EN 50527. The whole set-up shall be easy to fabricate, simply to apply, and movable in case of tests in the real employee's occupational environment. We proposed in this study a voltage injection system to

conduct *in vitro* tests of AIMD susceptibility to electric fields. Two shapes of systems were investigated.

1. Tank-shaped *in vitro* phantom

A tank-shaped *in vitro* phantom was used for the investigation of the AIMD susceptibility of cardiac implants under magnetic field exposures [63]. In the same way, we used a phantom (0.52 m×0.32 m×0.21 m) fabricated in PVC with cubic shape and filled with a saline solution of 0.2 S/m which represents the electrical conductivity of human tissue (*Figure 2-16*). Two plate electrodes made of aluminum (σ: 3.56×10^7 S/m) were placed on the sides in opposite directions. A voltage was injected on one of the electrodes with the other one grounded to generate uniformed EF between the two electrodes in the solution.

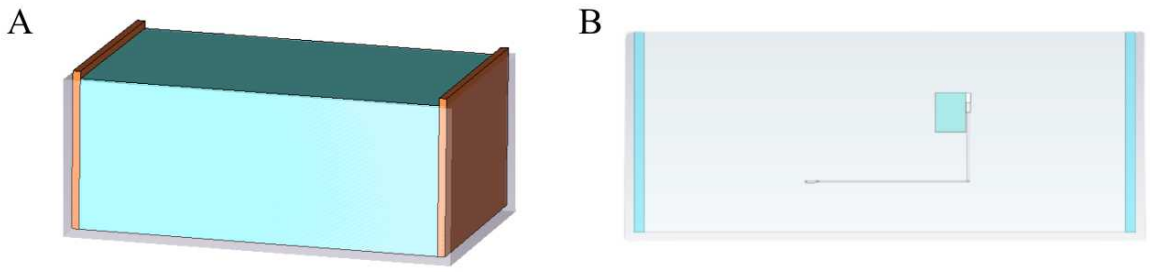

Figure 2-16 Voltage injection system: A) Tank-shaped in vitro phantom B) Tank-shaped in vitro phantom with an implant

The generated EF gave rise to an induced voltage on the cardiac implant placed in the phantom. Different levels of voltage injection were explored on the contact-voltage system. A voltage injection of 1.49 mV allows an induced voltage on the cardiac implant same to the voltage found in the controlled exposure system for unipolar sensing mode (421 µV); 2.4 mV for bipolar sensing mode (62 µV) (*Figure 2-17*).

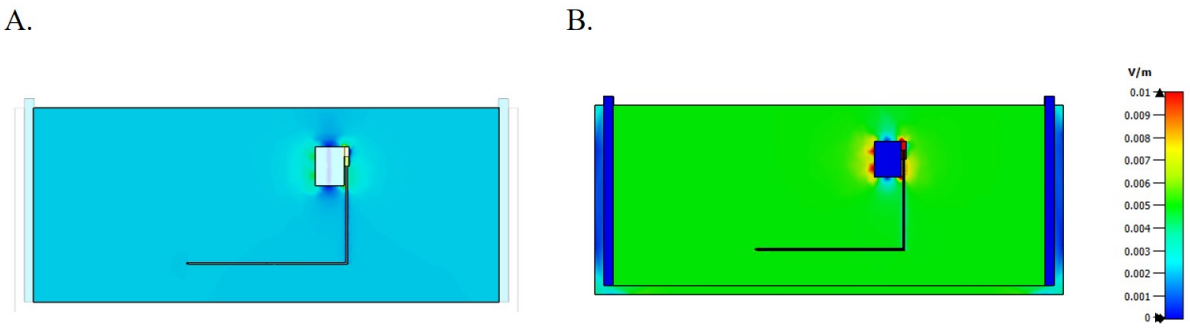

Figure 2-17 Voltage injection system with a voltage injection 1.49 mV (Left); Voltage injection system with a voltage injection 2.4 mV (Right)

In this tank-shaped phantom, the bipolar sensing probe is placed in an electric field of 4 mV/m which corresponds to the case in the controlled EF exposure system. However, for a unipolar probe of a cardiac implant, the sensing path from the electrode to the impulse generator

determines the induced voltage. Induced EF is greatly dependent on the complexity of the electrical properties of the human body. Even if we are able to obtain the relation between this set-up and the standard system, a set-up of the voltage injection system that reproduce the implantation conditions is required. Thus, the funnel-shaped *in vitro* phantom was reintroduced to the voltage injection system.

2. Funnel-shaped *in vitro* phantom

In view of the complexity of internal induced EF where the cardiac implants are usually installed in the human body, the funnel-shaped *in vitro* phantom was used instead of the tank-shaped phantom. In the voltage injection system, the phantom respects the same dimensions that were applied in the controlled EF exposure system, filled with the solution with the same electrical conductivity 0.2 S/m. The base of the phantom is grounded as well. Instead of exposing the phantom to the electric field, a piece of metal grid is placed on the top of the phantom, in contact with the solution. Voltages are injected to this grid to generate induced EF in the phantom between the grid and the grounded base (*Figure 2-18*). The level of the induced EF in the phantom can be managed by adjusting the level of voltage injection. Considering the practicability in the experimental set-up, the distance between the top of the phantom and the surface of the solution $D_{liquid-to-top}$ was fixed at 10 mm to stably support the metal grid while having enough space for implantation.

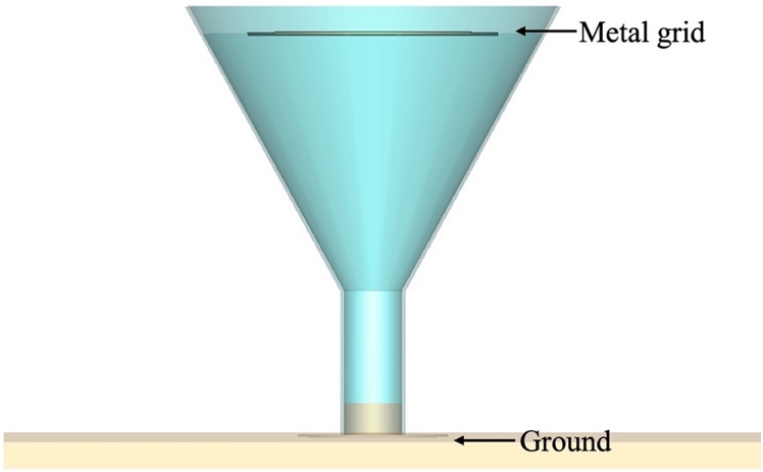

Figure 2-18 Voltage injection system

The EF induction in the voltage injection system was investigated with CST EM®. The EF was induced constantly in the lower part (cylinder part) of the phantom and gradually decreasing upwards in the upper part (*Figure 2-19*). It is found that a voltage injection of 0.52 mV reproduces an induced EF of 4 mV/m in the lower part (cylinder part) of the phantom, as the phantom exposed to an external EF of 1 kV/m in the controlled EF exposure system. The voltage injection system reproduces the EF induction as well in the heart where the probe tip is placed. In addition, the EF plots of the phantom in the voltage injection system with 0.52 mV of injection and in the controlled EF exposure system with 1 kV/m of exposure are nearly the same (*Figure 2-20*). Slight differences in the upper part of the phantom may be caused by the different polarization due to different exposure methods. Thus, the voltage injection system

represents another equivalent system to the virtual human body (standard system). This finding will be validated in the experimental measurements.

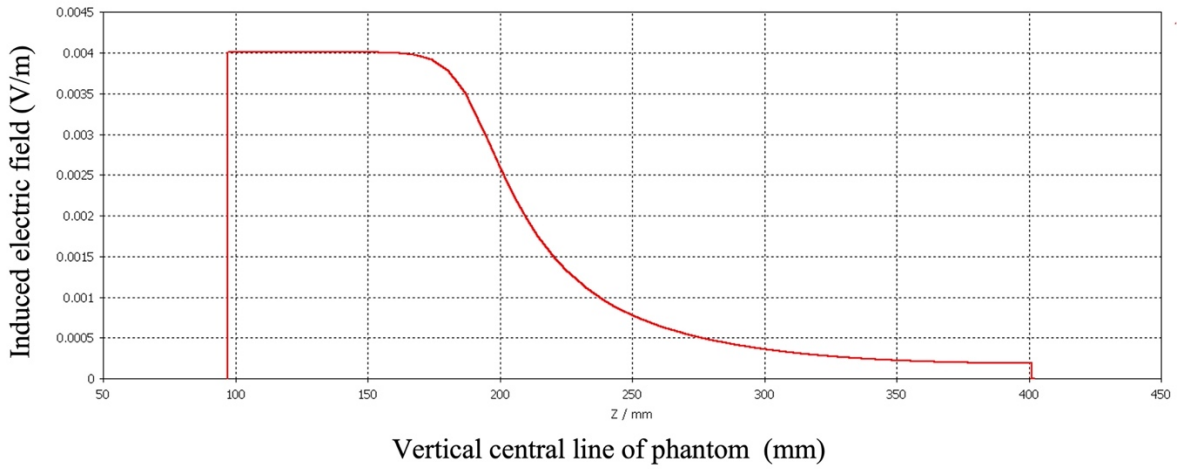

Figure 2-19 Voltage injection system with a voltage injection of 0.52 mV: Induced electric field in the central vertical line of the phantom

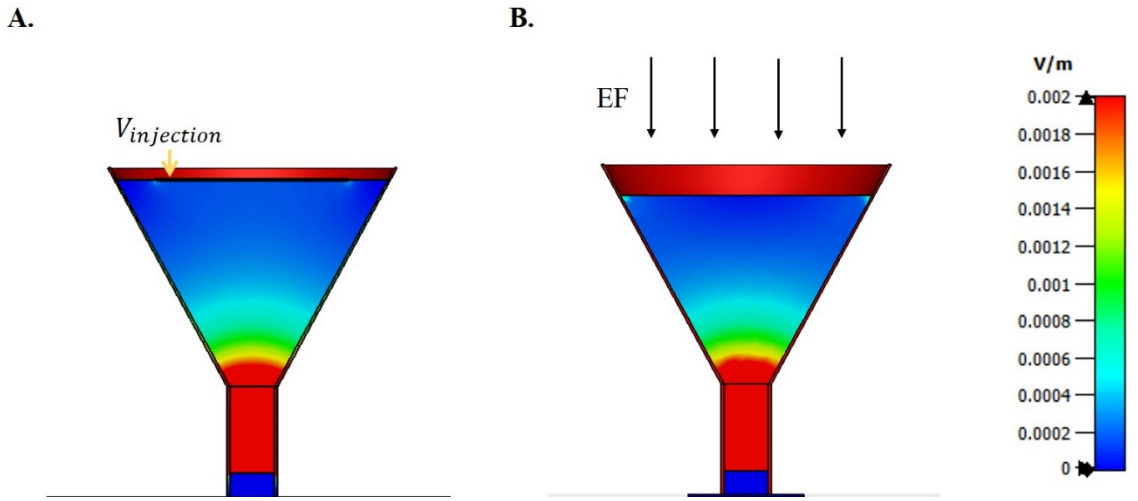

Figure 2-20 Induced electric field in the phantom: A) 0.52 mV injection to the metal grid in the voltage injection system $D_{liquid\text{-}to\text{-}top}$=10 mm; B)1 kV/m electric field external exposure in the controlled EF exposure system $D_{liquid\text{-}to\text{-}top}$=30 mm

3. *In vitro* phantom with cardiac implant

The model of a cardiac implant with the same dimensions and configurations as in the controlled EF exposure system was installed in the voltage injection system (*Figure 2-21*). The sensing paths were set:

- Unipolar sensing path: 220 mm between the housing and the lead tip;
- Bipolar sensing path: 12 mm between the ring and tip at the end of the lead.

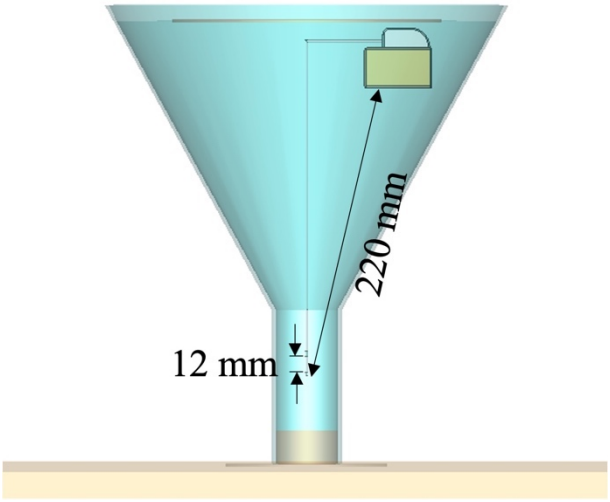

Figure 2-21 Voltage injection system with a PM model

With 0.52 mV of voltage injected to the metal grid, 347 µV was induced on the input of the cardiac implant for unipolar sensing mode; 61 µV was induced for bipolar sensing mode. The induced voltage found using the injection system stays at the same level as the values found in the controlled EF exposure system for bipolar sensing mode (62 µV). An injected voltage of 1 mV was investigated to obtain normalized induced voltage. With 1 mV of voltage injected to the metal grid, 668 µV were induced on the input of the cardiac implant for unipolar sensing mode; 117 µV were induced for bipolar sensing mode. The normalized values were used to contribute to the determination of the equivalence factors.

VI. Numerical validation of the risk assessment procedure

The objective of the numerical study is to build a risk assessment procedure for cardiac implants under occupational electric field at extremely low frequency (50 Hz). The establishment of the risk assessment procedure is based on the association of the three systems introduced in the previous parts of this chapter: virtual human body, controlled EF exposure system, and voltage injection system. We define the controlled EF exposure system as the *Equivalent system A* and voltage injection system as the *Equivalent system B*. Knowing the induced voltage on the cardiac implant under same exposure conditions in the ANSOFT virtual human body $U_{standard}$, in the controlled EF exposure system $U_{equivalent\ A}$, *Equation [5]* was applied to acquire the equivalence factors F_A. *Table 2-5* summarize the induced voltages on the cardiac implant found in the controlled EF exposure system (equivalent system A) systems and give the corresponding equivalence factors.

Table 2-5 Induced voltages on the cardiac implant found in the controlled EF exposure system (equivalent system A) and the corresponding equivalence factors

Induced voltage	Standard system	Equivalent system A	
	Virtual human body	Controlled EF exposure system	Equivalence Factor F_A
Unit	μV	μV	/
Unipolar	183	421	2.3
Bipolar	22	62	2.82

The equivalence factor describes the ability to substitute standard systems while retaining important characteristics. According to *Equation [6]*, a standard exposure $E_{standard}$ can be reproduced by exposure $E_{equivalent\ A}$ in the controlled EF exposure system by applying the equivalence factor. In the meantime, for 1 mV voltage injection in voltage injection system, an induced voltage of 668 μV was found in unipolar sensing mode and 117 μV in bipolar sensing mode.

On the basis of the results found in the simulation, the association of the three systems was numerically validated to build up the risk assessment procedure for the cardiac implants under EF exposures. To perform a risk assessment on the case that the patient with a cardiac implant exposed to an EF of 10 kV/m, it requires:

- An EF of 4.35 kV/m in the controlled EF exposure system for unipolar sensing mode;
- An EF of 3.55 kV/m in the controlled EF exposure system for bipolar sensing mode;
- An injection of 2.74 mV in the voltage injection system for unipolar sensing mode;
- An injection of 1.88 mV in the voltage injection system for bipolar sensing mode.

By applying the association of the three systems, same effects can be reproduced for a certain exposure level in the equivalent systems to investigate the susceptibility of the cardiac implant device.

VII. Discussion

The ANSOFT virtual human body was taken as the standard system in this study. The research on the equivalent systems were developed taking the findings on ANSOFT model as reference. The numerical study with the ANSOFT model was confirmed to have coherent findings with the other studies on the virtual human body under electric field exposure. The induced voltage found on the cardiac implant device used for the ANSOFT model was also proved to be in accordance with the previous studies.

Controlled exposure system was introduced as the equivalent system A to the standard system (ANSOFT virtual human body) with an equivalence factor of 2.3 for unipolar sensing mode and 2.82 for bipolar sensing mode. Voltage injection system was introduced as the equivalent system B. The equivalence factors were determined by the induced voltage value precisely

found on the input of the cardiac implants. Although the ANSOFT model represents the human body in real case, the equivalent systems with such configurations can reproduce the implantation and induction only for the ANSOFT model. If a different human body model was taken as the standard system, the equivalence factor will change accordingly, along with adjustments to the configuration. Thus, the equivalent system set-ups and the equivalence factors introduced in previous are applicable for the ANSOFT virtual human body. However, the concept of this approach applies to other numerical models as long as the induced voltage on the input of the cardiac implant can be determined. With some modifications to the configurations (e.g., $D_{liquid\text{-}to\text{-}top}$ of the experimental phantom), the controlled EF exposure system and the voltage injection system are able to serve other numerical studies for the establishment of *in vitro* experiments.

In the investigation of the voltage injection system, an injected voltage of 0.52 mV reproduces an induced electric field of 4 mV/m in the lower part of the phantom that represents the EF induction in the human heart for 1 kV/m EF exposure. In this case, an induced voltage of 347 µV for unipolar sensing mode and 61 µV for bipolar sensing mode were found which are fairly close to those in the controlled EF exposure system: 421 µV for unipolar sensing mode and 62 µV for bipolar sensing mode. Slight difference can be observed compared to the controlled EF exposure system for unipolar sensing mode. Considering the level of induced voltage depends on the sensing path between the housing and the extremity of the pacing lead, which crosses both parts of the phantom. We assumed that the difference may be caused by different mesh build-up; different polarizations in the upper part of the phantom due to different methods of exposure.

In addition, an equivalence relation can be built up between the controlled EF exposure system and the voltage injection system. To reproduce an electric field exposure of 1 kV/m in the controlled EF exposure system, it requires a voltage of 0.63 mV for unipolar sensing mode and 0.53 mV for bipolar sensing mode to be delivered to the voltage injection system.

VIII. Conclusion

In this chapter, a risk assessment process for cardiac implants under occupational electric field exposure at low frequency was proposed. The investigation was developed at high EF level at extremely low frequency (50 Hz). This risk assessment process is based on the establishment of the standard system and its equivalent systems. The conception was derived from the relation between the external EF exposure and the internal induced EF in a conductive object. A virtual human body was taken as the standard system which provided evidence of real-case study. Two equivalent systems were proposed for *in vitro* study, in which a funnel-shaped *in vitro* phantom was introduced to reproduce the electrical characteristics of the implantation area.

The three systems:

- Virtual human body (ANSOFT model);

- Controlled EF exposure system;
- Voltage injection systems

were all studied under exposures (or voltage injection) and implanted with a PM model to investigate the induced voltages on it. The controlled EF exposure system was proposed as an approach which could be conducted in the laboratory; the voltage injection system was proposed as an approach which allows simple and movable testing even in the real workplace.

The association of the three systems was introduced and validated by the numerical findings in the chapter. The values of the induced voltages and the equivalence factors will be taken as references for the experimental measurements. The numerical validation provides the evidence for transitioning from the *in vivo* study to the *in vitro* experiments and for the further experimental validation.

3

Design and implementation of experimental validation

I. Introduction

In vitro tests facilitate the estimation fairly close to the real situation without risks and protocol or ethical restrictions associated with *in vivo* studies. The steerability ensures that the tests are archivable, repeatable, and multiplied. In order to investigate electromagnetic interference on AIMDs in the human body, an *in vitro* experiment based on the numerical findings in chapter 2 is presented.

In this chapter, detailed description of the exposure set-ups and configurations for the experimental approach to conduct the measurement of the induced voltages on the input of the cardiac implant devices are presented. In the controlled EF exposure, the assembly of the devices allows high-voltage delivery to the experimental bench, consequently high-intensity electric field exposures. For safety control and monitor of the exposure set up are placed in a pilot room. All the components of the controlled EF exposure system are presented and justified. The voltage injection system is presented in detail as well on its experimental set-up and the phantom set-up in order to perform the *in vitro* tests.

Due to the small induced voltage at the input of the cardiac implant, a specific measuring system was designed to detect, amplify, and transmit the measured signal. The measuring system targets a real cardiac implant as the device under test (DUT). Two configurations were carried out to conduct tests for both unipolar and bipolar sensing mode. The optimizations were made to improve the performance of the measurement system in the aspect of isolation, transmission, and installation.

In addition, the measurement results in the controlled EF exposure system and in the voltage injection system are synthesized and compared with the simulation results. The equivalence between the two systems is shown based on the experimental measurements.

II. Design and implementation of controlled EF exposure system

The conception of the controlled EF exposure system was introduced in chapter 2 as an equivalent system A. *In vitro* tests require high-intensity electric fields to generate the equivalent exposures on the *in vitro* phantom. Besides the experimental bench analyzed in the numerical study, the controlled EF exposure system was designed more completely in practice on managing and monitoring the electric field, the transmission of the signal, and the generation of the electric field.

1. Experimental bench

The experimental bench is the equipment that generates the electric fields and contains the *in vitro* phantom. The homogeneous electric fields is produced by two conductive plates (2000 mm × 2000 mm) in Dibond® sheet of 3.2 mm thickness placed in parallel. The two plates are 750 mm apart with 4 PVC supports in between (*Figure 3-1*). The size and material of the

experimental bench were designed in the numerical approach. The upper plate was supplied with a high voltage; the lower plate was grounded. A metal rounded base was built in the center of the lower plate to connect the ground of the *in vitro* phantom. According to the simulation of the experimental bench in the software CST EM®, 60% of the electric field from the center remains at the desired level with 1% error rate, equivalent to a 1200 mm × 1200 mm square space in the center. The widest edge of the *in vitro* phantom is a circle with a diameter of 300 mm. Thus, with this experimental bench, the *in vitro* phantom can be placed in the qualified homogeneous electric field.

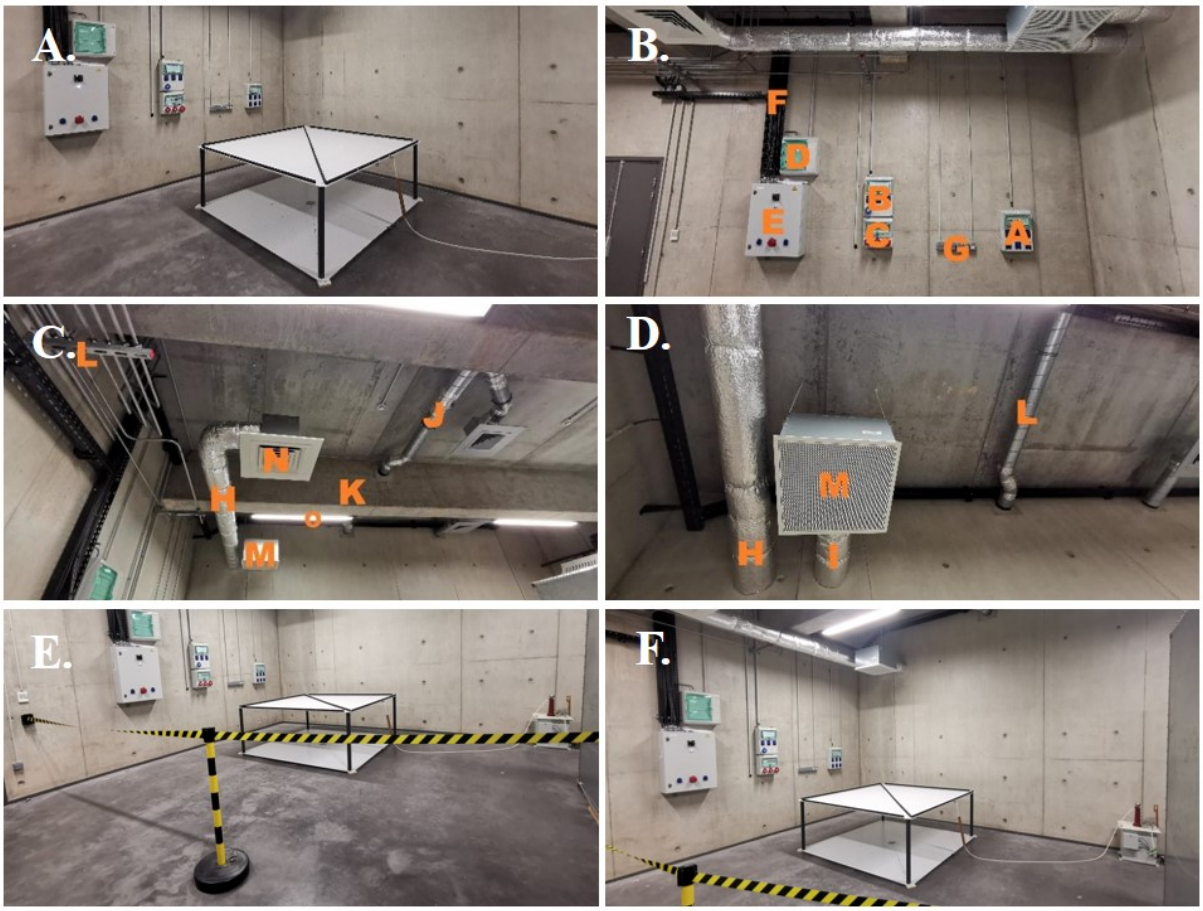

Figure 3-1 A) Experimental bench (conductive plates); B) Devices on the wall (switchgear and distribution box); C) Devices on the ceiling (ventilating ducts); D) Devices on the ceiling; E) Security cordon (2000 mm distant from the conductive plates) F) General view of experimental area

2. Experimental area

The experimental set-up was built up in the electromagnetic compatibility experimental room at the Jean Lamour Institute, Nancy (France). Due to the high level of the electric field reached in this study, it is important to guarantee security during exposures for people and for the installments in the room (*Figure 3-1 B, C, D*). A security cordon was set up to separate the experimental area from people (*Figure 3-1 E*). The experimental bench and the installments inside the experimental room were modeled in the simulation with two nearest concrete walls

(*Figure 3-2*) to investigate the impact on the electrical devices and on the performance of the EF exposure. All the facilities on the wall and the ceiling were modeled in metallic material to observe the worst-scenario case.

According to the finding in the simulation, the electric field generated by the experimental bench remains homogeneous in an ideal level for the exposure tests. The distances between the experimental bench and the walls were 500 mm and 1000 mm to ensure that the generated electric field was barely affected by the metallic devices on the wall. *Figure 3-2 B* and *Figure 3-2 C* shows the electric field plots of the horizontal cut plane in the middle of the experimental bench when generating an electric field of 1 kV/m at 50 Hz. It was found that the electric fields on the wall reach the level of 30% - 60% of the electric field expected in the experimental bench. Thus, for an electric field up to 50 kV/m, the electric fields that the devices on the wall are subjected are around 15-30 kV/m thus remaining without risk for them. The security cordon was placed at 2000 mm away from the experimental bench, ensuring that the maximum exposure outside of the protection area is less than 5 kV/m. The installation of the experimental bench respects the restrictions for occupational electric fields following the Directive 2013/35/EU [7].

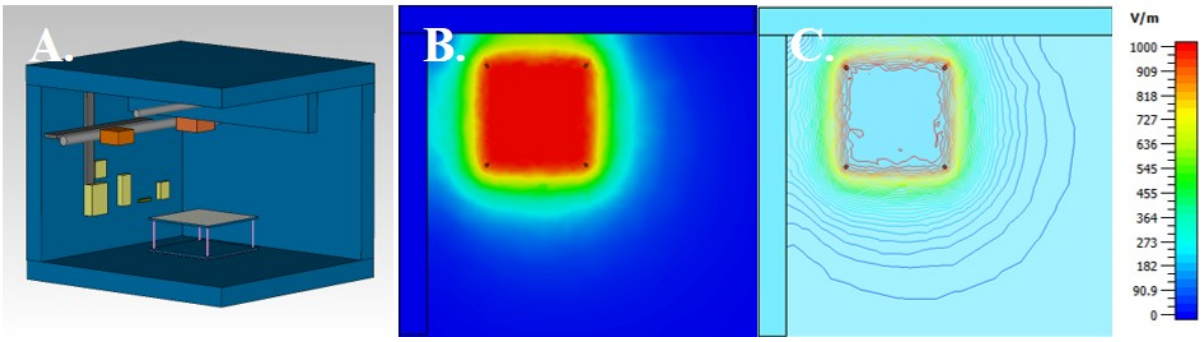

Figure 3-2 Numerical study on experimental room: A) Modeling of experiment area; B) EF plot of the experiment area of horizontal cut plane in the middle of experimental bench (contour); C) EF plot (isoline)

3. Control and supervision

An assembly of electrical devices was built up to deliver a high voltage to the upper plate of the experimental bench up to 80 kV at 50 Hz. For the safety concern, a Faraday cage besides the experimental area was taken as the pilot room for locating the personnel when the source is activated. A signal generator commanding sinusoidal signals at 50 Hz was placed at the control site in the pilot room, where found a power amplifier. The amplified signal is then sent outside of the pilot room to two transformers that allow high voltages up to 80 kV to be applied to the conductive plates. The devices used in the experimental setup are illustrated in *Table 3-1* as well as their specifications.

The high-voltage probe for measuring the voltage at the output of the high-voltage transformer is limited to 28 kV rms so that the voltage applied to the exposure system cannot be verified above this limit. A 3D H/E field meter (Maschek ESM-100) was used to measure the generated field while the room humidity was recorded and maintained at 30–55% during the experiments,

as was temperature, at 15–20 °C, in order to maintain the experimental conditions. The level of the generated electric fields was adjusted by the signal generator in the pilot room. The measured electric fields were recorded corresponding to the input of the generator and the output of the amplifier, given in *Annex I*. Thus, the electric field exposure levels can be determined by the level applied by the signal generator. They are also verified by measuring the output of the power amplifier during the tests on the measuring system and on the cardiac implant devices. An oscilloscope was placed in the pilot room to verify the delivered voltage level from power amplifier or from the high-voltage probe, and to check the waveforms. Fuses are installed between the output of the power amplifier and the input of the middle transformer to limit the current to 10 A, and between the two transformers to limit the current to 1 A. A copper claw was fixed on the upper conductive plate to ensure the receiving of high voltage from cable and two resistors of 1 MΩ were mounted between the claw and the cable to ensure a current limitation in case of breakdown (See *Figure 3-3*).

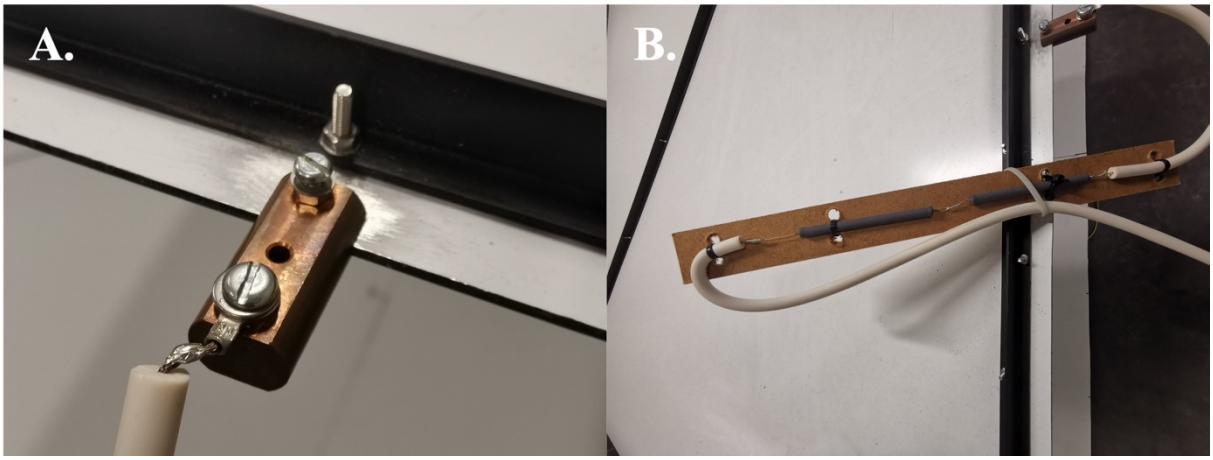

Figure 3-3 A) Copper claw; B) Current limiting resistor (black stripes in parallel) and high-voltage cables (white cables)

Table 3-1 Electrical device specifications

Appliance	Specification
Signal generator	▪ Function/arbitrary waveform generator ▪ Brand: Agilent ▪ Model: 33220A ▪ Max frequency: 20MHz ▪ Arbitrary frequency range: 1 μHz to 6 MHz ▪ Sample rate: 50 Msample/s ▪ Generate sinusoidal signals at 50 Hz ▪ Connected to power amplifier
Power amplifier	▪ Output voltage: 0-24 V ▪ Power: 500 VA ▪ Output voltage: 24 Vac ▪ Bandwidth: 40 Hz – 100 kHz ▪ Amplify the output signal of signal generator

	▪ Connected to middle transformer
Oscilloscope	▪ Digital oscilloscope ▪ Brand: Rohde & Schwarz ▪ Model: RTB2002 ▪ Sample rate: 2.5 Gsample/s ▪ Verify the output of power amplifier ▪ Verify the measurement of high voltage probe
Middle transformer	▪ Brand: Block ▪ Model: ST 250/23/24 ▪ Rated frequency: 50-60 Hz ▪ Rated output voltage: 24 Vac ▪ Rated power: 250 VA ▪ Transform the output of power amplifier (24 V/220 V) ▪ Deliver middle-level voltage to the high-voltage transformer
High voltage transformer	▪ Brand: Transfo Industrie ▪ Model: TMON-60-20 ▪ Rated frequency: 50-60 Hz ▪ Maximum output voltage: 60 kV ▪ Transform the output of middle transformer (209 V/60 kV) ▪ Deliver high voltage to the conductive plates
High voltage probe	▪ Brand: Testec ▪ Model: TT-HVP40 ▪ Input maximum voltage: (0 to 300Hz) 28 kVrms ▪ Input resistance: 1000 MΩ (±1%) ▪ Division: 1000:1 ▪ Measure the output of high voltage transformer ▪ Transmit the measurements by a coaxial cable to the pilot room
Field meter	▪ 3D H/E field meter ▪ Brand: Maschek ▪ Model: ESM-100 ▪ Range: 1 nT- 20 mT / 0.1 Vm – 100 kV/m ▪ Resolution: 1 nT / 100 mV/m ▪ Frequency range: 5 Hz – 400 kHz (-3 dB Limit) ▪ Accuracy: ± 5 %

4. *In vitro* phantom set up

The *in vitro* phantom was fabricated in glass with the thickness of 3.3 mm and placed in the center of the lower plate. The dimensions of the experimental phantom were the same as those of the numerical study: a funnel-shaped recipient with a total height of 350 mm, an upper diameter of 300 mm, a cone angle of 60° finished by a cylinder (lower part) of 46 mm diameter in which we place the end of the cardiac implant probe to be tested.

Gelatin filler for the phantom with dielectric properties equivalent to those of human tissue at the relevant frequencies was considered [63], which was used in the magnetic field studies on this subject in previous [64]. The advantage of gelatin is that it retains the positions of the DUT and its lead. Given the large number of tests expected, liquid solution provides more manageability and convenience. Saline water possessing conductivity of 0.19-0.21 S/m was filled inside, which is in accordance with the studies in IEC 62226 [65]. The conductivity of the solution was always checked using a conductivity meter, HI 99300 (accuracy: 2% full scale), before tests. The solution requires blending and periodic verification of the conductivity. In keeping with the observation of the simulation, the solution-level respects $D_{liquid-to-top} = 30\ mm$ to reproduce the electrical properties of the implantation area in the human body. Plexiglass support allowed the DUT to be positioned reproducibly in the recipient. The end of the probe was guided towards the lower part (cylindrical part) of the phantom by a wooden retainer, parallel to the direction of the EF, in order to produce the worst-case scenario, and in the center of the cylinder part. The DUTs were placed in a relatively identical configuration during tests. To ensure a perfect grounding of the experimental phantom, its metal bottom was connected to the lower grounded plate by 2 metallic O-rings (*Figure 3-4*).

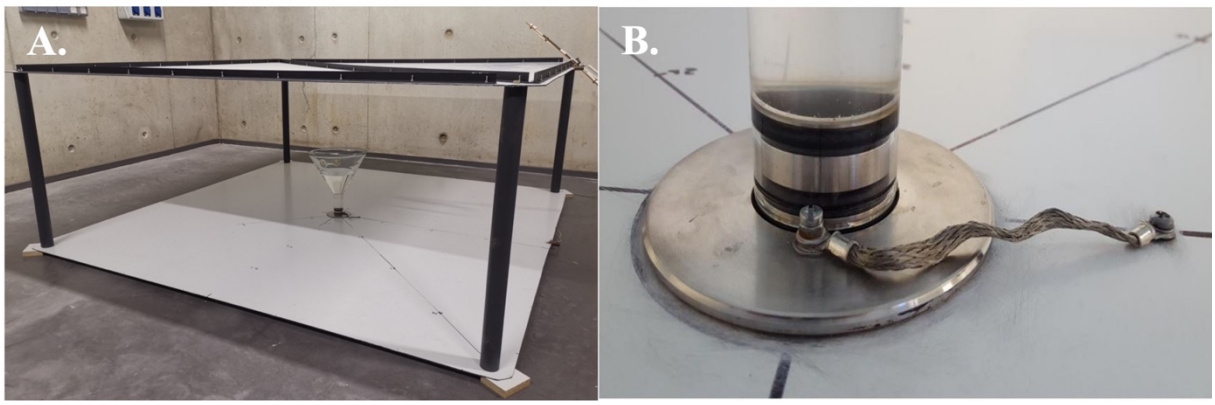

Figure 3-4 Experimental phantom in controlled EF exposure system: A) In vitro phantom and experimental bench; B) Grounding configuration

5. Experimental set up

The assembly of the experimental setup is shown in *Figure 3-5* for appliances in the pilot room and in the experimental area.

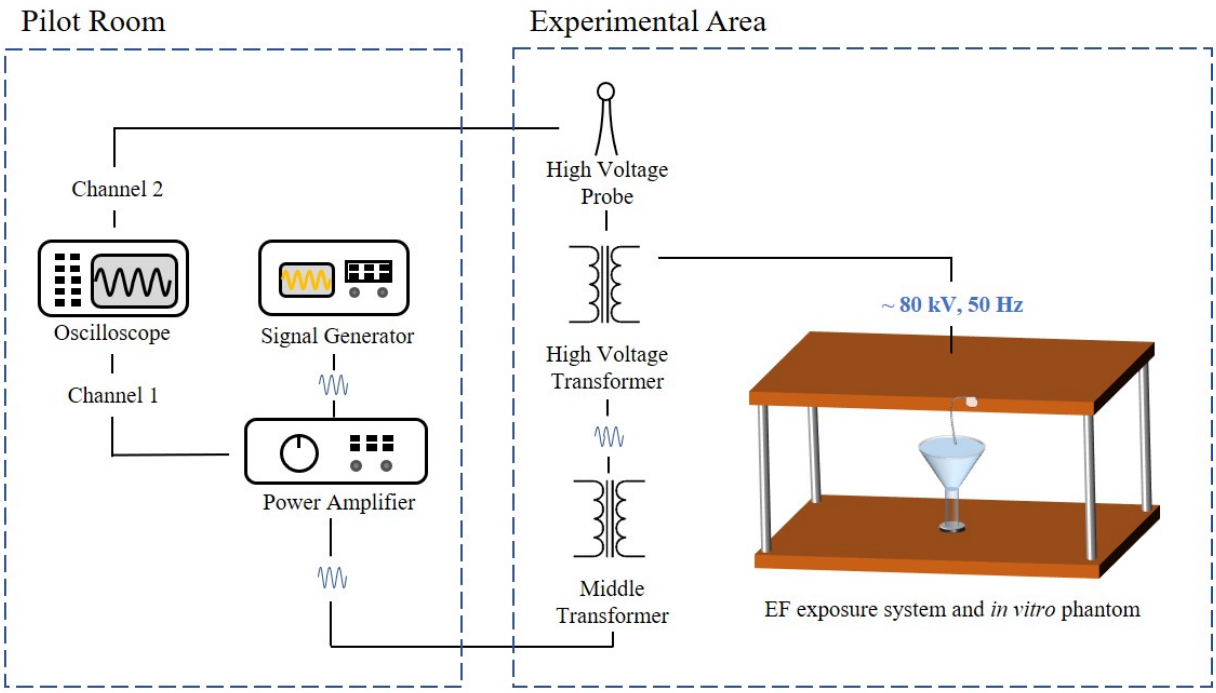

Figure 3-5 Experimental set-up of controlled EF exposure system

III. Design and implementation of voltage injection system

The conception of voltage injection system was proposed in *Chapter 2* as an equivalent system B. This system imitates the exposure in the controlled EF exposure system and reproduce the induction effects on the cardiac implant, with simple, easy, feasible, efficient, and risk-free configuration.

1. *In vitro* phantom set-up

The phantom used with the controlled EF exposure system was used as well as the voltage injection system. A piece of metal grid was fabricated with a diameter of 280 mm and placed on the top of the phantom solution. A banana socket at the top allows plugin of the injection cable (*Figure 3-6*). Voltages were injected to this grid from a signal generator to produce electric field induction in the phantom. The phantom base was connected to the common ground of the set-up. It has been proved (*Chapter 2*) that there is a constant induced electric field in the lower part of phantom and gradually varied induced electric field in the upper part. The distance between the surface of the solution and the top of the phantom recipient $D_{liquid-to-top}$ was fixed at 10 mm to ensure accordance with the numerical study of *Chapter 2*. To be mentioned, $D_{liquid-to-top}$ has great impact on the level of induced electric field in the phantom. For the voltage injection system, the equivalence factor differs for different values of $D_{liquid-to-top}$.

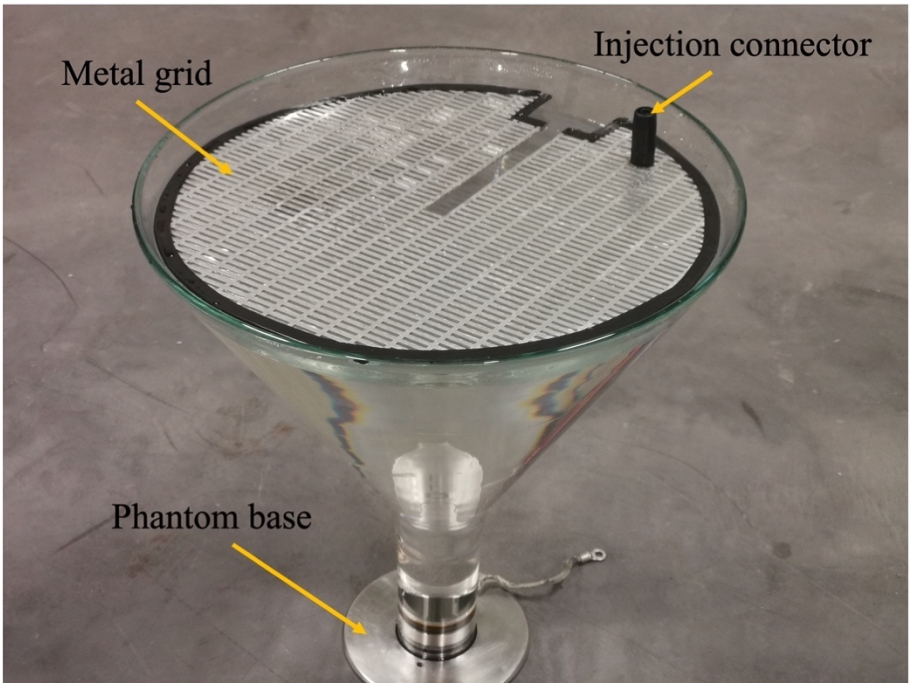

Figure 3-6 Experimental phantom set-up in the voltage injection system

2. Experimental set-up

According to the numerical analysis of cardiac implant exposed in the voltage injection system, an induced voltage of 668 μV on the probe is expected for 1 mV of injection for unipolar sensing mode and 117 μV for bipolar sensing mode. To reproduce the exposure of 1 kV/m in the controlled EF exposure system, it requires 0.63 mV of injection for unipolar sensing mode and 0.53 mV of injection for bipolar sensing mode. The levels of voltage injection are quite low compared to the output of a standard signal generator. A digital lock-in amplifier HF2IS from Zurich Instruments (*Figure 3-7*) was used to generate very small signals to the voltage injection system for induced voltage measurement and AIMD investigation. It possesses 2 signal generators with output level down to decade microvolts. It is equipped with the Zurich Instruments control platform LabOne®, which provides a web-based user interface featuring a spectrum analyzer, a sweeper and a basic oscilloscope, among others. LabOne® enables instrument control, data capture, data analysis, and data storage, which comes with an outstanding toolset for time- and frequency-domain analysis as well as sophisticated support to set up control loops, perform noise measurements, and interpret measurement data. Except serving as the signal generator that sends out signals with small amplitude, the injected voltage was also verified by HF2IS via its input portal and spectrum analyzer in LabOne®. As impedance of the system is close to the 50 Ω output of signal generator, it is necessary to measure the true voltage between grid and base. The levels of injected voltage were recorded with the values measured by HF2IS to acquire accuracy (Annex IV).

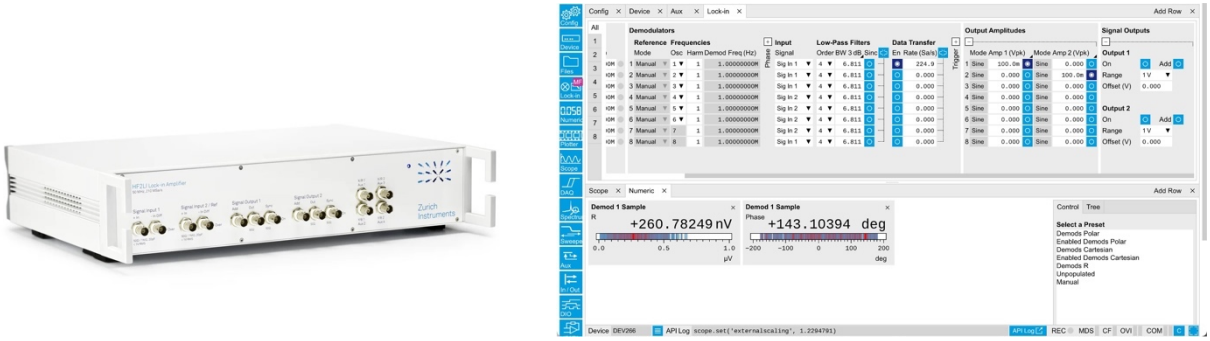

Figure 3-7 Digital lock-in amplifier HF2IS from Zurich Instruments; Interface of the instrument control platform LabOne®

For the purpose of having fixed position of the DUT, the plexiglass support and the wooden probe retainer were used in the voltage injection system as well to obtain identical configuration of the DUT with the controlled EF exposure system. The common ground was connected to the phantom base. The assembly of the experimental setup is shown in *Figure 3-8*.

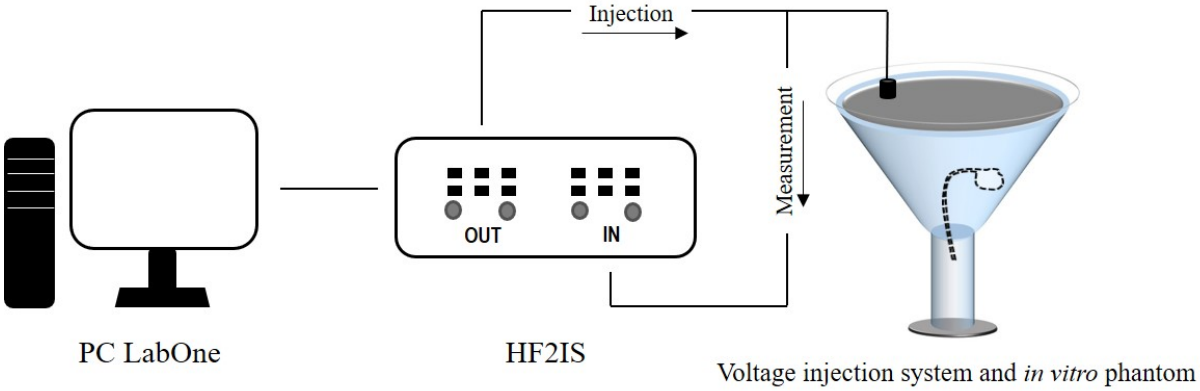

Figure 3-8 Experimental set-up of voltage injection system

IV. Design and implementation of measuring system

1. General design

For a cardiac implantable device wearer exposed to an electric field (EF) or a magnetic field (MF), internal EFs will be induced in the body tissues as well as on the device input. This may cause dysfunction or abnormal treatments by electromagnetic interference. For the purpose of assessing the immunity of cardiac implants to the electromagnetic interference, a measuring system for the evaluation of the induced voltage on the input of cardiac implants was required in the study. The electronic measuring system was expected to detect voltages at 50 Hz at microvolt level and to operate under low-frequency high-intensity electric field exposures without interfering the electric field to be measured. To allow measurements inside the exposed phantom solution, the measuring system had to be perfectly waterproof and isolated from the external electric field.

To investigate the interference that cardiac implants may be subjected to in real case, a real pacing lead was used to minimize the influence of the measuring system on the electric field

distribution in the phantom. In addition, a measuring circuit was inserted in a waterproof metal box which should possess the size of a PM/ICD impulse generator to simulate the real implantation. Considering the small scale of the signals to be measured, an amplification is necessary before treating them. For documenting and analyzing the measurements, data transmission was required. A set-up for ECG signal generation was designed and implemented to reproduce the real implantation environment during the tests of cardiac implants. Different types of the ECG signal allow specific cases to be taken into consideration. The general design of the electronic measuring system is given in *Figure 3-9* and detailed in the following parts.

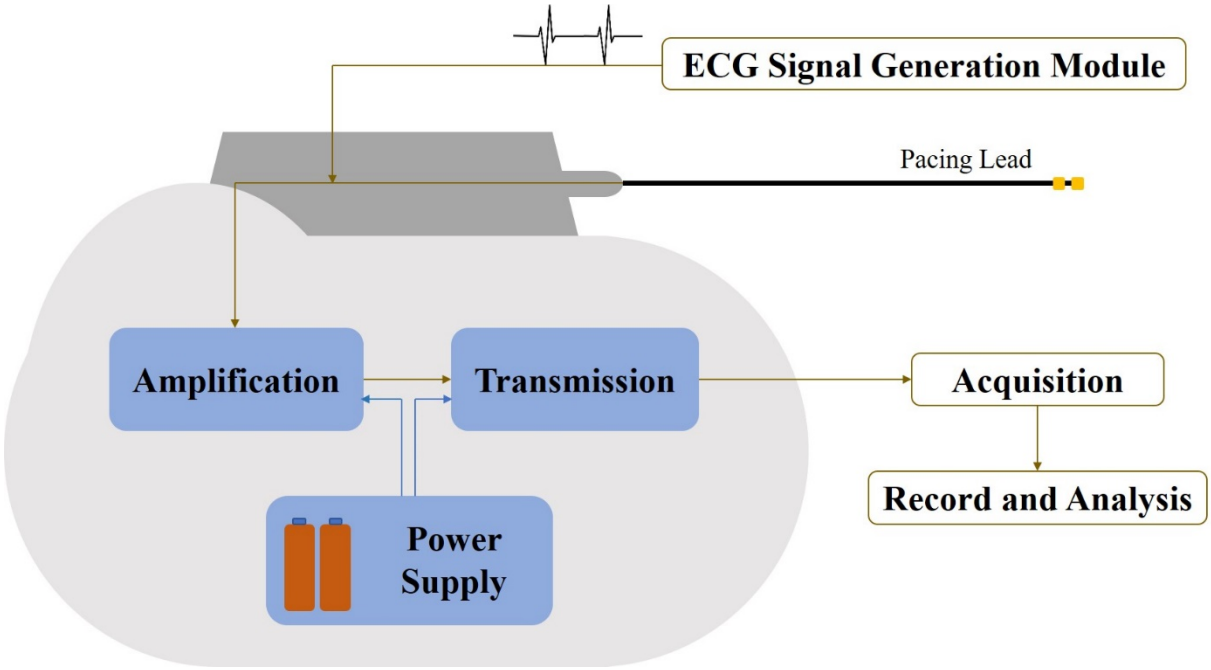

Figure 3-9 General design of measuring system

2. Measuring circuit

When the cardiac implant probe is submitted to an electric field, an induced EF appears at the surface of the probe. Thus, a potential difference can be detected between the two electrodes on the probe in bipolar sensing mode or between the cardiac implant housing and the electrode at the tip of the probe in unipolar sensing mode.

A bipolar pacing lead of standard IS-1 was used as the input of the measuring system to measure the induced voltage that the implanted device is subjected to. Two sensing electrodes are on one extremity of the lead to conduct detection and pacing; two connectors are on the other extremity of the lead to connect to the housing (impulse generator) (*Figure 3.10)*. The positive pair is isolated from the negative pair, except in saline where there are few hundreds of ohms between them. Thus, the induced voltage is determined by the potential difference between the positive pair and the negative pair.

Figure 3-10 Bipolar pacing lead

To conduct such measurements of the induced voltage on cardiac implants, we have designed and implemented three measuring circuits with different configurations.

- Circuit A

In order to receive the signals from the pacing lead, a n-channel junction field-effect transistor (JFET) 2N3819 was selected in the adaptation part of the circuit. According to the tests conducted on the JFET 2N3819, its specifications can be determined as below (*Table 3-2*):

Table 3-2 Specifications of 2N3819

Pinch off voltage	V_p	3	V
Drain current for zero bias	I_{dss}	8	mA
Cut off voltage	$V_{gs}(off)$	-2.2	V

The grid of JFET is influenced by this charge and a voltage was generated. The self-biasing configuration allows us to always have gate-source voltage of -2.2 V $<V_{gs}<$ 0, so the JFET is turned on. Drain current increases as V_{gs} increase which allows us to have V_d as a phase reversed output for a given amplification. This amplification depends on the self-biasing configuration and the load r_L and can be derived by

$$A = -g_m r_L$$

Where g_m is the transconductance and r_L is the load. With this configuration, we obtained an unloaded gain of -1.8 (the phase is reversed). The final gain of the circuit is governed by the loads following impedance matching. One electrode was taken as the input of the circuit and the other was connected to ground (GND) of the circuit to obtain the potential difference between the two electrodes. We have connected GND to the shielding box to avoid floating ground. In other words, a unipolar sensing mode could be performed with this circuit. Overall, circuit A (*Figure 3-11*) is a method to conduct measurements for unipolar sensing mode with a gain of 10.

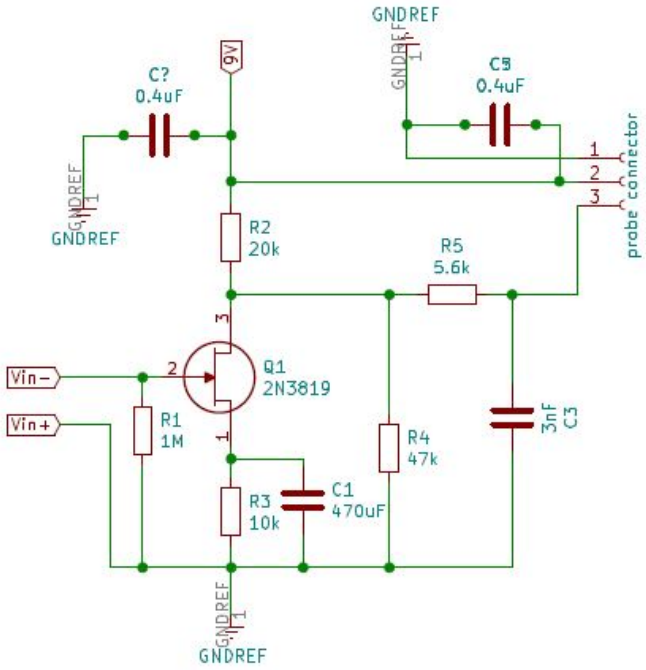

Figure 3-11 Circuit A: a measuring circuit with 2N3819 adaptation part

- Circuit B

A module based on AnalogDevices620 instrumentation amplifier (AD620) was used as circuit B (*Figure 3-12*). This circuit is a low cost, low power consuming, high accuracy amplification module, with two adjustable resistors to respectively adjust the gain of 1.5 to 1000 and the offset, powered from 3.5 to 10V on the VIN pin and adjacent GND pin. This module provides a platform for amplification of small AC or DC signals between 100 µV and 300 mV from analog sensors, strain gauges, and similar devices. Differential inputs on circuit B allow us to have the induced voltage for bipolar sensing mode while the adjustable resistors permit different gains and offsets during the test.

The inputs of AD620 (S+ and S-) have a 1 KΩ series resistor respectively to limit input current to a safe level. The gain is adjusted using a 100 KΩ potentiometer (R6). The output of the AD620 is passed through one of the two LM358 operational amplifiers configured as a unity gain buffer. The output of this buffer is available on the pin labeled VOUT. The input of the other LM358 operational amplifier is a 10 KΩ potentiometer which is placed between two resistors of 1 KΩ in series to tie the power rails between V+ and V-. The output of this LM358 is fed into the V_{ref} pin on the AD620 to adjust the offset. The 7660 voltage converter takes in the V+ voltage and generates a negative voltage for the -Vs pin on the AD620 (V-). This configuration sets the AD620 both positive and negative power rails.

The circuit has better performance with a gain of 50 and an offset around 3 V. First measurements were carried out by circuit B for bipolar sensing mode. However, the settings of gain and offset are not stable on circuit B. Since gain value is proportional to the inverse of adjustable resistors, which was taken as R_g, it is difficult to correctly adjust high gain and obtain

good stability with this circuit. Slight changes can disturb its performance largely. It is suspected that the switched capacitor voltage converter interferes with the measurement during exposure tests. For this reason, we decided to preset constant gains in the further development for unipolar sensing mode and bipolar sensing mode.

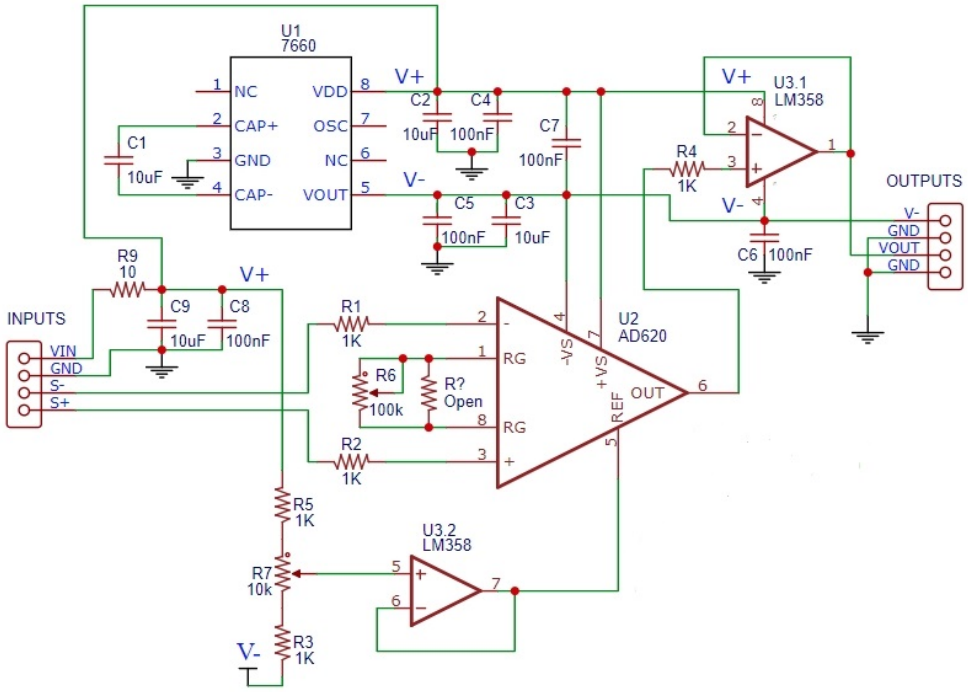

Figure 3-12 Circuit B: AD620 instrumentation amplifier module

- Measuring circuits

After the investigation on the measuring circuits for induced voltage in previous, a measuring circuit was designed based on the circuit B (AD620 module) to be compatible with both unipolar sensing mode and bipolar sensing mode. The instrumentation amplifier AD620 takes charge of amplification of the input induced voltage. To preset the resistor R_g, the gain of amplification can be fixed. The gain of the instrumentation amplifier AD620 is determined by:

$$Gain = \frac{49.4 \times 10^3}{R_g} + 1$$

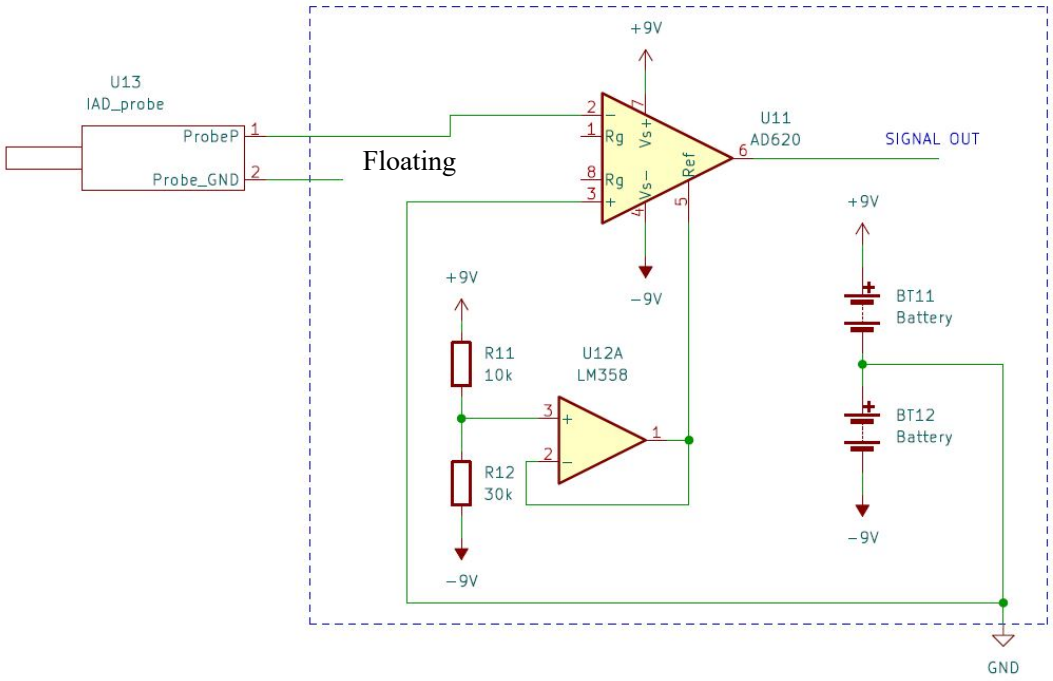

Figure 3-13 Measuring circuit for unipolar sensing mode with gain of 1

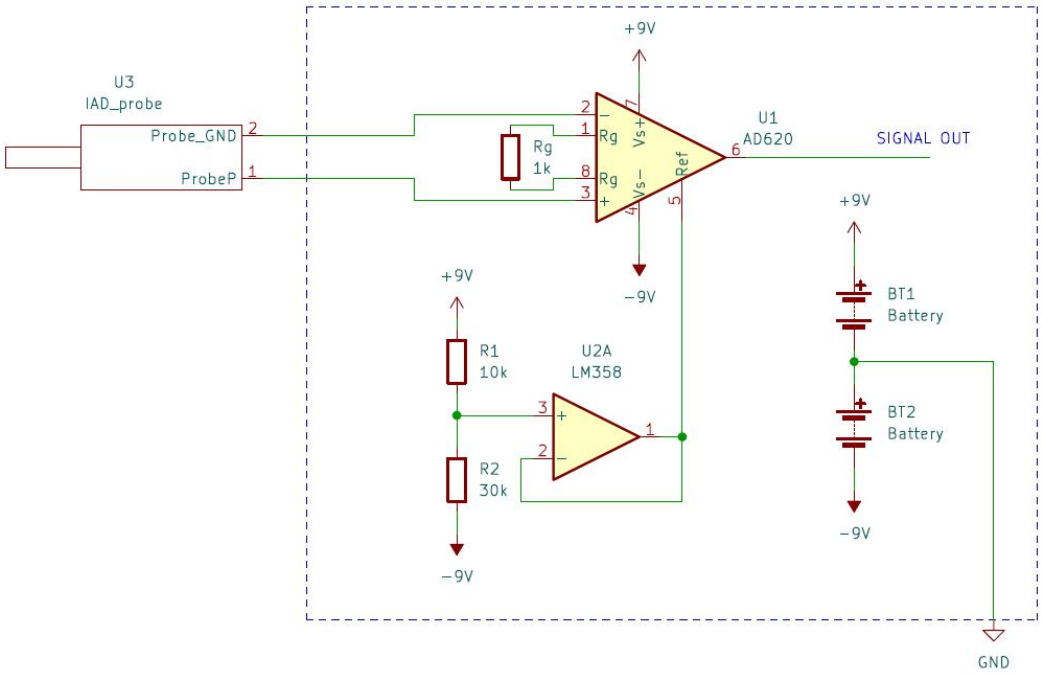

Figure 3-14 Measuring circuit for bipolar sensing mode with gain of 50

For unipolar sensing mode, one of the inputs of pacing lead was disconnected and R_g was removed for obtaining a gain of 1 (*Figure 3-13*). The negative input of the instrumentation amplifier AD620 takes the potential of the metal container which was taken as the reference GND in the circuit and one of the inputs of the pacing lead as its inputs. Thus, this measuring circuit measures the potential difference between the metal container and the electrode at the extremity of the pacing lead.

For bipolar sensing mode, AD620 takes both inputs from the two electrodes of the pacing lead as its inputs (*Figure 3-14*). Thus, the circuit measures the potential difference between the two electrodes at the end of the pacing lead. Considering the induced voltages in bipolar sensing mode are expected to be weak, a resistor of 1070 Ω (± 0.1%) was used as R_g, so the theoretical gain for bipolar measuring circuit is:

$$47.12 < Gain_{Bipolar} < 47.21$$

According to the experimental verification, the gain of the measuring circuit for bipolar sensing mode was confirmed at 47.168. The circuits were supplied by two batteries of 9V to obtain a stable reference GND and avoid possible problems due to switched capacitor voltage converter. Two resistors R1 and R2 built up a voltage divider to fix a voltage reference level at 4.5 V. An operational amplifier was used to set AD620 reference (offset) at 4.5 V. These two circuits were finally used for the experimental measurements. Reasonable gain, stable reference level, and small scale provided better performance than the others. The output of the circuit was then delivered to the transmission module.

3. Transmission and reception

Once the measuring circuit detects the induced voltage and amplified it to an observable level, its output signal is transmitted to an acquisition module for recording and analysis. An optical fiber probe set (Langer A100-1) was applied for optoelectronics transmission. This optical fiber probe possesses good immunity performances under EMF and allows us to observe the measurement results in real time. Two sensors (AS120 and AS100) provide multiple choices of extra gain or precision (*Table 3-3*). Sensor AS100 with a range of 10 V gives us the identical signal output which was used in the tests. The sockets for the sensor AS100 were embedded in the measuring circuits and supplied by the 9 V battery (*Figure 3-15 A*).

Table 3-3 Specifications of optical link Langer sensors AS 120 and AS 100

Model	Measuring Range	Frequency Range	Gain	Offset
AS 120	1V	10 Hz – 2.5 kHz	10	5V
	0.1V	300 Hz – 2.5 kHz	100	
AS 100	50V	10 Hz – 2.5 kHz	0.2	0V
	10V	10 Hz – 2.5 kHz	1	

The optical sensor AS100 was connected to the optical receiver AE100 via optical fiber to conduct the transmission under electromagnetic field exposures without interference. The receiver AE100 was mounted on an oscilloscope to observe the measurements in real time (*Figure 3-15 B*). In order to avoid different reference grounds from devices, the optical receiver AE100 was power supplied by a 12 V battery.

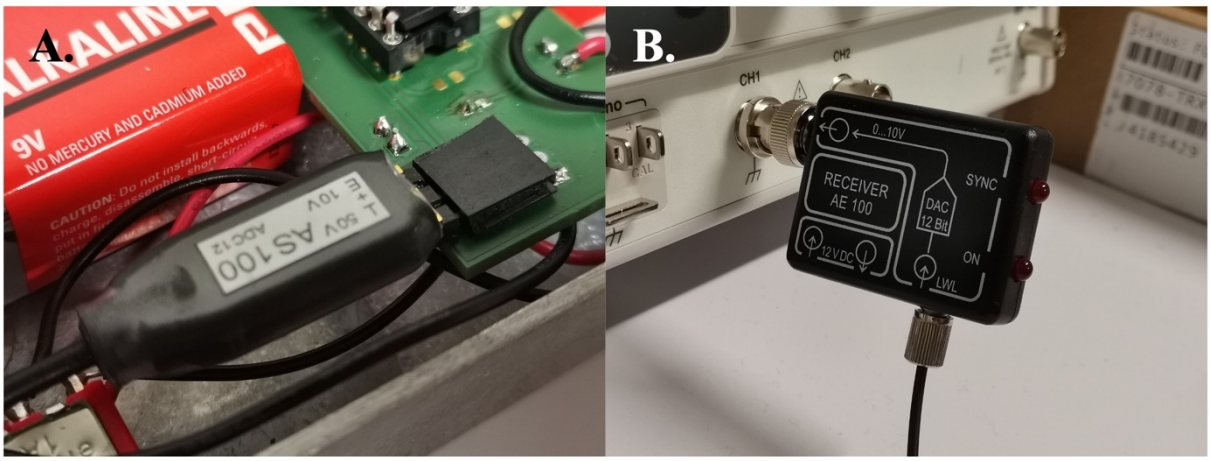

Figure 3-15 Optical fiber probe set for transmission: A) Optical sensor AS100 mounted on the measuring circuit; B) Optical receiver AE100 mounted on the oscilloscope

A PC oscilloscope from Pico Technology 5000 series replaced ordinary laboratory oscilloscope for receiving the signals from the optical receiver AE100 (*Figure 3-16*). This device is power supplied via USB by PC, the concern about that different reference GNDs of experimental devices may affect the results can be eliminated. Besides, time efficiency was achieved for having results directly on the PC and saving the measurements for further analysis.

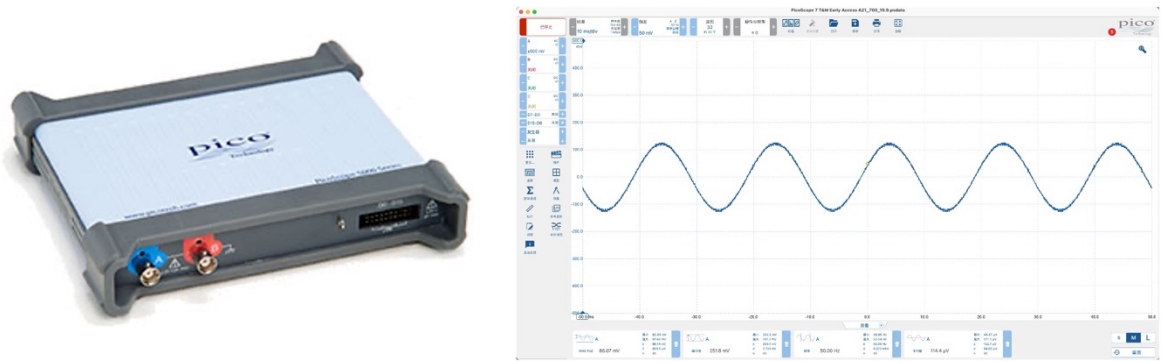

Figure 3-16 PC oscilloscope from Pico technology series 5000; PicoScope 7 user interface for instrument control and measurement observation

4. Optimization

- Waterproof shielding container

With the measuring circuit introduced above, different measurements were conducted without waterproof container as preliminary tests. Thus, the measuring system was placed outside the phantom and submitted to a high intensity electric field. In these tests, we found that even though the metal box served as electromagnetic shielding, it was not well sealed and charges induced on the metal box affected the performances of the measuring circuit. The measurement results were always much higher than expected and sometimes saturated.

A shielding container was fabricated with rubber gasket to seal the container, and waterproof cable glands for passing the pacing lead and the optic fiber through (*Figure 3-17*). The measuring circuit and two 9 V batteries serving as its power supply were installed in this

container, as well as the optical sensor of the optical link set with the optical fiber passing out of the container to transmit the measured signals. This well-insulated shielding container ensured the measuring system to be fully placed in the high-intensity electric fields and in the phantom solution as the way that cardiac implants are installed.

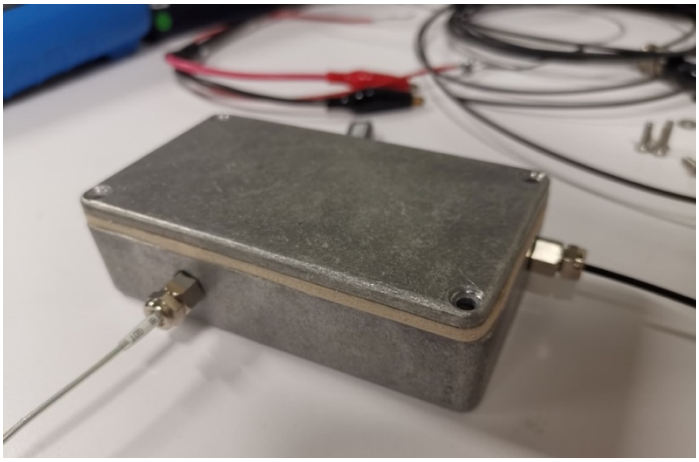

Figure 3-17 Waterproof shielding container of measuring system

The measuring system simulates the structure of a cardiac implantable device, containing a metal shielding box and a sensing lead, in order to create the same scenario as a cardiac implant under exposure. However, the dimension of the shielding box used in the experimental measurements was 115×65×33 mm, larger than the true size of a pacemaker (50×30×7 mm) or an ICD (50×50×15 mm). As we observed in the simulation, this difference doesn't have a serious impact on the induced electric field in the lower part of the phantom, so for the bipolar sensing mode, the induced voltages can be measured properly. However, for the unipolar sensing mode, the size of the metal box in the upper part of phantom may have influence on the induced electric field in this area so as the voltage induced between that metal box and that probe. Overall, a measuring system with a smaller scale will be better to limit the influence brought by the measuring system, therefore, to better simulate the real case exposure and polarization in the unipolar sensing mode.

- DUT holder

During the exposures, the shielding container of the measuring system representing the cardiac implant housing (impulse generator) was immersed in the phantom solution to mimic the real-case implantation. In the measurement of the induced voltage, the shielding container and its lead was taken as the DUT; in the immunity test under EF exposure, the cardiac implant device with its lead was taken as the DUT (see further in *Chapter 4*).

To ensure that the position of the DUT is manageable and reproducible, a plexiglass DUT holder was fabricated to fix the housing of the DUT (*Figure 3-18*). This holder is composed of two parts: the main support mounted on the edge of the phantom, with a slot for the installation of the shielding container; the accessible part mounted in the slot on the main support, for the installation of the cardiac implant housing. With fixing the position of the housing and the extremity of the pacing lead thanks to the pacing lead retainer, the distance between the housing

and the extremity of the lead is fixed. In other words, in the tests with a certain pacing lead, the sensing paths for unipolar sensing mode and for bipolar sensing mode are fixed. To be in accordance with the numerical approach, the sensing path of unipolar sensing mode is 220 mm, and the sensing path of bipolar sensing mode is 12 mm.

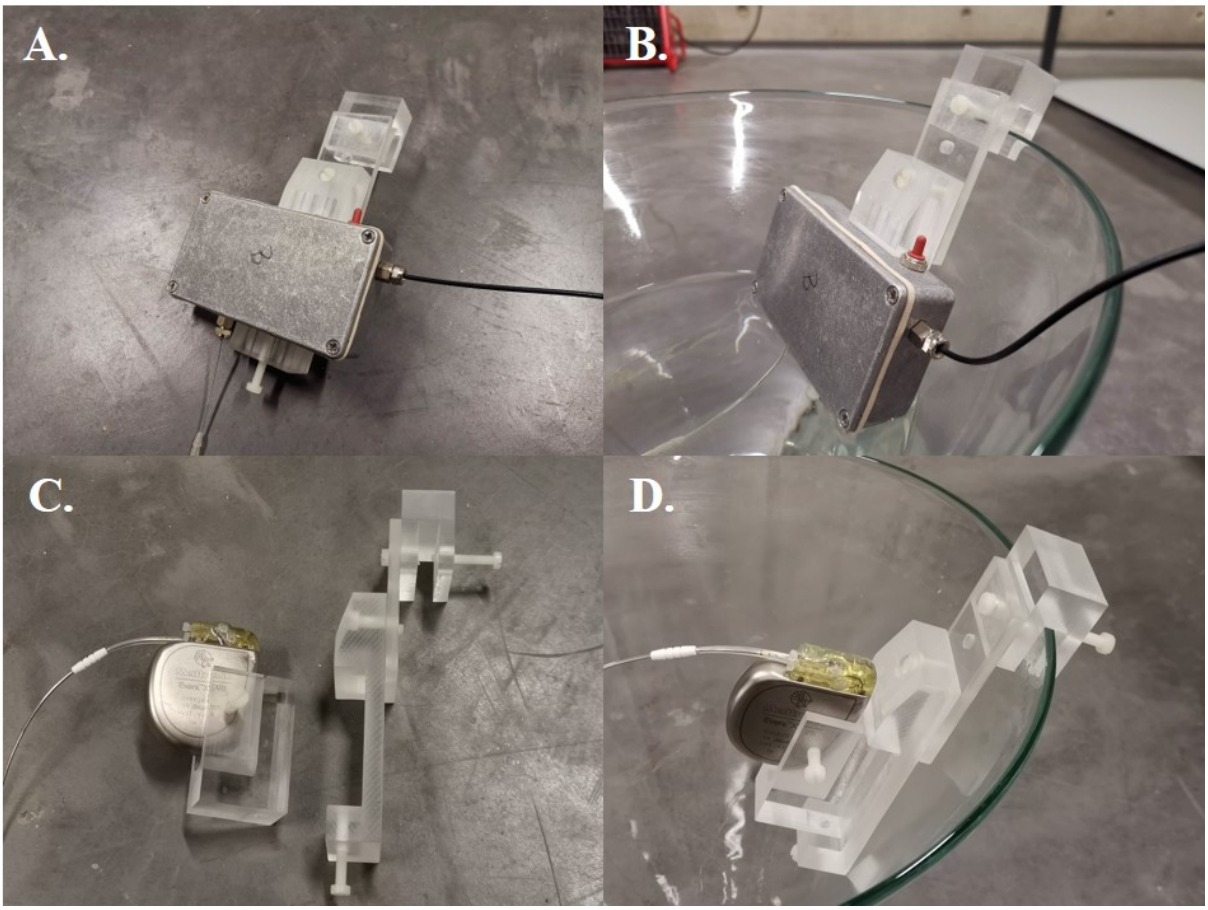

Figure 3-18 Plexiglass DUT holder: A)&C) DUT holder (separated DUT holder, big slot on the main part for fixing the measuring system and small slot on the accessional part for fixing the cardiac implant devices); B)&D) DUT holder mounted on the experimental phantom

- Pacing lead retainer

According to the studies on the electric field interference on cardiac implant probe and previous works, in bipolar sensing mode, the worst-case scenario occurs when the direction of the pacing lead is placed in parallel with the direction of external electric field. To generate such condition and to ensure reproducible results, a pacing lead retainer for fixing the position of the probe was required.

A pacing lead retainer containing a wooden stick and a plastic plug was firstly designed and tested (*Figure 3-19*). The plug was placed in the middle of the phantom (between the upper part and the bottom part) to stabilize the retainer. There are some holes in the plug for passing through polarization of the field. The cardiac implant lead was attached to the wooden stick passing through the plug. According to the simulation, the induced electric field in the phantom can be slightly changed caused by the existence of the retainer. Considering the plastic plug

was in the middle, which may have a noticeable impact on the distribution of the electric field, a better solution was needed. In addition, a variation of the induced electric field can be observed at the end of the wooden stick. To avoid this influence, the end of the pacing lead should be attached to the stick with a sufficient distance. We have chosen 40 mm for the distance between the end of the pacing retainer and the end of the pacing lead for the following tests.

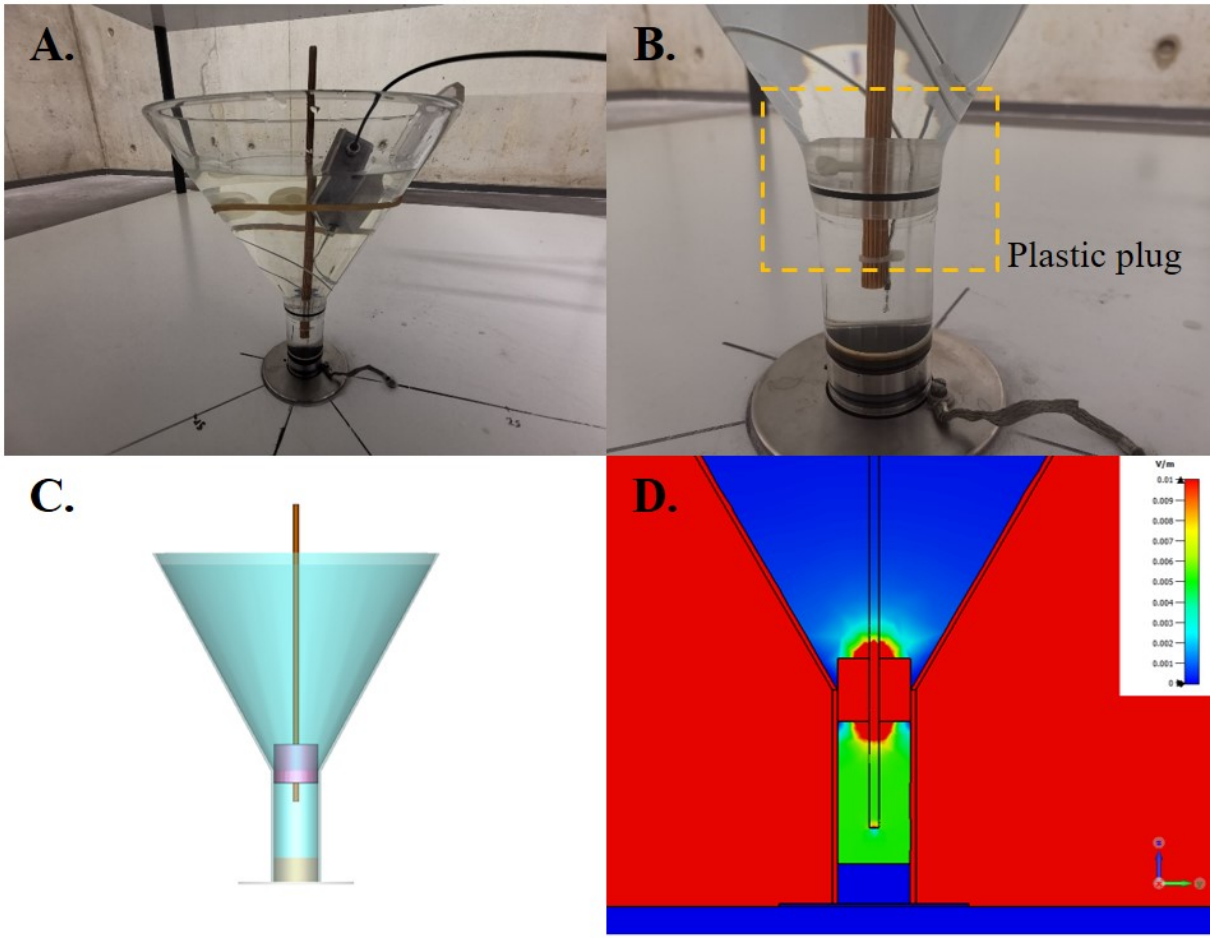

Figure 3-19 Pacing lead retainer with a plastic plug: A) Installation of retainer B) Plastic plug of retainer C) Modeling of retainer D) Simulation of retainer under 1 kV/m EF exposure

For the purpose of avoiding the influence of the plastic plug in the middle of the phantom, a new wooden cross-shaped pacing lead retainer was fabricated. This retainer contains a stick locating on the top of the phantom recipient horizontally to provide stability, and another stick locating vertically in the middle to retain the position of the probe. According to the simulation for this retainer, this probe retainer has less impact on the induced electric field in the phantom (*Figure 3-20*). Under 1 kV/m EF exposure, the induced EF in the phantom remained at 4 mV/m, the same value as without the retainer, except for the area near the tip. Thus, the distance between the end of the pacing lead and the tip of the retainer was fixed at 40 mm. Due to its performance, this pacing lead retainer was used in the experimental measurements.

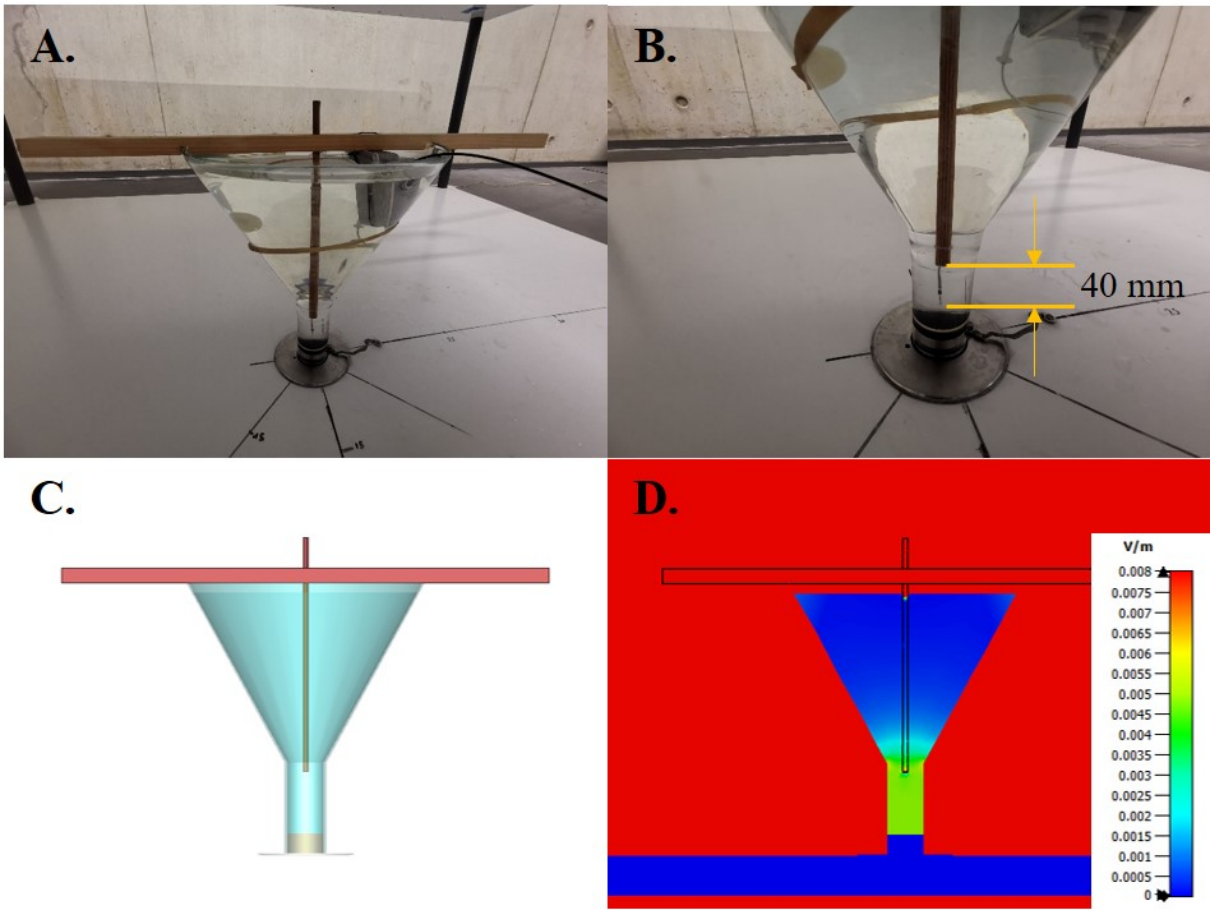

Figure 3-20 Cross-shaped wooden retainer: A) Installation of cross-shaped retainer B) Distance between the end of the pacing lead and its retainer C) Modeling of cross-shaped retainer D) Simulation Modeling of cross-shaped retainer under 1 kV/m EF exposure

- Postprocessing

Thanks to the PC oscilloscope from Pico Technology, the measuring results can be observed directly on a PC. The supporting software PicoScope shows the signal's features, such as amplitude, frequency, RMS value, etc. All the values documented in this study are all RMS values, so the RMS value in PicoScope was recorded for the experimental measurements.

However, for the measured signals with relatively low levels, the electrical parasitic elements have a great impact on the observed results. Thus, the measuring results were processed after the experimental measurements by the FFT method in MATLAB, to obtain the component at 50 Hz. The results were always recorded for the RMS quantity observed with the software PicoScope and for the amplitude at 50 Hz obtained by postprocessing.

5. Measuring system set up

The assembly of the measuring system setup is shown in *Figure 3-21* for induced voltage measurement where "DUT in Experimental Set-up" represents the DUT (shielding container and its lead) in the controlled EF exposure system as well as in the voltage injection system, of which the experimental set-ups were introduced in the previous parts.

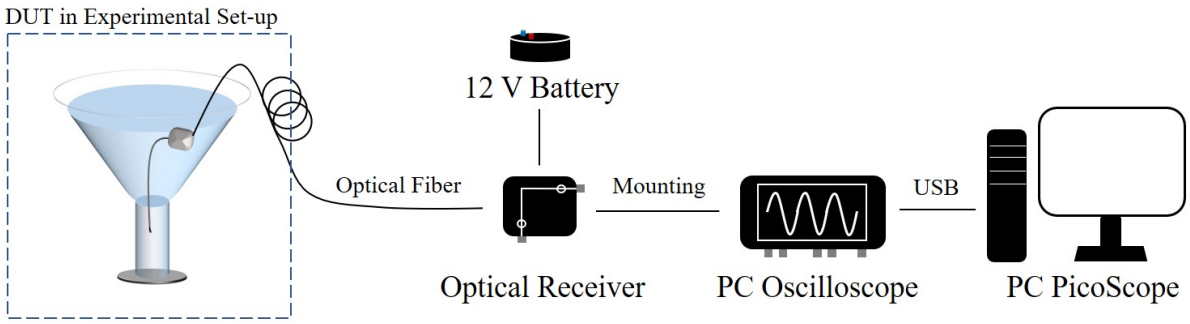

Figure 3-21 Measuring system set up

V. Experimental measurements

The experimental measurements were conducted in the controlled EF exposure system and in the voltage injection system. The results of the induced voltage obtained by the measuring system in the two systems are attached in the Annex II, III, IV, and V. Results from the PC oscilloscope Pico-tech 5000 (RMS value) and from signal processing in MATLAB are included.

Significant effect of noise on the measurements can be observed at lower exposure levels in which the electrical parasitic elements have a great impact on the results, especially in unipolar sensing mode. *Figure 3-22* shows the measured signal observed in the software PicoScope for exposure of 1.52 kV/m and 20 kV/m in the controlled EF exposure system as an example. Distinct noise can be observed at the exposure of 1.52 kV/m compared to the exposure of 20 kV/m. Thus, as previously explained, we applied FFT method on the recorded results in MATLAB as postprocessing, in order to obtain the component at 50 Hz.

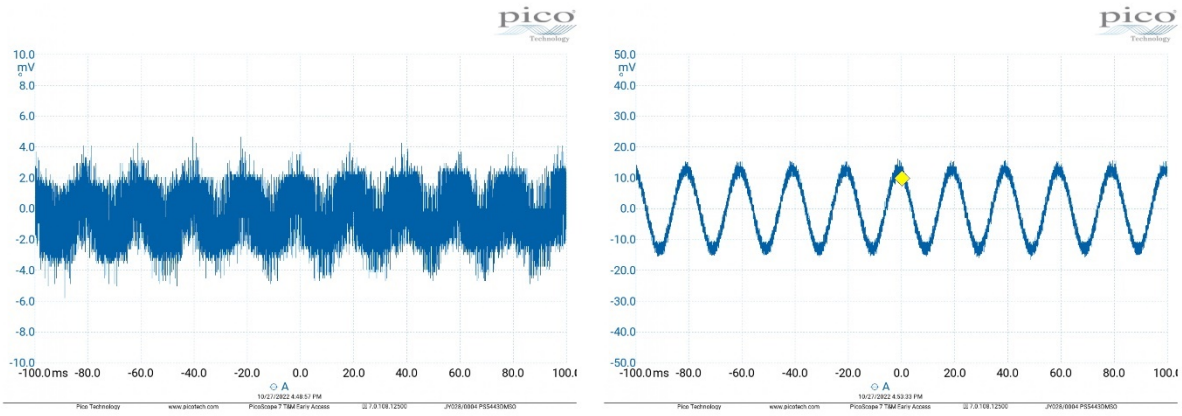

Figure 3-22 Measurement results obtained by unipolar measuring system under EF exposures of 1.52 kV/m (left) and 20 kV/m (right)

In addition, according to the observation of measured results, the received signals begun to deform starting at an input of 1600 mVpp from the signal generator, i.e., a generated electric field exposure of 50 kV/m. Thus, only the measurements of exposures up to 50 kV/m were validated and analyzed. Evident distortion is shown in *Figure 3-23* for an EF exposure of 70 kV/m.

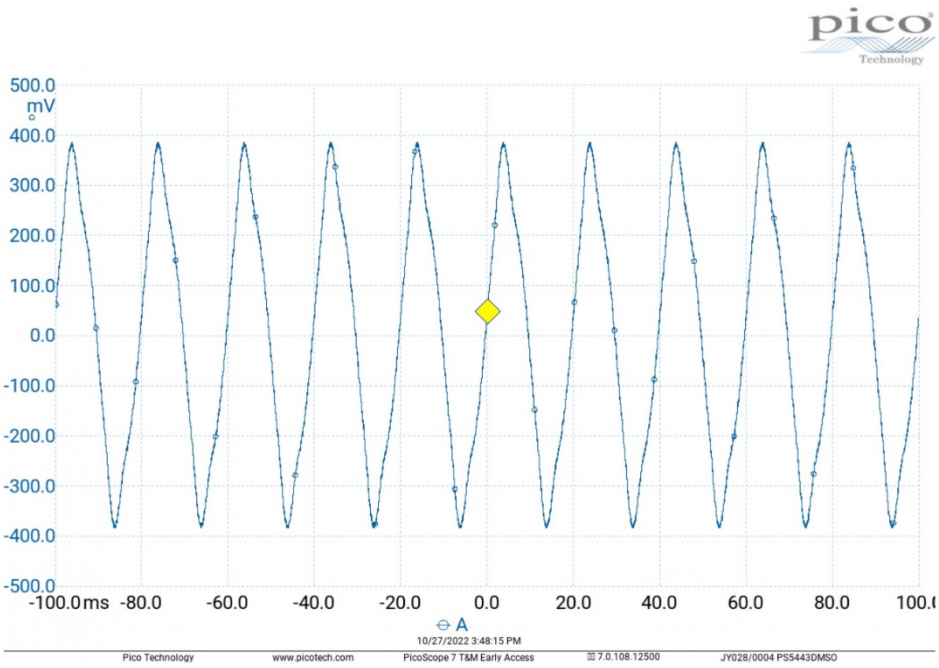

Figure 3-23 Distorted signal received on the PC oscilloscope for an EF exposure of 70 kV/m

Annex II and *Annex III* show the induced voltages measured in the controlled EF exposure system for unipolar sensing mode and for bipolar sensing mode. The measuring results after postprocessing (FFT) are plotted in *Figure 3-24* and *Figure 3-25* with blue dots. Linearity between the external EF exposure and induced voltage can be observed for both bipolar and unipolar sensing mode. The orange lines represent the linear relation between the EF exposure and the induced voltage in the numerical simulation. For unipolar sensing mode in the controlled EF exposure system (*Figure 3-24*), we can see that the induced voltages on the DUT measured in the experiments are almost overlap to the simulation results. The gradient of the trend line of the results was taken as the mean induced voltage for normalized EF exposure (1 kV/m), which we obtained 438 µV for the experimental measurements and 421 µV for the numerical simulation, with a difference of 4%. For bipolar sensing mode in the controlled EF exposure system (*Figure 3-25*), the induced voltages on the DUT measured in the experiments are also close to the simulation results. We obtained 80 µV for the experimental measurements and 62 µV for the numerical simulation, with a difference of 29%.

Annex IV and *Annex V* show the induced voltages measured with the voltage injection system for unipolar sensing mode and for bipolar sensing mode. The measuring results after postprocessing (FFT) and the simulation results are plotted in *Figure 3.26* and *Figure 3.27* on which linearity of the experimental measurement results (blue dots) and numerical simulation results (orange line) can be observed as well. For unipolar sensing mode, we obtained 772 µV in the experimental measurements as the mean induced voltage for normalized voltage injection (1 mV) from the gradient of the trend line of the results and 668 µV for the numerical simulation, with a difference of 15.6%. For bipolar sensing mode, we obtained 121 µV in the experimental measurement as the mean induced voltage for normalized voltage injection (1 mV) and 117 µV for the numerical simulation, with a difference of 3.4%.

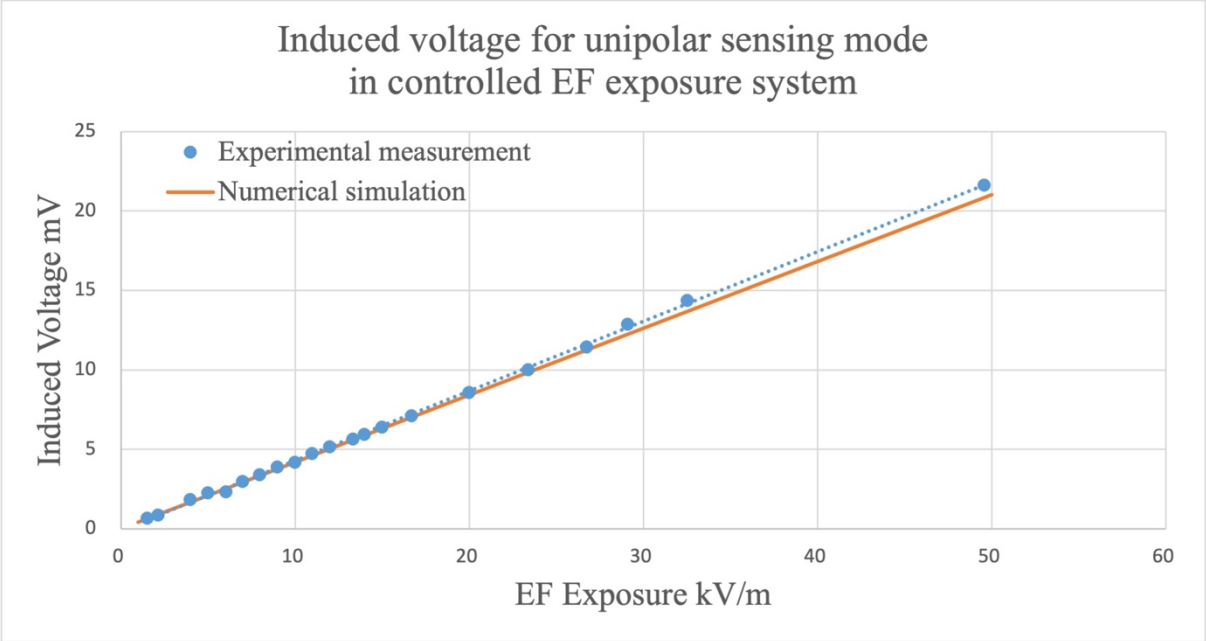

Figure 3-24 Measurement results for unipolar sensing mode in controlled exposure system

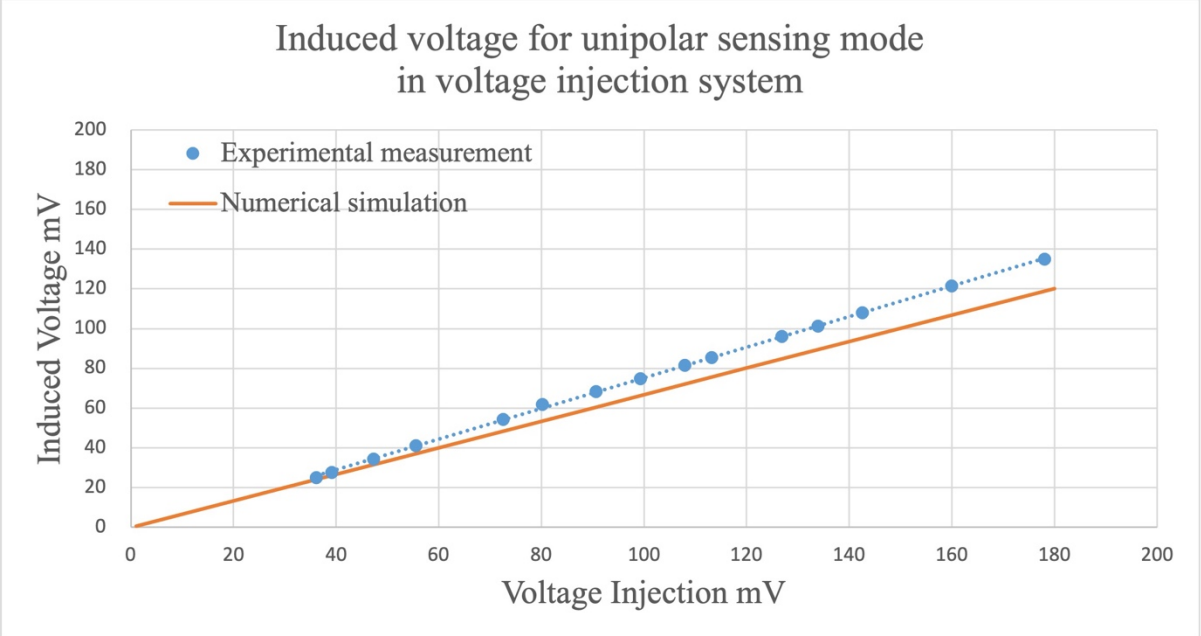

Figure 3-25 Measurement results for bipolar sensing mode in controlled exposure system

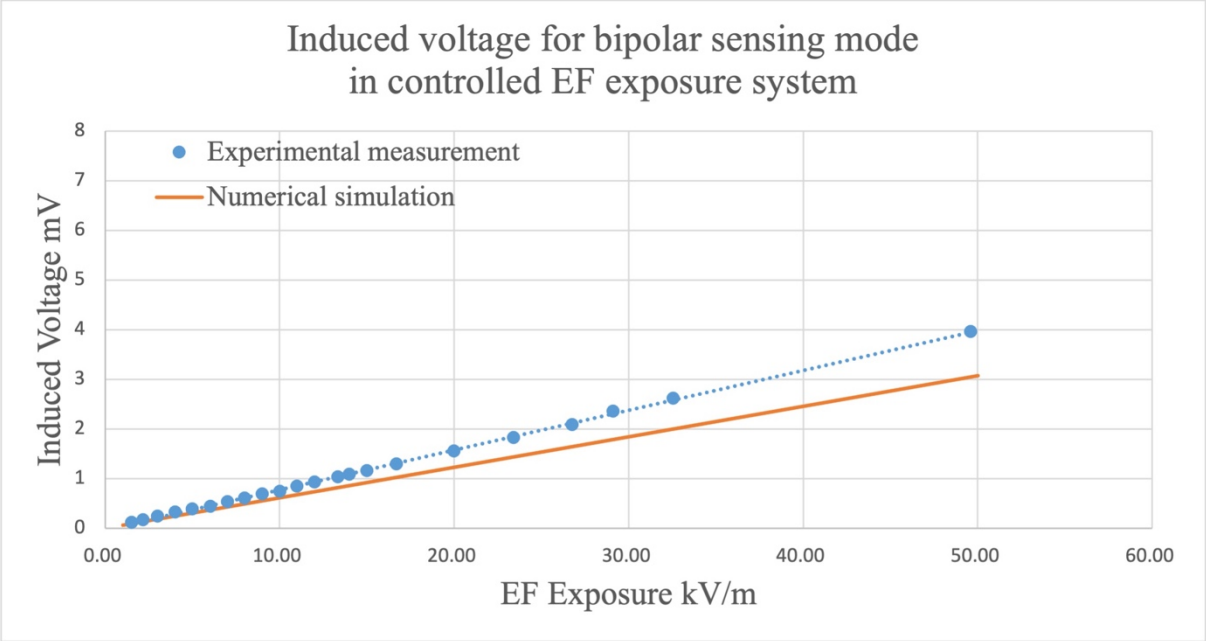

Figure 3-26 Measurement results for unipolar sensing mode in voltage injection system

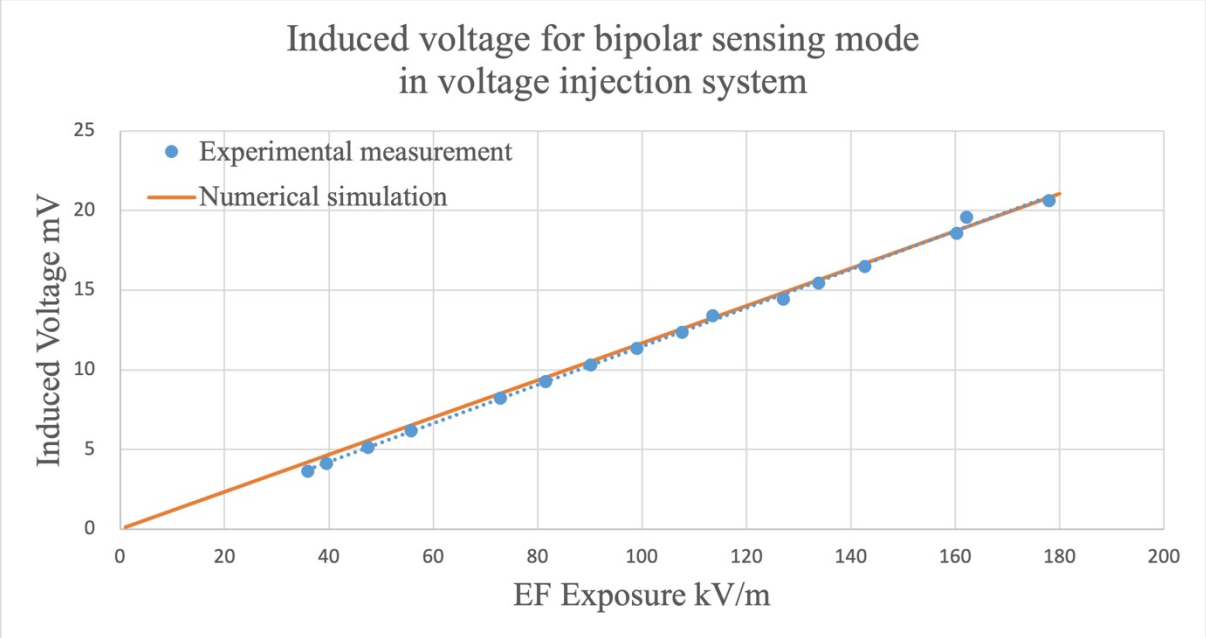

Figure 3-27 Measurement results for bipolar sensing mode in voltage injection system

Following the analysis of numerical approach in the *Chapter 2*, the equivalence factors for the controlled EF exposure system are summarized in *Table 3-4*. This parameter represents the equivalence between the equivalent system A and the standard system (real case) and was defined previously in detail (*Chapter 2*). In addition, using the voltage injection system, an induced voltage of 772 µV was found in unipolar sensing mode for 1 mV voltage injection and 121 µV in bipolar sensing mode.

Table 3-4 Induced voltages for the virtual human body and for the controlled EF exposure system for 1 kV/m EF exposure at 50 Hz

Induced voltage	Standard system	Equivalent system A	
	Virtual human body	Controlled EF exposure system	Equivalence Factor F_A
Unit	µV	µV	/
Unipolar	183	438	2.39
Bipolar	22	80	3.64

On the basis of the equivalences found in the experimental measurements, the association of the three systems was experimentally validated to build up the risk assessment procedure for the cardiac implants under EF exposures. To perform a risk assessment on the case that the patient with a cardiac implant exposed to an EF of 10 kV/m, it requires:

- An EF of 4.18 kV/m in the controlled EF exposure system for unipolar sensing mode;
- An EF of 2.75 kV/m in the controlled EF exposure system for bipolar sensing mode;
- An injection of 2.37 mV in the voltage injection system for unipolar sensing mode;
- An injection of 1.82 mV in the voltage injection system for bipolar sensing mode.

VI. Discussion

In the numerical approach, the ANSOFT virtual human body was taken as the standard system. The equivalences researched between the standard system and the equivalent system were carried out for the ANSOFT model. The feasibility of the application on other numerical studies was discussed in the *Chapter 2*. In the experimental approach introduced in this chapter, the ANSOFT model serves as the standard system, i.e., real case, as well. Thus, modifications of the experimental configuration allow these set-ups to be used for equivalent tests for other numerical studies, even for *in vivo* experimental studies if possible.

Compared to the induced voltages found in the numerical studies (*Table 3-6*), in controlled EF exposure system, there is a difference of 4% between numerical simulation and experimental measurement in unipolar sensing mode and a difference of 29% in bipolar sensing mode. These differences may be caused by the material limits of the experimental set-up, such as old cables, inaccurate facilities, and variations of the experimental conditions. Particularly in the bipolar sensing mode, the difference was found higher than one fourth, of which an explanation was proposed that the bipolar measuring circuit possesses a gain of 50, so that some parasites might

be amplified as well and affected the measurements, considering the induced voltages in bipolar sensing mode were relatively low.

In voltage injection system, a difference of 15.6% was found between numerical simulation and experimental measurement in unipolar sensing mode and a difference of 3.4% in bipolar sensing mode. An inquiry was conducted on the difference in unipolar sensing mode. We assumed that because the housing of DUT located near the metal grid, the DUT may be subjected to a slightly higher electric field in this area, which resulted in a higher induced voltage.

Table 3-5 Comparison between results in numerical approach and in experimental approach

Approach	Controlled EF exposure system (For 1 kV/m exposure)		Voltage injection system (For 1 mV exposure)	
	Numerical	Experimental	Numerical	Experimental
Unit	µV	µV	µV	µV
Unipolar	421	438	668	772
Bipolar	62	80	117	121

In the controlled exposure system, an induced voltage of 438 µV was found in the cardiac implant in unipolar sensing mode and 80 µV in bipolar sensing mode under 1kV/m electric field exposure. By applying the normalized induced voltage found in the experimental measurements, for a voltage injection of 0.52 mV, we have 401 µV in unipolar sensing mode and 63 µV in bipolar sensing mode. Furthermore, to reproduce an electric field of 1 kV/m in the controlled EF exposure system, it requires a voltage of 0.57 mV for unipolar sensing mode and 0.66 mV for bipolar sensing mode to be delivered to the voltage injection system. The induced voltages found in the experimental measurements remain at the same level as the numerical simulation which validates the equivalence between the controlled EF exposure system and the voltage injection system (*Table 3-6*). In other words, the performance of the voltage injection system is validated for reproducing the same exposure to the DUT without an exceptional experimental environment.

As mentioned in previous sections, in the controlled EF exposure system, the measured signals begun to deform from an input of 1600 mV in peak to peak on the signal generator, i.e., a generated electric field exposure of 50 kV/m. It was verified that distortion occurred at the same level of EF exposure for the measuring system with different gains. We assume that the distortion is caused by the configuration of the exposure system. According to the equivalence factor between virtual human body representing the real case and controlled EF exposure system (2.39 for unipolar sensing mode and 3.64 for bipolar sensing mode), an electric field exposure of 50 kV/m in the laboratory system is equivalent to an exposure of 119.5 kV/m for unipolar sensing mode and 182 kV/m for bipolar sensing mode, above 6 times higher than the high action level (AL) 20 kV/m in Directive 2013/35/UE. Thus, the controlled EF exposure system possesses adequate ability to perform the risk assessments on the cardiac implants.

In the experimental investigations, the external factors may have a great impact on the measurements. For example, the electrical conductivity of the phantom solution determines the

electric field distribution which determines the induced voltage on the input of the cardiac implant. Thus, the characteristics of the phantom solution should be maintained constantly by stirring to keep the homogeneity of the conductivity. In addition, gelatin phantom material can be taken into consideration to achieve a homogeneous phantom and fixed DUT position.

VII. Conclusion

In this chapter, the establishment of the risk assessment for cardiac implants under high-intensity electric field exposures at extremely low frequency (50 Hz) was validated by experimental approach. The equivalent systems: controlled EF exposure system and voltage injection systems were built up in the experimental room with performance verification and optimization. The configurations of the two systems were detailed presented.

A measuring system was introduced in this chapter to measure the induced voltages that cardiac implant devices are subjected during EF exposures. Two measuring circuits were designed and implemented for both sensing methods and the measuring system allows unaffected signal transmission via optical fiber, and direct observation in real time.

The measured induced voltages in experimental approach are close to the results obtained in numerical approach, which validated the equivalences that we proposed between the three systems. This validation is vital for the establishment of the risk assessment procedure for the immunity test on the cardiac implant devices, which is introduced in the *Chapter 4*.

4

Risk assessment procedure for AIMD: establishment and application

I. Introduction

Following the European Directive 2013/35/EU, employers are obliged to "assess all risks for workers arising from electromagnetic fields in the workplace." In this study, a risk assessment method under high intensity electric field (EF) exposures at low frequency (50 Hz) was proposed for the device performance evaluation of cardiac implants. This approach was validated by the numerical simulations and the experimental results in the *Chapters 2* and *3*.

In this chapter, the establishment of the risk assessment procedure for cardiac implant devices under occupational EF exposures is introduced based on the estimation of the induced voltages on the input of the devices investigated in the previous chapters. The association of the three exposure systems: ANSOFT virtual human body (standard system), controlled EF exposure system (equivalent system A), and voltage injection system (equivalent system B), was built up by adopting the exposure level limits in the standards and guidelines as reference. The estimation of the induced voltage was on the basis of those discovered in the standard system and the equivalence factors for the corresponding equivalent systems.

As the validation and application of the risk assessment procedure, four cardiac implant devices (two pacemakers and two ICDs) were tested for their performance of immunity to high-intensity electric field exposures. *In vitro* tests were conducted on these devices with the same experimental set-ups of controlled EF exposure system and voltage injection system. The interference thresholds were investigated in the four cardiac implants and the two exposure systems. The proposed risk assessment procedure is applied to these four cardiac implant devices.

II. Establishment of risk assessment procedure

The conception of risk assessment procedures for potential hazards of electromagnetic interference on cardiac implant devices was introduced in the *Chapter 2*. A risk assessment procedure based on the association of the three exposure systems (*Figure 4-1*) was proposed for the devices under occupational electric field exposure at extremely low frequency (50 Hz). The estimation of the induced voltage and the equivalence factors were investigated in the previous chapters. In this chapter, the establishment of the risk assessment procedure is carried out on the basis of the induced voltages found in the standard system and the equivalences for the corresponding equivalent systems which were validated in the experimental measurements.

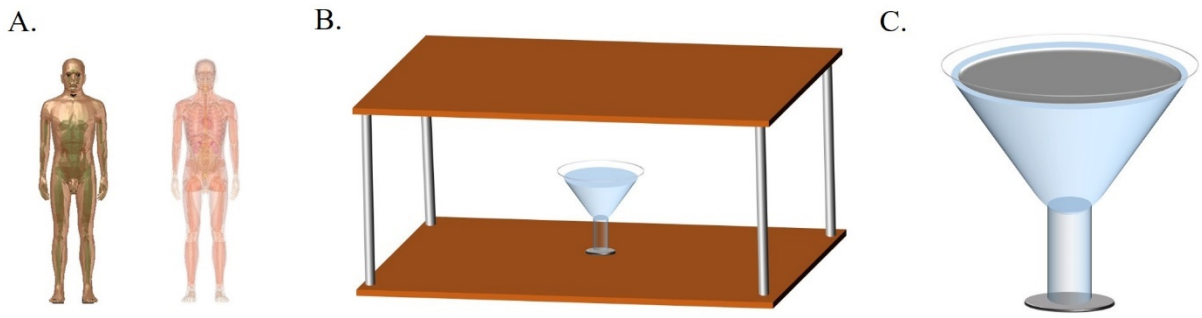

Figure 4-1 Three exposure systems: A) Standard system: ANSOFT virtual human body; B) Equivalent system A: controlled EF exposure system; C) Equivalent system B: voltage injection system

Table 4-1 specifies the exposure limitation indicated in the IEEE Standard C95.1, and ICNIRP Guideline. The voltages induced on the input of the cardiac implant devices were estimated employing those investigated on the ANSOFT virtual human body (Unipolar: 22 μV; Bipolar: 183 μV). Equivalent exposure tests can be built up in the controlled EF exposure system and in the voltage injection system to have the same voltages induced on the input of the cardiac implant devices.

Table 4-1 Induced voltages under EF exposure levels indicated in the European Standard 2013/35/EU, IEEE Standard C95.1, and ICNIRP Guideline

Exposure Limit in standard and guideline		**Induced Voltage**	
		Unipolar	Bipolar
ICNIRP Reference Level (Public) / IEEE C95.1-2019 (Unrestricted)	5 kV/m	0.92 mV	0.11 mV
2013/35/UE Low Action Level / ICNIRP Reference level (Occupational)	10 kV/m	1.83 mV	0.22 mV
2013/35/EU High Action Level / IEEE C95.1-2019 (Restricted)	20 kV/m	3.66 mV	0.44 mV

Figure 4-2 demonstrates the association of the three exposure systems for unipolar sensing mode. For a certain exposure on the ANSOFT virtual human body (horizontal axis), the EF levels that are required to conduct equivalent exposure tests in the controlled EF exposure system can be found on the left axis; the injected voltages that are required in the voltage injection system can be found on the right axis. *Figure 4-3* demonstrates the association for bipolar sensing mode. The exposure limitation indicated by the standards and guidelines were labelled in the figure. Thus, to perform an equivalent exposure test on the cardiac implant device, the exposure indicator can be verified in these figures.

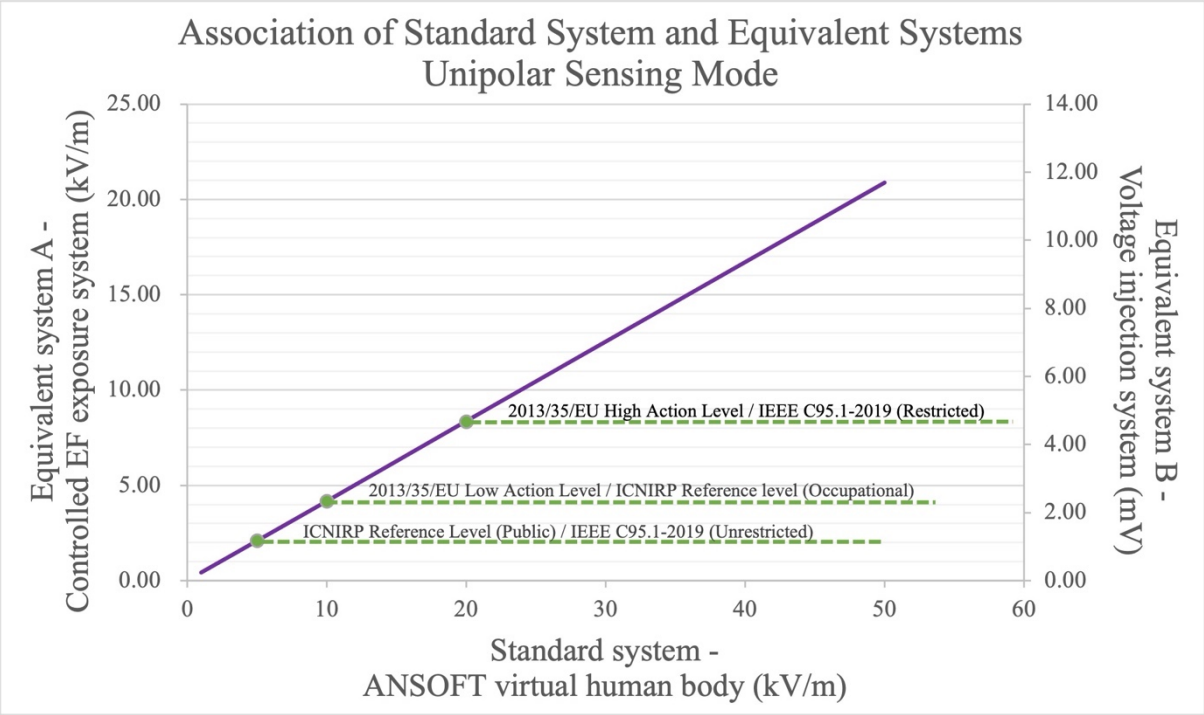

Figure 4-2 Association of standard system and equivalent systems for unipolar sensing mode

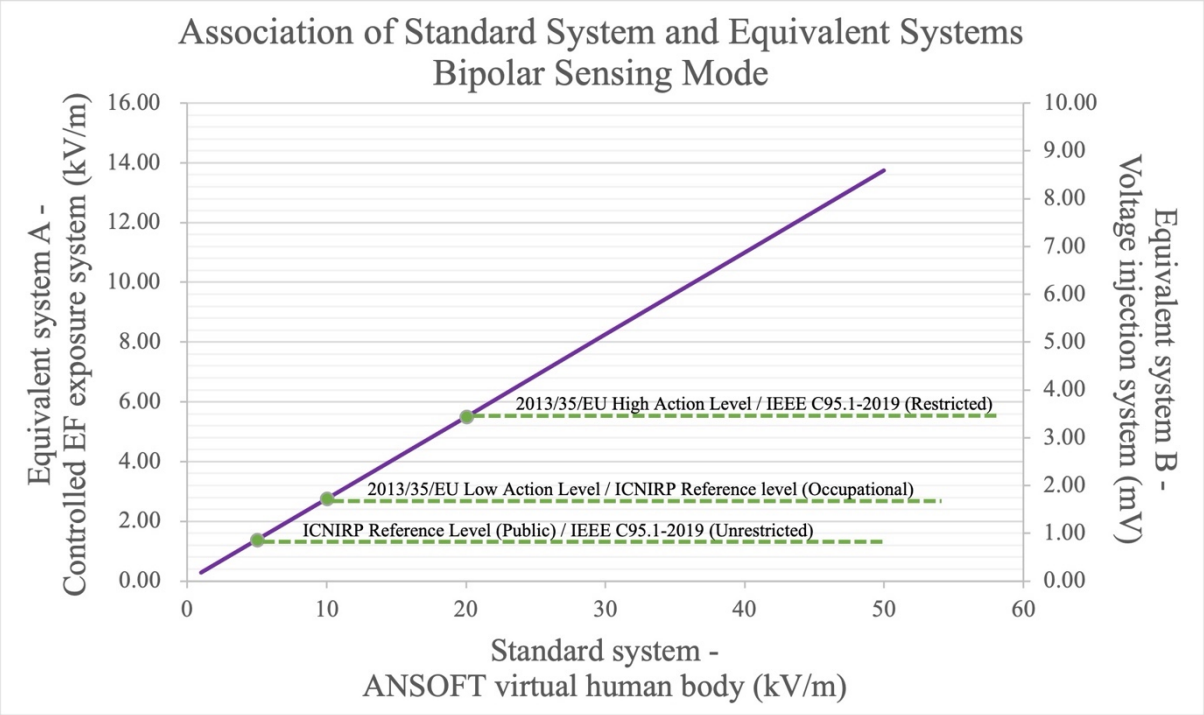

Figure 4-3 Association of standard system and equivalent systems for bipolar sensing mode

For most of the enterprises, due to their diversity, it is not practical and efficient to conduct immunity tests in the controlled EF exposure system which requires rigorous experimental configuration and maintenance. Meanwhile, the voltage injection system is an ideal alternative for conducting such tests since it is simple and does not require sophisticated material. Thus, the voltage injection system is proposed for the risk assessment procedure at the workplace.

The risk assessment procedure is illustrated in *Figure 4-4* for the cardiac implant device bearer. Here he is defined as AIMD-employee according to NF EN 50527. He might work under high-intensity occupational exposure in the workplace. The *in vitro* experimental set-ups and the associations of the systems are applied in the step *Immunity test to the exposure*. *In vitro* tests are built up in the voltage injection system according to the surveys. The required voltage injection can be determined in the *Figure 4-2* and *Figure 4-3*. After executing this risk assessment procedure, the AIMD-employee should be informed: areas of continuous stay, areas of transient exposure, and areas of non-access.

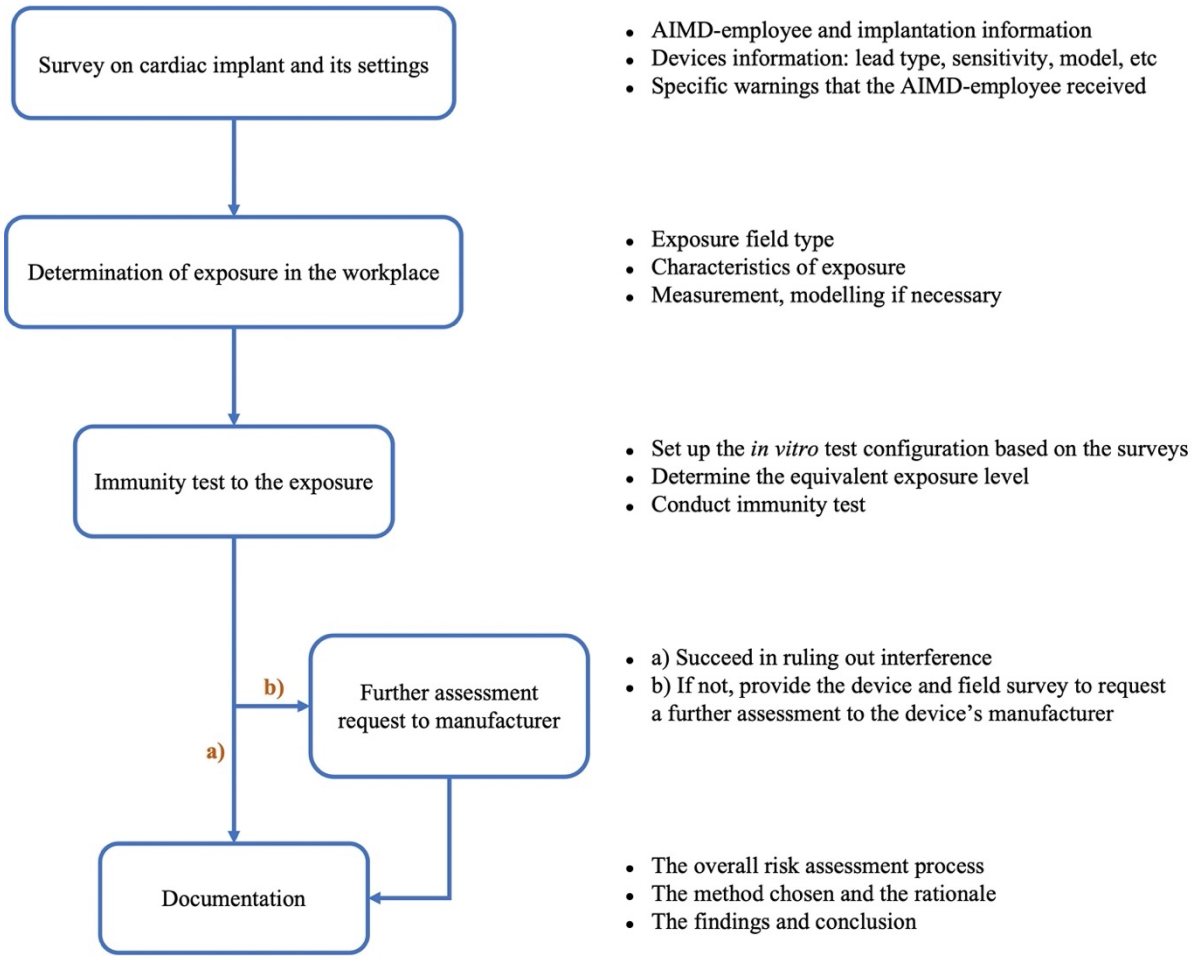

Figure 4-4 Risk assessment procedure for AIMD-employee (adapted from NF EN 50527)

III. Immunity tests on cardiac implant devices

The induced voltage on the input of the cardiac implant devices is taken as the evaluation quantity for the interference that the devices are subjected to. As the estimation of the induced

voltages were carried out in the three exposure systems numerically and experimentally, *in vitro* immunity test was proposed to the cardiac implants in the equivalent exposure systems to investigate their interference thresholds under EF exposures at 50 Hz. Same experimental conditions and configurations were retained in order to maintain accordance with previous experimental measurements.

1. Devices under test (DUTs)

Four AIMDs from Medtronic were tested in this study: two pacemakers (PMs) and two implantable cardioverter defibrillators (ICDs). The integrations with pacing leads were checked for the pacing impedance within a range from 200 to 2000 Ω (standard values corresponding to impedance when AIMD is implanted in the body).

- Advisa SR MRI™ SureScan™

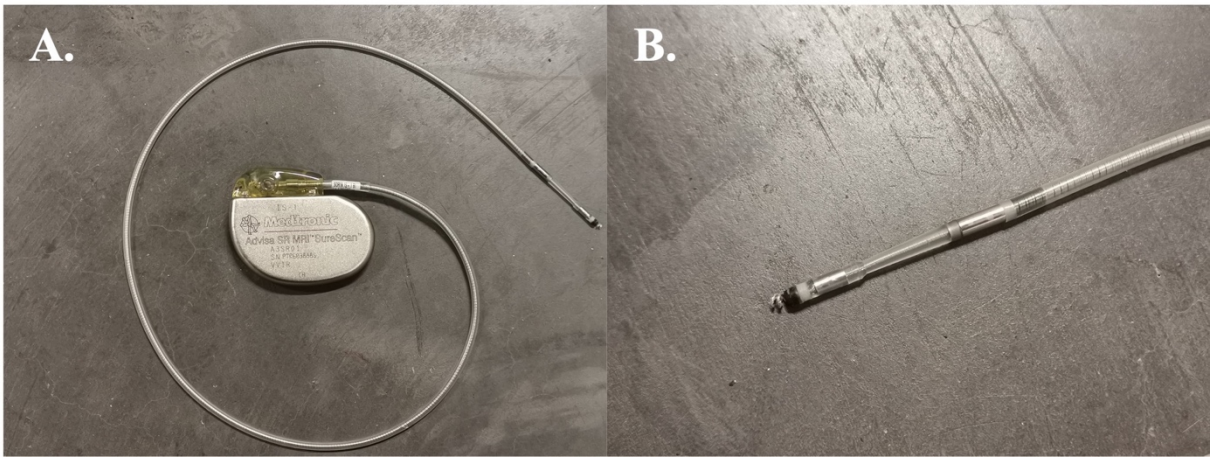

Figure 4-5 Medtronic pacemaker Advisa SR MIR SureScan: A) Impulse generator and pacing lead; B) Electrodes on pacing lead

Advisa SR MRI SureScan is a single chamber implantable pacemaker that monitors and regulates the patient's heart rate by providing single chamber rate-responsive bradycardia pacing therapies. The device senses the electrical activity of the patient's heart using the electrodes of the implanted pacing lead and then analyzes the heart rhythm based on selectable detection parameters. The device responds to brady-arrhythmia by providing bradycardia pacing therapy. The device provides diagnostic and monitoring information that assists with system evaluation and patient care.

Table 4-2 Specification sheet of Advisa SR MIR SureScan

Brand	Medtronic
Pacing system	ADVISA SR MRI™ SureScan™
Model	A3SR01
VT Monitor Interval (Rate)	280; 290 … $360_{nominal}$ … 500 ms
Mode	$VVIR_{nominal}$; VVI; VOO; OVO
Lower Rate	30; 35 … $60_{nominal}$; 70; 75 … 150 min^{-1}
RV Amplitude	0.5; 0.75 … $3.5_{nominal}$ … 5; 5.5; 6; 8 V

RV Pulse Width	0.03; 0.06; 0.1; 0.2; 0.3; $0.4_{nominal}$ … 1.5 ms
RV Sensitivity	0.45; 0.60; 0.90; 1.20; 2.00; 2.80; 4.00; 5.60; 8.00; 11.30 mV Bipolar: $0.90_{nominal}$ mV Unipolar: $2.80_{nominal}$ mV
RV Pace Polarity	Bipolar; Unipolar
RV Sense Polarity	Bipolar; Unipolar
Min Limit	$200_{nominal}$; 300; 400; 500 Ω
Max Limit	1000; 1500; 2000; $3000_{nominal}$ Ω

- Adapta ADVDD01

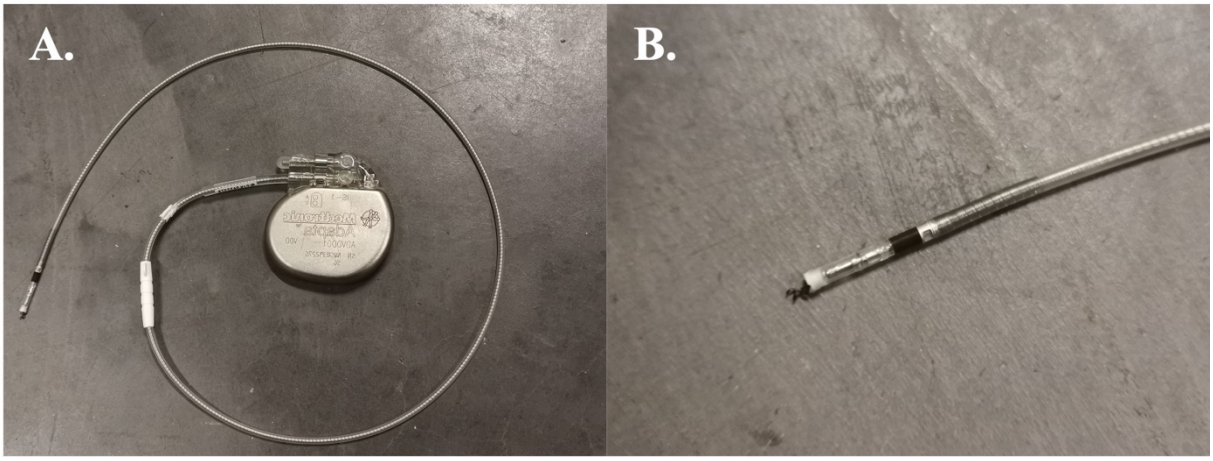

Figure 4-6 Medtronic pacemaker Adapta ADVDD01: A) Impulse generator and pacing lead; B) Electrodes on pacing lead

The Adapta™ pacemaker models combine physiologic pacing with automaticity. Adapta ADVDD01 implantable pulse generators (IPGs) are contraindicated for VDD mode operation in patients with sinus disorders. The device is also indicated for atrial tracking modes in patients who may benefit from maintenance of AV synchrony. Atrial tracking modes are specifically indicated for the treatment of conduction disorders that require restoration of both rate and AV synchrony, which includes various degrees of AV block to maintain the atrial contribution to cardiac output and VVI intolerance (for example, pacemaker syndrome) in the presence of a persistent sinus rhythm.

Table 4-3 Specification sheet of Adapta ADVDD01

Brand	Medtronic
Pacing system	ADAPTA
Model	ADVDD01
Mode	$VDD_{nominal}$; VVIR; VDIR; VVI; VDI; VVT; VOOR; VOO; ODO; OVO; CAO
Lower Rate	30; 35; 40… $50_{nominal}$; 170 min^{-1}
RV Amplitude	0.5; 0.75; 1.0 … $3.5_{nominal}$ … 4; 4.5; 5; 5.5; 6; 7.5 V

RV Pulse Width	0.12; 0.15; 0.21; 0.27; 0.43; $0.4_{nominal}$, 0.46; 0.52; 0.64; 0.76; 1; 1.25; 1.5 ms
Ventricular Sensitivity	1; 1.4; 2; $2.8_{nominal}$; 4.5; 6.8; 11.2 mV
Atrial Sensitivity	0.18; $0.25_{nominal}$; 0.35; 0.5; 0.7; 1; 1.4; 2; 2.8; 4 mV
Pacing Polarity	Bipolar; Unipolar
Sensing Polarity	V: Bipolar; Unipolar A: Bipolar
Min Limit	200 Ω
Max Limit	$1000; 2000; 3000; 4000_{nominal}$ Ω

- Evera XT VR

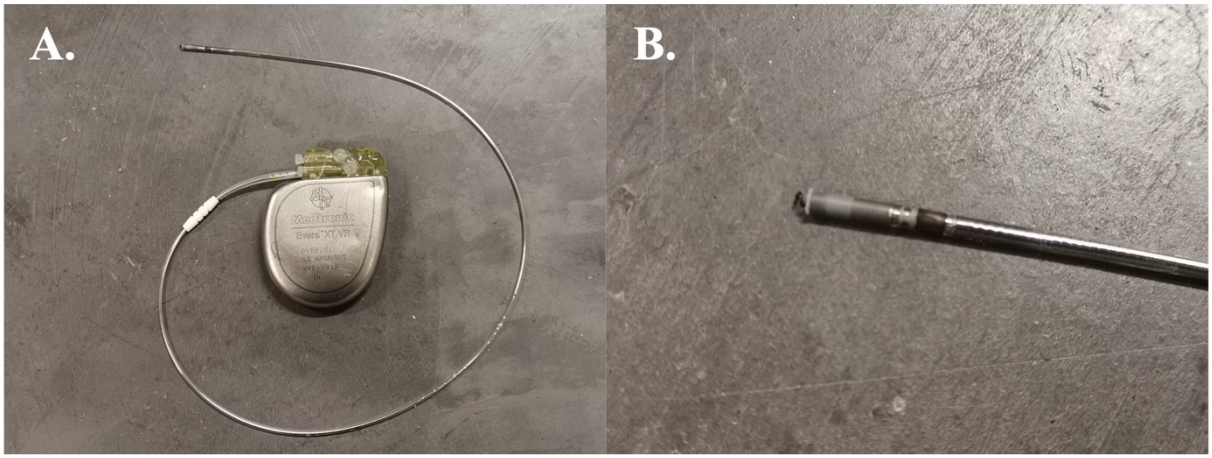

Figure 4-7 Medtronic ICD Evera XT VR: A) Impulse generator and pacing lead; B) Electrodes on pacing lead

The Medtronic Model DVBB2D1 Evera XT VR single-chamber, implantable cardioverter defibrillator (ICD) is a multiprogrammable cardiac device that monitors and regulates the patient's heart rate by providing a single chamber, rate-responsive bradycardia pacing and ventricular tachyarrhythmia therapies. The device can detect ventricular tachyarrhythmias (VT/VF) automatically and can provide treatment with defibrillation, cardioversion, and antitachycardia pacing therapies. The device responds to bradyarrhythmias by providing bradycardia pacing therapy. The device also provides diagnostic and monitoring information that assist with system evaluation and patient care.

Table 4-4 Specification sheet of Evera XT VR

Brand	Medtronic
Pacing system	Evera XT VR
Model	DVBB2D1
VF Interval (Rate)	240; 250 … $320_{nominal}$ … 400 ms
FVT Interval (Rate)	200; 210 … $240_{nominal}$ … 600 ms
VT Interval (Rate)	280; 290 … $360_{nominal}$ … 650 ms
VT Monitor Interval (Rate)	280; 290 … $450_{nominal}$ … 650 ms

Mode	DDDR; DDD; AAIR⇔DDDR$_{nominal}$; AAI⇔DDD; DDIR; DDI; AAIR; AAI; VVIR; VVI; DOO; AOO; VOO; OVO
Lower Rate	30; 35 … 60$_{nominal}$; 70; 75 … 150 min^{-1}
RV Amplitude	0.50; 0.75 … 3.5$_{nominal}$ … 5.00; 5.50; 6.00; 8.00 V
RV Pulse Width	0.03; 0.06; 0.10; 0.20; 0.30; 0.40$_{nominal}$ … 1.5 ms
RV Sensitivity	0.15; 0.30$_{nominal}$; 0.45; 0.60; 0.90; 1.20 mV
RV Pacing Polarity	Bipolar; Tip to coil
RV Sensing Polarity	Bipolar; Tip to coil

- Secura DR

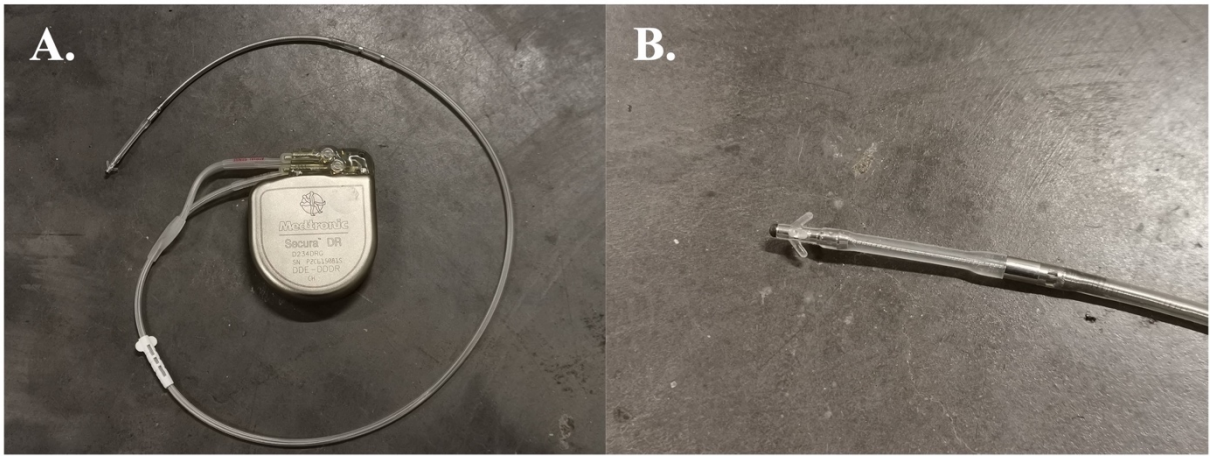

Figure 4-8 Medtronic ICD Secura DR: A) Impulse generator and pacing lead; B) Electrodes on pacing lead

The Medtronic Model D234DRG Secura DR dual chamber, implantable cardioverter defibrillator (ICD) is a multiprogrammable cardiac device that monitors and regulates the patient's heart rate by providing a single or dual chamber, rate-responsive bradycardia pacing; ventricular tachyarrhythmia therapies; and atrial tachyarrhythmia therapies. The device senses the electrical activity of the patient's heart using the electrodes of the implanted atrial and right ventricular leads. It then analyzes the heart rhythm based on selectable detection parameters. The device can automatically detect ventricular tachyarrhythmias (VT/VF) and provides treatment with defibrillation, cardioversion, and antitachycardia pacing therapies. The device can also automatically detect atrial tachyarrhythmias (AT/AF) and provides treatment with cardioversion and antitachycardia pacing therapies. The device responds to bradyarrhythmias by providing bradycardia pacing therapy. The device also provides diagnostic and monitoring information that assist with system evaluation and patient care.

Table 4-5 Specification sheet of Secura DR

Brand	Medtronic
Pacing system	Secura DR
Model	D234DRG
VF Interval (Rate)	240; 250 … $320_{nominal}$ … 400 ms
FVT Interval (Rate)	200; 210 … 240 $_{nominal}$ … 600 ms
VT Interval (Rate)	280; 290 … 360 $_{nominal}$ … 650 ms
VT Monitor Interval (Rate)	280; 290 … 450 $_{nominal}$ … 650 ms
Mode	$VVI_{nominal}$; VVIR; VOO; OVO
Lower Rate	30; 35; $40_{nominal}$; 45 … 60; 70; 75 … 150 min^{-1}
RV Amplitude	0.50; 0.75; … $3.5_{nominal}$ … 5.00; 5.50; 6.00; 8.00 V
RV Pulse Width	0.03; 0.06; 0.10; 0.20; 0.30; $0.40_{nominal}$ … 1.5 ms
RV Sensitivity	0.15; $0.30_{nominal}$; 0.60; 0.90; 1.20 mV
RV Pacing Polarity	Bipolar; Tip to coil
RV Sensing Polarity	Bipolar; Tip to coil
Atrial Amplitude	0.5; 0.75 … 3.5 … 5; 5.5; 6; 8 V
Atrial Pulse Width	0.03; 0.06; 0.1; 0.2; 0.3; 0.4 … 1.5 ms
Atrial Sensitivity	0.15 mV (±75%); 0.3; 0.45; 0.6 mV (±50%); 0.9; 1.2; 1.5; 1.8; 2.1; 4.0 mV (±30%)

2. Cardiac implant configuration

Medtronic CareLink™ programmer for Medtronic/Vitatron devices with 2067 programming head was used to program the configurations of the DUTs. The programmer is a portable computer system used to manage cardiac devices in the clinic and procedure room. Enabled with Conexus® wireless telemetry, the programmer provides efficiency at implants and follow-up. All the DUTs (cardiac implants) were programmed and their detection and pacing parameters checked and synchronized with in the system. High voltage or ATP therapy during *in vitro* testing was disabled to prevent dangerous shocks to the test personnel.

- Pacing and sensing mode

Depending on the number of leads and the model of device, different stimulation modes can be programmed on the PMs and ICDs. An international code (NBG) developed by the North American Society of Pacing and Electrophysiology Mode Code Committee and the British Pacing and Electrophysiology Group, is defined for the classification of the various stimulation modes (*Table 4-6*). The various stimulation modes are qualified by a 4- or 5-letter code allowing understanding their basic functioning.

- The first letter defines the pacing site(s): ventricle (V), atrium (A), both (D), single chamber (S) or none (0).
- The second letter defines the detection site(s): same letters.

- The third letter indicates the operating mode: inhibited (I), triggered (T), both (D), none of the above (0).
- The fourth letter indicates the frequency control (R) or its absence (0).
- The fifth letter indicates the presence of multisite pacing: absence (0), atrial (A), ventricular (V), and dual (D: A+V).

Table 4-6 NASPE/BPEG Generic (NBG) Pacemaker Code

I	II	III	IV	V
Chamber(s) Paced	Chamber(s) Sensed	Response to Sensing	Rate Modulation	Multisite Pacing
O = None A = Atrium V = Ventricle D = Dual (A+V)	O = None A = Atrium V = Ventricle D = Dual (A+V)	O = None T = Triggered I = Inhibited D = Dual (T+I)	O = None R = Rate Modulation	O = None A = Atrium V = Ventricle D = Dual (A+V)

In order to ensure the comparability of the immunity tests on the AIMDs, all four cardiac implants were programmed with VVI mode, i.e., ventricles paced, ventricles sensed, the pulse generator inhibits pacing output in response to a sensed ventricular event. This mode of pacing prevents ventricular bradycardia and is primarily indicated in patients with atrial fibrillation with a slow ventricular response.

- Sensitivity

The sensitivity of a cardiac implant is defined as the minimum myocardial voltage required to be detected as a P wave or R wave, measured in mV, which is programmed in its system, lower the number, higher the sensitivity of the cardiac implant. The general range of sensitivity for a normal pacemaker is 0.4-10 mV for the atria, and 0.8-20 mV for the ventricles [66]. Using maximal sensitivity settings could cause the pacemaker to mistake various random fluctuations of electrical activity for cardiac activity. When the patient is subjected to EMI, it could lead to serious dysfunction or improper treatment. Automatic sensitivity function is available on some models of PMs and ICDs. When the automatic sensitivity function is activated, the device monitors the amplitude of the sensed signals. Depending on the results, the sensitivity is automatically increased or decreased to preserve a sufficient sensing margin, commensurate with the patient's sensed P and R waves.

To ensure the comparability and reproducibility of the immunity assessment on the AIMDs, the tests were conducted with the maximum sensitivity and the nominal sensitivity (*Table 4-7*).

Table 4-7 DUT models and tested sensitivities

DUT model	Tested sensitivity		
	Sensitivity Max.	Sensitivity Nom.	Other sensitivity
Advisa SR MRI SureScan	0.45 mV	Unipolar: 2.8 mV Bipolar: 0.9 mV	4 mV
Adapta	1 mV	2.8 mV	4 mV
Evera XT VR	0.15 mV	0.3 mV	0.6 mV
Secura DR	0.15 mV	0.3 mV	0.6 mV

- Pacing lead selection

The integration of the cardiac implant device and the pacing lead are crucial and play a major role for the functions of the cardiac implants. Several pacing lead types exist with different connection standard, fixation type and tip-ring spacing. According to the previous study, the tip-ring spacing plays an important role in the induced voltages on the input of the cardiac implants. Thus, the tip-ring spacings were all taken into consideration in the analysis (*Table 4-8*). In addition, active fixation leads with extendable screws in the tip which enable fixation to any place within the heart are mostly used now. Passive fixation leads as the old generation of pacing lead, designed with a lumen inside which enabled a stylet to guide the lead to the desired location, are still existing [68][69]. One passive fixation lead with tip-ring spacing of 28 mm was selected for the ICD Secura DR to observe its impact.

Table 4-8 Tested pacing lead specification

DUT	Standard	Pacing lead type	Tip-ring spacing
Advisa SR MRI SureScan	IS-1 BI	Active fixation lead	23 mm
Adapta	IS-1 BI	Active fixation lead	10 mm
Evera XT VR	IS-1 BI	Active fixation lead	10 mm
Secura DR	IS-1 BI	Passive fixation lead (old generation)	28 mm

3. Experimental set-up

In vitro immunity tests on cardiac implants were carried out in the controlled EF exposure system and in the voltage injection system. In order to be in accordance with the measurements of induced voltage conducted on the measuring system, the experimental set-up remains the same as in the experimental measurements presented in the *Chapter 3*. The probe retainer and DUT holder were employed in the immunity tests (*Figure 4-9*). To be in accordance with the experimental measurements for induced voltage, the sensing path of unipolar sensing mode was fixed at 220 mm and the sensing path of bipolar sensing mode being dependent on the physical characteristics of the lead; a distance of 40 mm was fixed between the end of the probe retainer and the extremity of the pacing lead. The exposure supplying method and the measurement transmission were all kept the same as introduced in the *chapter 3*.

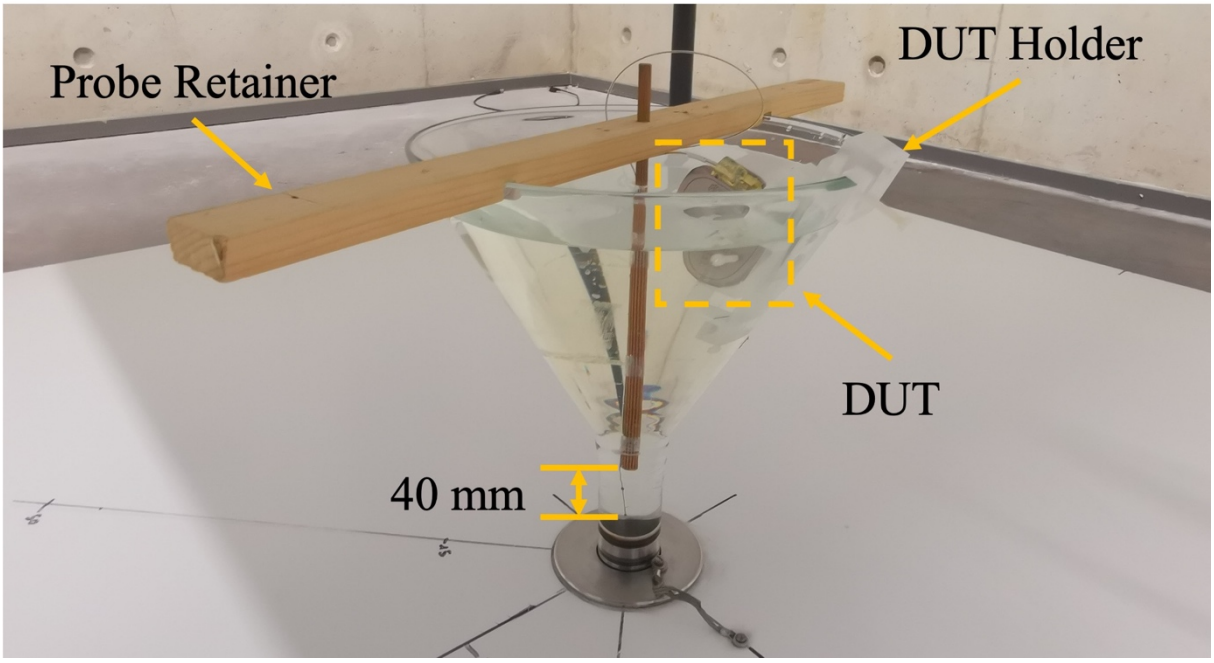

Figure 4-9 In vitro test on cardiac implants set-up for controlled EF exposure system

The cardiac implants detect abnormal heart signals and respond to cardiac events. To simulate the real-case implantation environment and to observe cardiac events generated by the electric field interference, heart signals were sent to the cardiac implants during the immunity test. The arbitrary waveform generator 33120A from Agilent delivers cardiac signals at adjustable frequency and amplitude. *Table 4-9* shows the specifications of the cardiac signal generator 33120A and an ECG generation module was built up for the immunity tests on the cardiac implants.

Table 4-9 Specifications of cardiac signal generator

Appliance	Specification
Cardiac signal generator	▪ Brand: Agilent ▪ Model: 33120A ▪ Amplitude resolution: 12 bits ▪ Bandwidth: 15 MHz ▪ Sample rate: 40 MSa/s ▪ Waveforms: Sine, square, triangle, ramp, noise, sin(x)/x, exponential rise exponential fall, cardiac, dc volts. ▪ Generate heart signal to DUTs (cardiac implants)

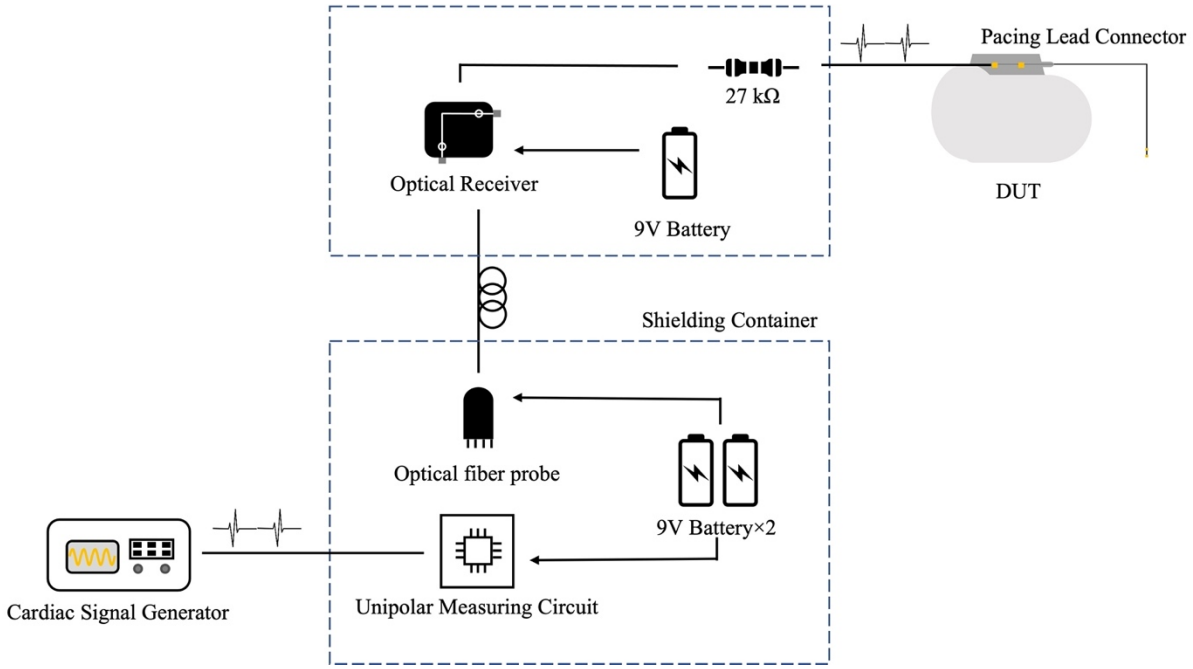

Figure 4-10 Cardiac signal generation set up

The unipolar measuring circuit was reused to receive the cardiac signals sent by the cardiac signal generator and conduct the signal transmission via optical fiber. The optical receiver AE100 was installed in a waterproof shielding container to pass the cardiac signals to the cathode connector via thin wire. Due to the low level of heart signal in real case, a resistor of 27 kΩ was placed between the output of the circuit and the connector to divide the voltage in order to obtain small amplitude. A 9 V battery supplies the optical receiver AE100. The shielding container is attached to the cardiac implant to connect the GND reference. *Figure 4-10* illustrates the experimental set-up of the cardiac signal generation module. The generated cardiac signal was verified for its form and set at a frequency of 1 Hz (*Figure 4-11*).

Typically, the amplitude of cardiac signal ranges from 0.5 mV to 1 mV. However, due to the diversity of patients' cardiac signals, the amplitude may differ between individuals. Accordingly, appropriate sensitivity setting is required. The sensitivity is usually set 3-4 times lower than the sensitivity threshold (when the cardiac signal can be detected by the pulse generator). During the test, the maximum sensitivity, nominal sensitivity, and a sensitivity with a higher value were selected for all the cardiac implants. Therefore, the cardiac signals delivered to the DUT possesses an amplitude that is 4 times the sensitivity value.

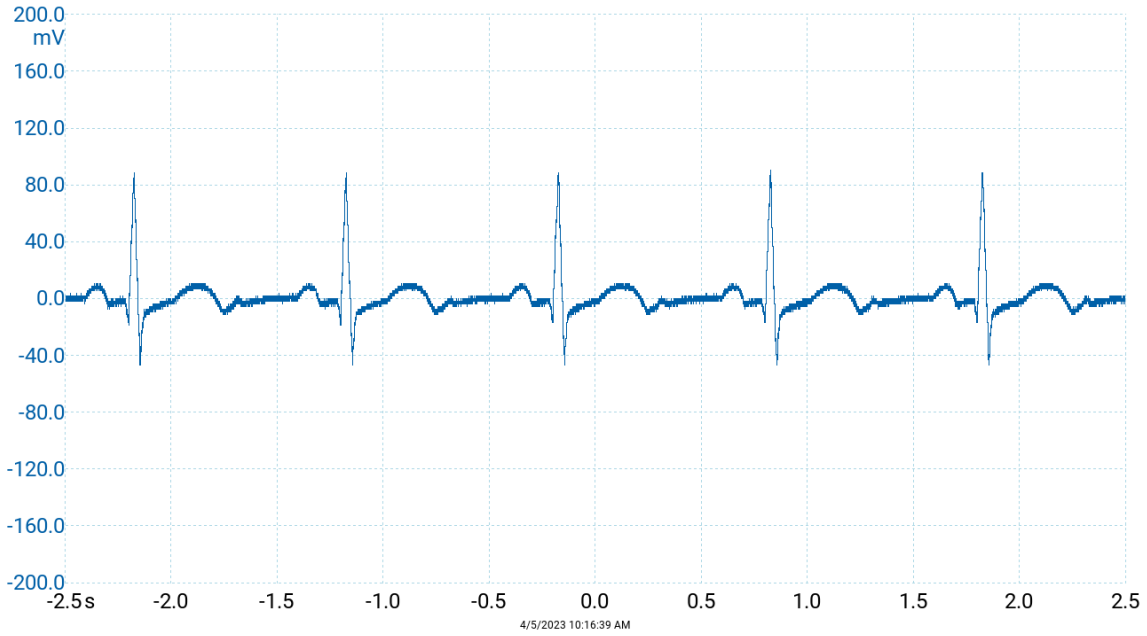

Figure 4-11 Cardiac signals delivered by the ECG signal generation module

Due to different functions that pacemakers and ICDs possess, the definitions of 'Proper functioning' and 'Dysfunction occur' are different. *Table 4-10* presents their definitions and other terms in the immunity test. The determination of the interference threshold is to perform a certain level of EF to the exposure system, then increase or decrease the intensity of the field until the maximum level of EF is reached three times in which the device is properly functioning.

Table 4-10 Definition of terms in immunity tests

Term	Device Type	Definition
VS	/	Ventricular detection
VP	/	Ventricular stimulation
VF	/	Ventricular fibrillation
TV	/	Ventricular tachycardia
FD	/	Fibrillation detected
FS	/	Fibrillation sense
TD	/	Tachycardia detected
TS	/	Tachycardia sense
Proper functioning	Pacemaker	Pacemaker reads the cardiac signals as VS
	ICD	ICD reads the cardiac signals as VS
Dysfunction occurs	Pacemaker	Device mis-reads the cardiac signals and provides pacing VP
	ICD	Device detects some events FV/TV

IV. Results and Discussion

The immunity tests were conducted on four cardiac implants for three sensitivities including the maximum sensitivity and nominal sensitivity. The PMs were tested in both unipolar and bipolar polarities of sensing and the ICDs in bipolar sensing mode (unipolar mode does not exist for ICDs).

During the immunity tests of cardiac implants, it contains four states from no perturbation to the device totally disturbed. *Figure 4-12* and *Figure 4-13* are the states of devices observed on the programmer. Cardiac signals were delivered to the PM DUTs, so the states of PMs were determined by cardiac signal sensing. The interference thresholds for ICDs were justified since with or without cardiac signal injection no difference was observed, so the states of ICDs were determined by the mistaken events. Thus, the interference threshold is the maximum level that reaches State II three times.

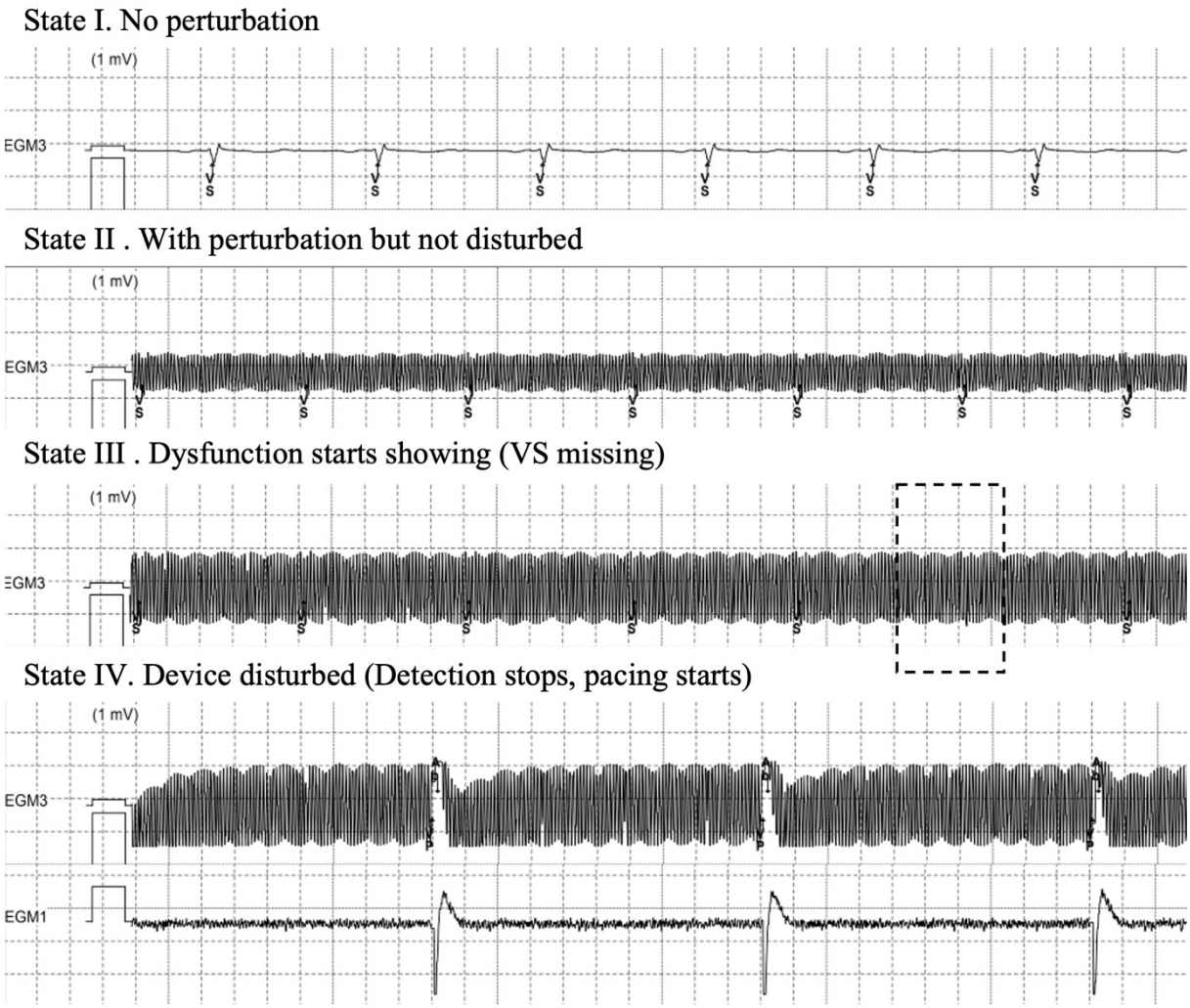

Figure 4-12 Four states of PMs in the immunity test

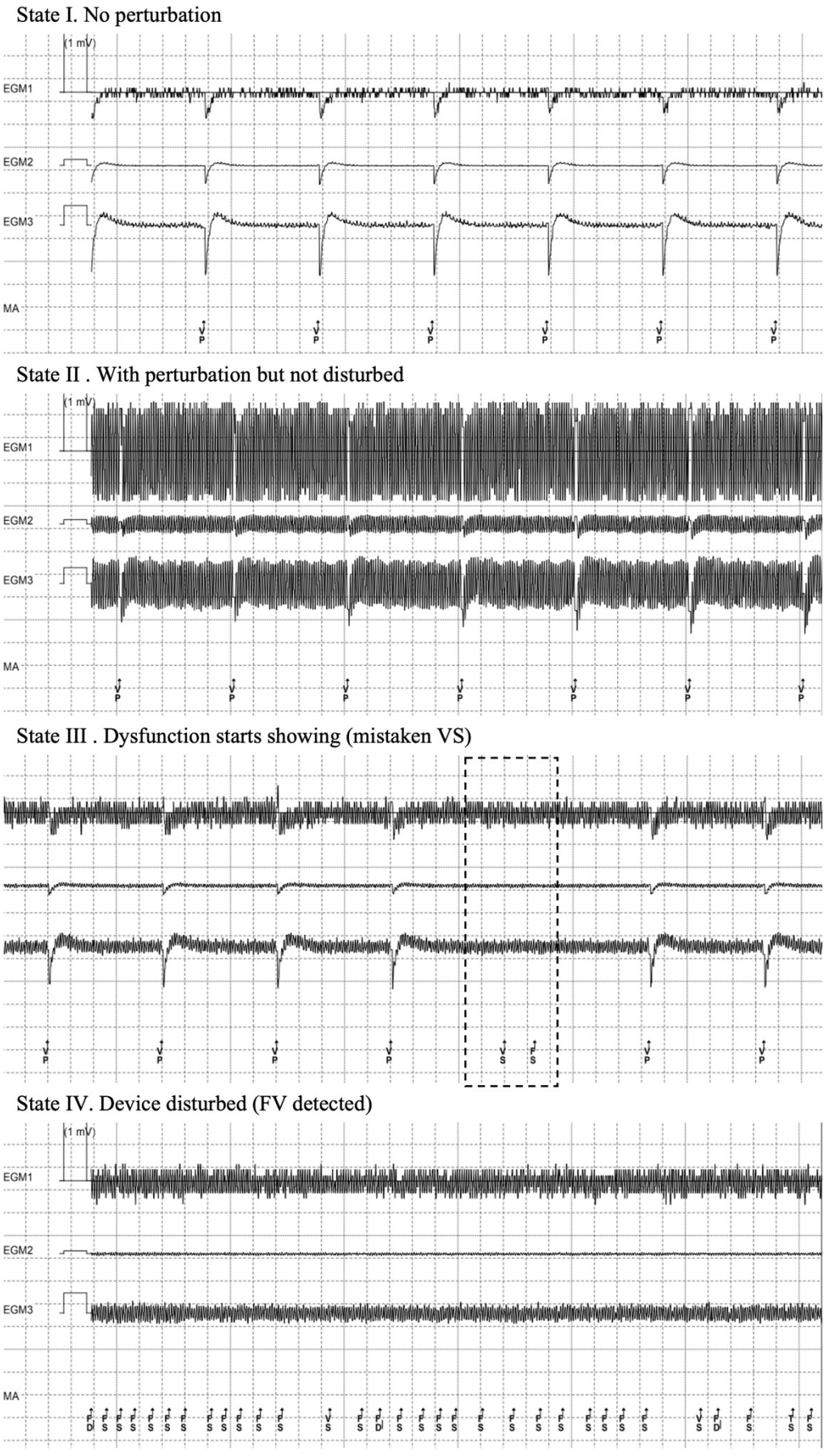

Figure 4-13 Four states of ICDs in the immunity test

The interference thresholds to the electric field exposures were investigated for the controlled EF exposure system and for the voltage injection system (*Table 4-11* for PMs and *Table 4-12* for ICDs). The interference thresholds for ANSOFT virtual human body are presented in the tables by applying the equivalences that were found previously.

Table 4-11 Interference thresholds for pacemakers Advisa SR and Adapta in controlled EF exposure system and voltage injection system for unipolar and bipolar sensing modes, and interference thresholds for ANSOFT virtual human body (real case)

Polarity	Model	Sensitivity	Controlled exposure system		Voltage injection system	
			TH.[1]	TH. $_{real\ case}$[2]	TH.[3]	TH. $_{real\ case}$[2]
		mV	kV/m	kV/m	mV	kV/m
Unipolar	Advisa SR	0.45	7.6	18.19	4.45	18.77
		2.8	7.4	17.71	4.45	18.77
		4	7.4	17.71	4.45	18.77
	Adapta	1	6	14.36	2.83	11.94
		2.8	15	35.90	9.19	38.77
		4	21.76	52.08	13.43	56.66
Bipolar	Advisa SR	0.45	26.2	95.27	12.09	66.50
		0.9	25.87	94.07	11.95	65.73
		4	23.86	86.76	11.81	64.96
	Adapta	1	44.38	161.38	32.38	178.09
		2.8	50+ [4]	182+	89.08	489.94
		4	50+	182+	129.73	713.52

1. TH. : interference threshold acquired in the controlled EF exposure system.
2. TH. $_{real\ case}$: equivalent interference threshold in the standard system (ANSOFT virtual human body).
3. TH. : interference threshold acquired in the voltage injection system.
4. The maximum level of EF in the controlled exposure system is 50 kV/m. Above this value, the quality of EF exposure cannot be ensured.

For the pacemaker Advisa SR, the interference thresholds for different sensitivities are approximate in both polarity settings and relatively high. To further investigate this phenomenon, a pacemaker from the same series, Advisa DR MRI SureScan™, was tested with the voltage injection system for bipolar sensing mode. The interference thresholds found for Advisa DR (*Table 4-12*) for three sensitivities remain in the same level as well. The algorithms embedded in the devices are not available for scientific research due to commercial copyright problems. There is no assured explanation for this case, however, we assumed that the pacemaker series Advisa was designed with the technology MRI SureScan™ to have a higher tolerance to electromagnetic interferences.

Table 4-12 Interference thresholds for pacemakers Advisa DR using voltage injection system for bipolar sensing mode, interference thresholds for ANSOFT virtual human body (real case)

Polarity	Model	Sensitivity	Voltage injection system	
			TH.	TH. real case
		mV	mV	kV/m
Bipolar	Advisa DR	0.45	16.4	96.45
		0.9	16.5	97.04
		2.8	16.2	95.28

Different from the performance of Advisa SR, the interference thresholds for the pacemaker Adapta follow the increasing of sensitivities and showed a linearity feature. The thresholds for ANSOFT virtual human body derived from the controlled EF exposure system and the voltage injection system agree to each other at specific sensitivity with small difference. When setting the device in bipolar sensing mode, in the controlled EF exposure system, no dysfunction was observed up to 50 kV/m which is the exposure limit to ensure exposure quality, i.e., up to 182 kV/m for ANSOFT virtual human body. In addition, the advantage of bipolar polarity was well presented on the pacemaker Adapta, the interference thresholds for bipolar sensing mode in the two exposure systems are more than 10 times higher than those in unipolar sensing mode for the same sensitivity setting.

Table 4-13 Interference thresholds for ICDs Secura DR and Evera XT VR in controlled EF exposure system and voltage injection system for bipolar sensing mode, and interference thresholds for ANSOFT virtual human body (real case)

Model	Sensitivity	Controlled EF exposure system		Voltage injection system	
		TH.	TH. real case	TH.	TH. real case
	mV	kV/m	kV/m	mV	kV/m
Secura DR	0.15	0.67	2.44	0.42	2.31
	0.3	1.52	5.53	0.95	5.23
	0.6	3	10.91	1.91	10.51
Evera XT VR	0.15	1.84	6.69	1.13	6.22
	0.3	4	14.55	2.47	13.59
	0.6	8.35	30.36	4.95	27.23

Linearity of the interference thresholds on ICDs along the increasing of sensitivity was well presented in *Table 4-13*. According to the immunity tests on the ICD Secura DR, a threshold of 2.44/2.31 kV/m (derived from controlled EF exposure system / voltage injection system) was found at the maximum sensitivity 0.15 mV in bipolar sensing mode. In this case, the dysfunction occurred under the reference public exposure limit in the ICNIRP which gave rise to a serious alert. Secura DR was integrated with a passive fixation lead from the old generation, with a tip-

to-ring spacing of 28 mm. To further investigate the susceptibility caused by the passive fixation lead, Secura DR was tested in the voltage injection system, integrated with an active fixation lead with a tip-ring spacing of 10 mm. The interference thresholds for Secura DR with the active fixation lead (10 mm tip-ring spacing) were found (*Table 4-14*) more than 3 times higher than with the passive fixation lead (28 mm tip-ring spacing).

Table 4-14 Interference thresholds for Secura DR with an active fixation lead (tip-ring spacing 10 mm) in voltage injection system, and interference thresholds for ANSOFT virtual human body (real case)

Model	Sensitivity	Voltage injection system	
		TH.	TH. $_{\text{real case}}$
	mV	mV	kV/m
Secura DR	0.15	1.4	8.23
	0.3	3.1	18.23
	0.6	6.1	35.88

It is justified that Secura DR was subjected to more interference with integrating to the passive fixation pacing lead. The difference between the interference thresholds is certainly caused by the different tip-ring spacings but doesn't completely conform to their ratio (28/10). Thus, we can assume that the fixation method may have influence on the immunity of cardiac implants. Due to lack of proper leads, further studies haven't been carried out yet and may be expected from the perspective. The tip-to-ring spacing has influence on the voltage induced on the input of the device and the typical tip-to-ring spacing for a bipolar lead is 10-14 mm. The devices within the scope of the European Standards are tested by their manufacturers to ensure the immunity under standardized exposure levels. However, the device shall not demonstrate malfunction when set to a sensitivity of 0.3 mV, with the assumption of bipolar sensing leads having a tip-to-ring spacing of 20 mm [70]. The measurements conducted in the experimental set-up took a bipolar lead with a tip-to-ring distance of 12 mm. Further investigation was carried out on the induced voltages on specific DUTs with considering their tip-to-ring spacing (*Table 4-15*).

Table 4-15 Induced voltage on the DUTs per unit dose of exposure indicator

Model	Tip-ring spacing	Polarity	Induced voltage per unit dose of exposure indicator[1]	
			Controlled EF exposure system	Voltage injection system
	mm		mV	mV
Advisa SR	23	Unipolar	0.84	1.48
		Bipolar	0.15	0.23
Adapta	10	Unipolar	0.37	0.64
		Bipolar	0.07	0.10
Secura DR	28	Bipolar	0.19	0.28
Evera XT VR	10	Bipolar	0.07	0.10

1. The unit dose of exposure indicator is: 1 kV/m EF exposure in the controlled EF exposure system; 1 mV voltage injection in the voltage injection system.

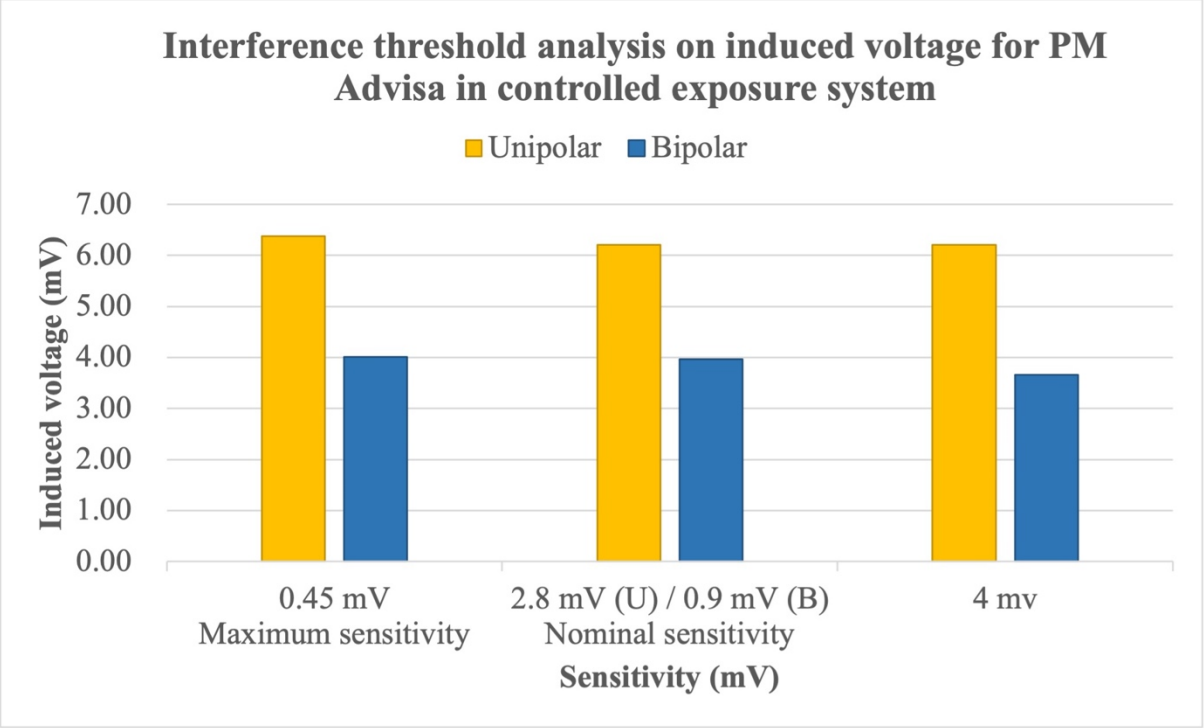

Figure 4-14 Interference threshold analysis on induced voltage for PM Advisa SR in controlled exposure system

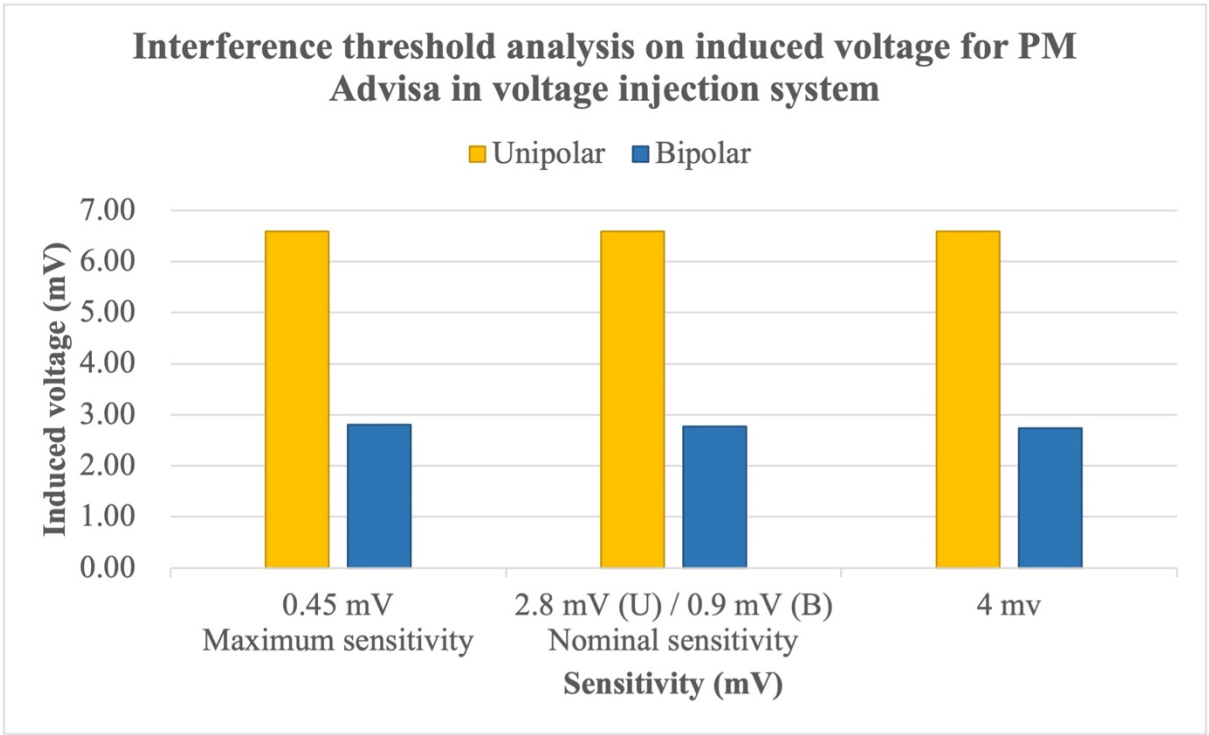

Figure 4-15 Interference threshold analysis on induced voltage for PM Advisa SR in voltage injection system

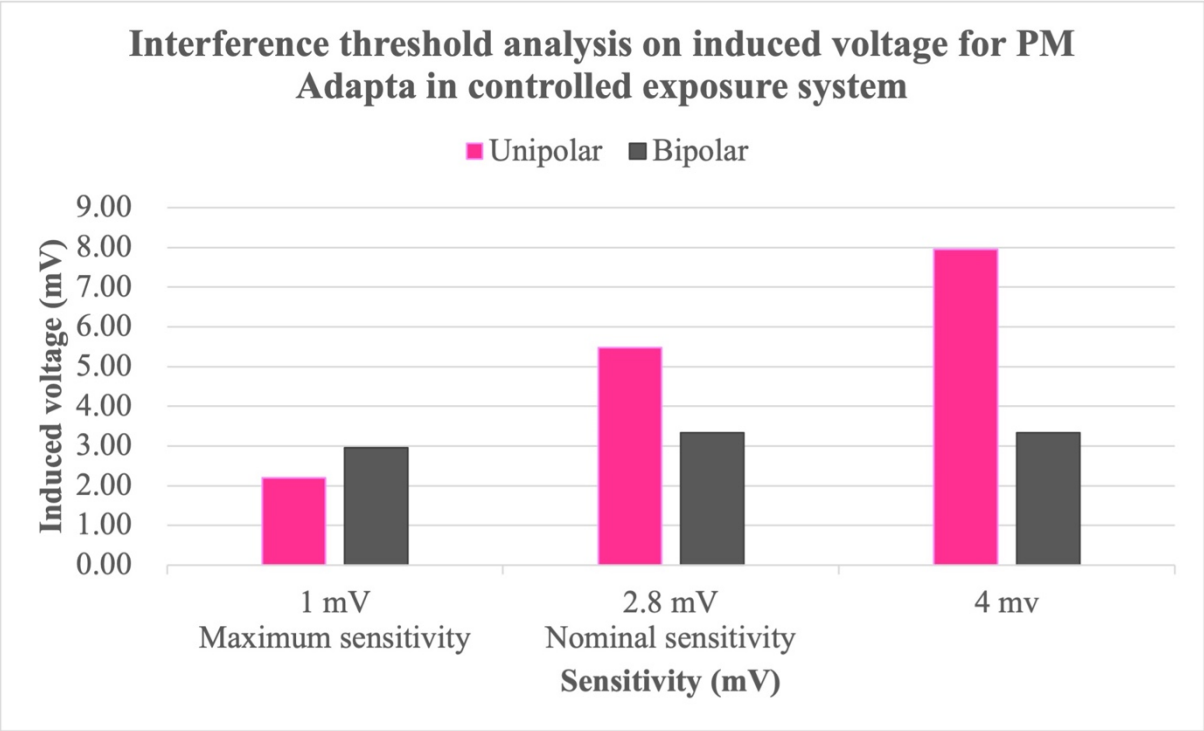

Figure 4-16 Interference threshold analysis on induced voltage for PM Adapta in controlled exposure system

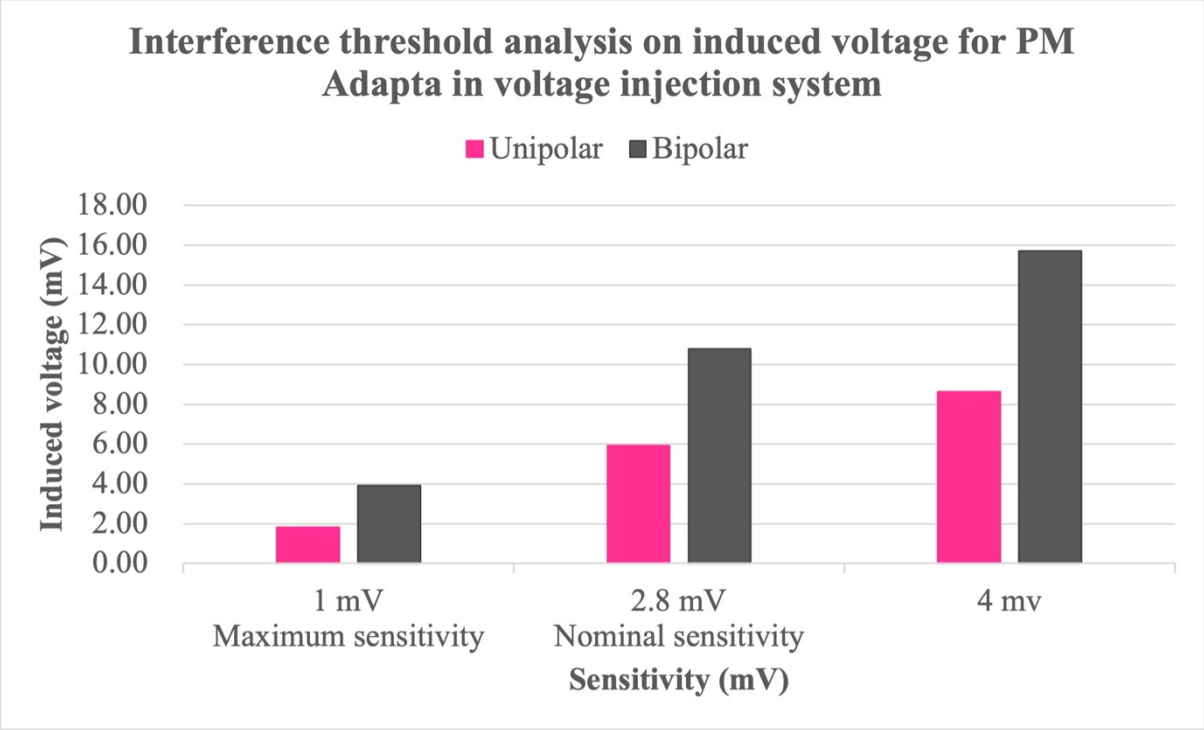

Figure 4-17 Interference threshold analysis on induced voltage for PM Adapta in voltage injection system

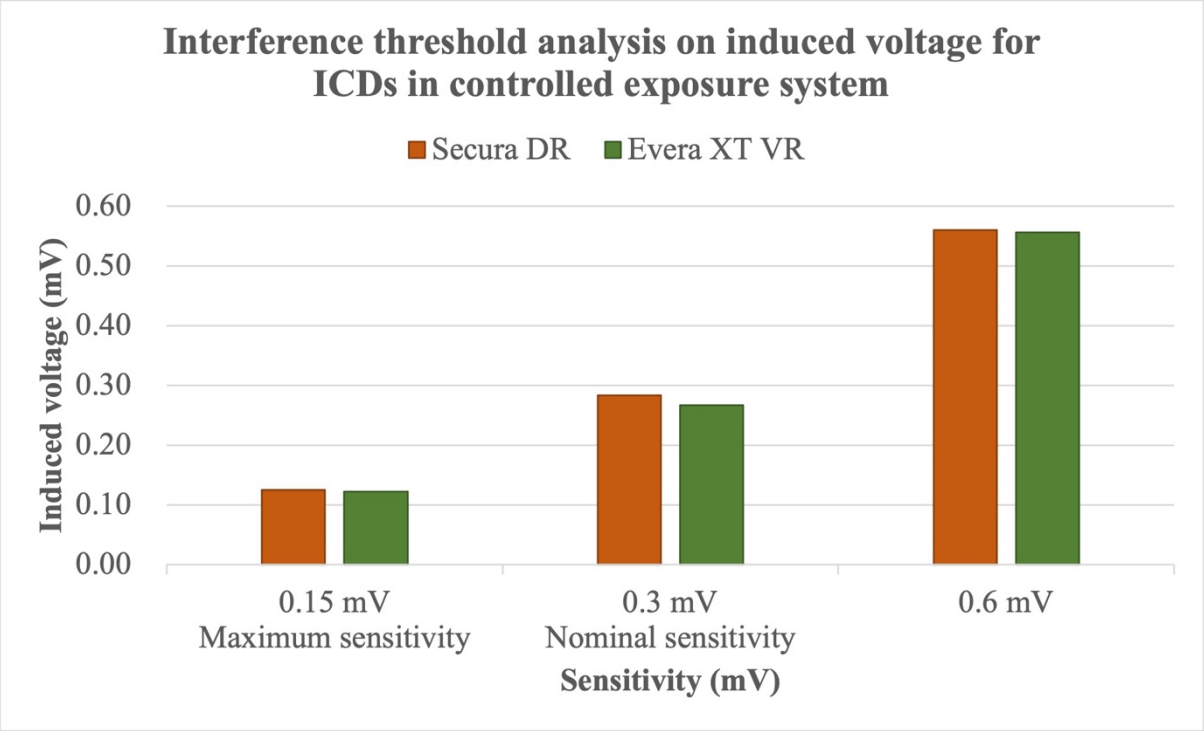

Figure 4-18 Interference threshold analysis on induced voltage for ICDs in controlled exposure system

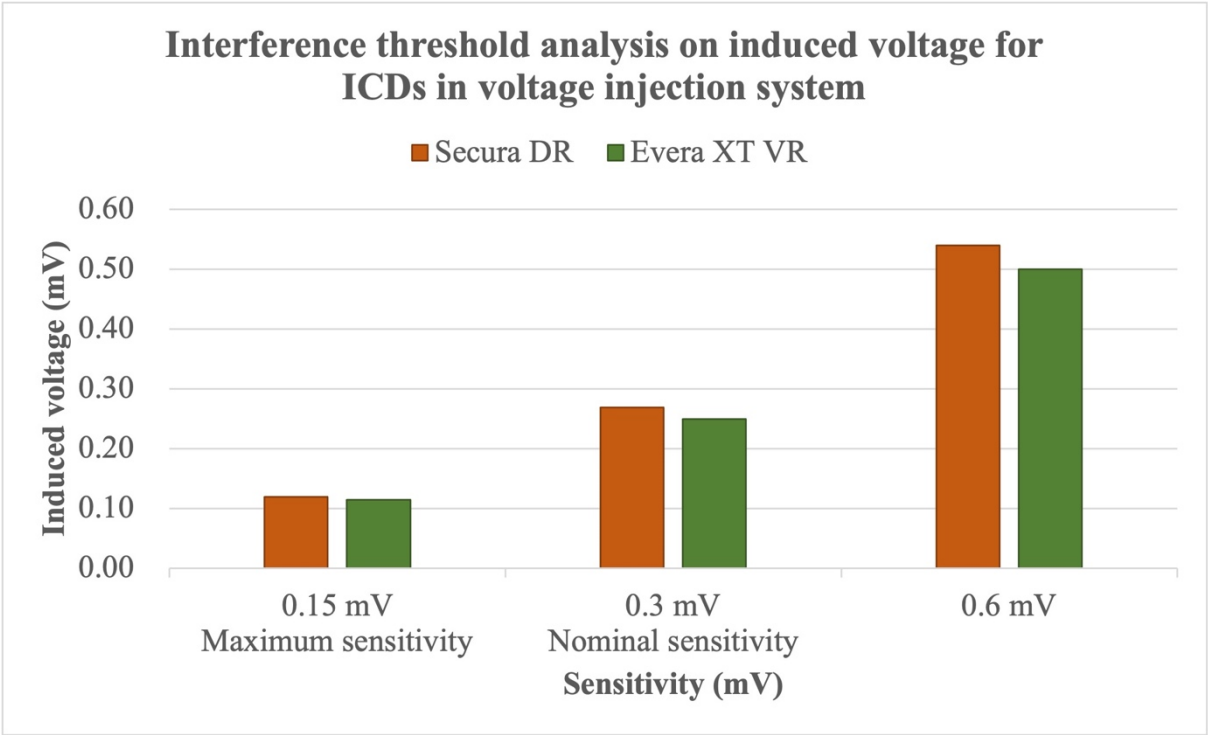

Figure 4-19 Interference threshold analysis on induced voltage for ICDs in voltage injection system

Figure 4-14, 4-15, 4-16, 4-17 present the estimation of the induced voltage for the controlled EF exposure system and for the voltage injection system, based on the interference threshold analysis for pacemaker DUTs in unipolar and bipolar sensing mode. Except Advisa SR and Adapta with a sensitivity of 4 mV in bipolar sensing mode, the induced voltages were all found above the level of sensitivity setting.

Figure 4-18, 4-19 present the estimation of the induced voltage based on the interference threshold analysis for ICD DUTs. For the ICDs, the induced voltages were all found below the level of sensitivity setting. Thus, ICDs are more susceptible, in other words, ICDs are subjected to more interference and have relatively low thresholds to the electric fields. The configuration of devices and the selection of pacing leads should be conducted cautiously. The integration of ICD Secura DR and the passive bipolar lead with a long tip-to-ring spacing is not adequate for public and occupational occasions. In the investigation of the interference thresholds for ICD under EF exposures (Gercek C., 2016), 6 ICDs out of a total of 11 were found at the maximum sensitivity (0.15 mV) with thresholds 5-6 kV/m, which is coherent to our findings. By applying the method introduced in previous, the induced voltages on the tested devices in this study can be estimated with configuration specified.

V. Conclusion

Based on the numerical approach and the experimental approach introduced in the *Chapter 2* and *Chapter 3*, the risk assessment for AIMDs exposed to occupational EF at extremely low frequency (50 Hz) was established in this chapter. The risk assessment procedure was proposed in *Figure 4-4* for AIMD-employees in the workplace. To perform an equivalent exposure test on a cardiac implant device, the exposure indicator can be verified in *Figure 4-2* and *Figure 4-3* which include the exposure level limits on the standards and guidelines as references.

Four AIMDs (two PMs and two ICDs) were selected to conduct immunity test in the experimental set-ups of controlled EF exposure system and voltage injection system as the vitally important step in the risk assessment procedure. Interference thresholds were investigated in the four DUTs and corresponding analysis on the induced voltage were carried out. In addition to the equivalence between the three systems that we obtained during the validation of the risk assessment procedure; it was justified that the voltage injection system is a qualified equivalent system that reproduces the same effect on the input of the cardiac implants as high-intensity EF exposure. Thus, it can be used in the risk assessment for AIMD-employees in the workplace.

General Conclusion & Perspectives

In light of concerns regarding the occupational safety and health of workers wearing cardiac implants, a novel and simple approach for conducting immunity test on AIMDs was proposed in order to build up the risk assessment procedure for AIMD-employees who are likely to be subjected to EMI in the workplace. In this study, the immunity tests on cardiac implants was studied with numerical and experimental approaches in parallel. Three exposure systems were proposed on the basis of the estimation of the induced voltage at the input of cardiac implants under electric field exposure: 1) ANSOFT virtual human body as the standard system to study the real-case exposure; 2) Controlled EF exposure system as equivalent system A to reproduce the same effect on the cardiac implant under equivalent exposure; 3) Voltage injection system as equivalent B to reproduce the same effect on the cardiac implant with a manageable parameter. The association of the three systems validated the innovated immunity test on cardiac implants under high-intensity electric field exposures for the risk assessment in the workplaces.

Retro background and literature study were conducted in ***Chapter 1***. The histories, developments, challenges, and causes underlie the interference to cardiac implants were introduced as well as the related contents of standards, guidelines, and studies.

Theoretical and numerical studies on the subject were carried out in ***Chapter 2***. The association of the standard system and equivalent systems was proposed based on the estimation of the induced voltage at the input of the cardiac implant. The principles of the systems and the phantoms were detailed described and justified by simulation in the software CST EM®. The association was numerically validated for the purpose of establishing the risk assessment process. Taking ANSOFT virtual human body as a standard system, we obtained an equivalence factor of 2.3 for unipolar sensing mode and 2.82 for bipolar sensing mode for controlled EF exposure system; an equivalence factor of 3.65 for unipolar sensing mode and 5.32 for bipolar sensing mode for voltage injection system.

The design and implementation of the experimental approach were conducted in ***Chapter 3***. The equivalent exposure systems were built up according to the conception introduced in *Chapter 2*. A measuring system was designed and fabricated to measure the induced voltage on the cardiac implants under exposures. From the experimental measurements, we obtained an equivalence factor of 2.39 for unipolar sensing mode and 3.64 for bipolar sensing mode for controlled EF exposure system; an equivalence factor of 4.22 for unipolar sensing mode and 5.50 for bipolar sensing mode for voltage injection system. The equivalences between the systems led to the immunity test in the risk assessment procedure introduced in *Chapter 4*.

The risk assessment procedure was defined and applied to four cardiac implants in ***Chapter 4***. Exposure limitation indicated by the standards and guidelines were explored for exposure levels in the association of the three systems and their induced voltage. Four cardiac implants (two PMs and two ICDs) were investigated for the interference thresholds by applying the immunity test and the transformation between systems in order to analyze the potential risk for the devices. The induced voltages derived from the interference thresholds follow the adjustments of cardiac

implants' sensibility in most of the cases. The performance was unfavorable when a passive lead with a tip-ring spacing of 28 mm was selected on an ICD.

In conclusion, the interference to AIMD carriers caused by high-intensity electric field at 50 Hz was investigated and analyzed from physical characteristic aspect with *in vitro* study. An immunity test process for cardiac implants was proposed to construct the risk assessment procedure for AIMD-employees in the workplace.

In perspective of the establishment of the risk assessment procedure, normative documents are required for the description of immunity test construction and the expression of risk assessment process flow. The *in vitro* test in controlled EF exposure system and voltage injection system may serve to other virtual human bodies as its equivalent systems. Further investigation can be conducted for *in vivo* studies if it is possible to obtain the interference thresholds in patients, that corresponding physical quantities can be determined and analyzed for cases in the *in vivo* studies.

In perspective of the experimental approach, considering the small scale of the voltages to be measured, certain aspects can be refined to further simulate the real situation. The saline water, as phantom liquid material does not allow to maintain the homogeneity of the phantom steadily. Along with the downward movement of NaCI in the liquid, the lower part of the phantom may possess higher conductivity than upper part. Thus, gel can be taken into consideration for maintaining both the position of DUT and the homogeneity of the conductivity distribution. Although the sensing path configuration was precisely controlled to measure the induced voltage on cardiac implants, the size of measuring system is still four times larger than typical implant housing. A measuring system with reduced size may have less influence on the field distribution near it and less impact on the measurement of unipolar sensing mode. In the immunity test on cardiac implants, an experimental set-up was used to deliver standard heart signals to the phantom. Yet in real cases, heart signals vary in amplitude, frequency, and formation, especially for patients who suffer from heart diseases.

In addition, workers are typically exposed to electric fields, magnetic fields, and the combination of both. This thesis has been focused on the occupational electric field exposure at extremely low frequency (50 Hz). The utility frequency in the Americas and parts of Asia is typically 60 Hz. The immunity test configuration can be slightly adjusted to perform the tests at 60 Hz thereby building up the risk assessment procedure for those regions. Furthermore, research work can be carried out in magnetic fields following the same pattern with different configurations, as well as the combination of the electric field and magnetic field.

Abbreviations and units

ABBREVIATIONS

AIMD	active implantable medical device
CVD	cardiovascular disease
CHD	coronary heart disease
EMF	electromagnetic field
EMI	electromagnetic interference
EMC	electromagnetic compatibility
EF	electric field
MF	magnetic field
PM	pacemaker
ICD	implantable cardioverter defibrillator
CRT	cardiac resynchronization therapy
MRI	magnetic resonance imaging
AL	action level
ELV	exposure limit value
DRL	dosimetric reference limits
ERL	exposure reference levels
ICNIRP	International Commission on Non-Ionizing Radiation Protection
EN/IEC	European standard
AC	alternative current
HVAC	high voltage alternating current

INDICATIONS

ε	dielectric permittivity
σ	electrical conductivity
$\vec{E}$	electric field

k_E	shape factor
F	equivalence factor
f	frequency
U	voltage (induced)
V	voltage (injected)
rms	root mean square
GND	ground

Units of measurement

kV/m	kilovolt per meter
Vpp	voltage in peak to peak
V/m	volt per meter
mT	millitesla
µV	microvolt
mm	millimeter
Hz	hertz
S/m	Siemens per meter
Ω	ohm
ms	millisecond

Annex

I. Measured electric fields corresponding to the input of the generator and the output of the amplifier.

Generator input	Amplifier output	Measured EF	Generator input	Amplifier output	Measured EF
mVpp	Vpp	kV/m	mVpp	Vpp	kV/m
30	0.786	0.89	280	7.5	9
37	0.88	1	280	7.94	9.44
40	1.04	1.2	300	8.4	10
50	1.3	1.52	308	8.36	10
60	1.56	1.84	338	9.16	11
68	1.65	2	368	10	12
70	1.85	2.16	390	11	13
80	2.11	2.5	400	11.3	13.35
90	2.38	2.81	420	11.8	14
100	2.64 / 2.57	3	450	12.6	15
110	2.9	3.4	500	14	16.7
120	3.18	3.74	600	17	20
130	3.35	4	700	19.8	23.4
130	3.44	4.07	800	22.5	26.76
140	3.71	4.4	900	25.2	29.11
150	4.1	4.73	925	25.9	30
160	4.3	5	1000	28	32.54
160	4.36	5.06	1220	34	40
170	4.7	5.48	1250	34.8	41
180	5.2	6.04	1500	42.2	49.6
190	5.1	6	1510	42.6	50
190	5.48	6.38	1750	50.2	59.4
200	5.78	6.73	1780	50.6	60
220	5.9	7	2000	59	70
220	6.3	7.4	2010	58.6	70
225	6.46	7.5	2215	66.2	80
240	6.86	7.8	2250	68.4	83
250	6.7	8	2410	75	90
260	7.4	8.7	2500	80	97

II. Induced voltage measured (Gain: 1) in the controlled EF exposure system for unipolar sensing mode, results from oscilloscope Picotech 5000 (RMS value) and results from signal processing in MATLAB.

EF	Measuring System Output	Induced Voltage	Induced Voltage per 1 kV/m Exposure	Measuring System Output at 50 Hz	Induced Voltage at 50 Hz	Induced Voltage per 1 kV/m Exposure
kV/m	mVrms	uVrms	uV	mVpeak	uVrms	uV
	Oscilloscope			FFT		
1.52	8.093	2861	1882	0.96	677.28	446
2.16	8.93	3157	1461	1.25	881.57	408
4.00	11.53	4076	1019	2.60	1837.59	459
5.00	16.93	5985	1197	3.22	2276.60	455
6.04	17.12	6052	1002	3.32	2344.08	388
7.00	18.23	6444	921	4.21	2979.77	426
8.00	16.74	5918	740	4.82	3408.26	426
9.00	17.67	6246	694	5.50	3887.78	432
10.00	19.91	7038	704	5.92	4188.09	419
11.00	21.02	7431	676	6.71	4745.50	431
12.00	23.44	8286	691	7.33	5181.29	432
13.35	24.37	8615	645	7.99	5651.07	423
14.00	24.74	8746	625	8.43	5957.26	426
15.00	25.49	9011	601	9.05	6396.70	426
16.70	27.53	9732	583	10.06	7113.49	426
20.00	33.02	11673	584	12.14	8580.23	429
23.40	36.74	12988	555	14.18	10024.06	428
26.76	40.93	14469	541	16.18	11439.41	427
29.11	44.18	15618	537	18.24	12893.86	443
32.54	48.84	17265	531	20.33	14376.43	442
49.60	66.93	23660	477	30.64	21659.82	437
70.00	101.3	35810	512	42.77	30237.93	432

III. Induced voltage measured (Gain: 47.168) in the controlled EF exposure system for bipolar sensing mode, results from oscilloscope Picotech 5000 (RMS value) and results from signal processing in MATLAB.

EF	Measuring System Output	Induced Voltage	Induced Voltage per 1 kV/m Exposure	Measuring System Output (50 Hz)	Induced Voltage (50 Hz)	Induced Voltage per 1 kV/m Exposure
kV/m	mVrms	uVrms	uV	mVpeak	uVrms	uV
	Oscilloscope			FFT		
1.52	21.4	160	106	7.68	115	76
2.16	27.44	206	95	11.14	167	77
3.00	38.14	286	95	16.34	245	82
4.00	48.37	363	91	21.53	323	81
5.00	58.14	436	87	25.57	383	77
6.04	64.19	481	80	28.94	434	72
7.00	77.67	582	83	35.17	527	75
8.00	88.31	662	83	40.70	610	76
9.00	98.54	739	82	45.96	689	77
10.00	106	794	79	49.53	742	74
11.00	119	892	81	56.49	847	77
12.00	130.1	975	81	61.65	924	77
13.35	143.2	1073	80	68.82	1032	77
14.00	149.7	1122	80	72.25	1083	77
15.00	161.6	1211	81	77.54	1162	77
16.70	178.3	1336	80	86.23	1292	77
20.00	213.5	1600	80	103.93	1558	78
23.40	251.8	1887	81	121.69	1824	78
26.76	289.2	2167	81	139.38	2089	78
29.11	326.5	2447	84	156.94	2352	81
32.54	363.8	2726	84	174.60	2617	80
49.60	540.9	4054	82	263.94	3956	80
70.00	820.7	6151	88	368.93	5530	79

IV. Induced voltage measured (Gain: 1) in the voltage injection system for unipolar sensing mode, results from oscilloscope Picotech 5000 (RMS value) and results from signal processing in MATLAB.

Voltage Injection	Measuring System Output	Induced Voltage	Induced Voltage per 1 mV injection	Measuring System Output (50 Hz)	Induced Voltage (50 Hz)	Induced Voltage per 1 mV injection
mVrms	mVrms	uVrms	uV	mVpeak	uVrms	uV
	Oscilloscope			FFT		
36.1	75.81	26798.84	742.35	35.32	24969.62	691.68
39.2	83.25	29428.88	750.74	39.13	27663.03	705.69
47.3	102.3	36163.05	764.55	48.65	34392.52	727.11
55.6	124.6	44046.10	792.20	58.16	41120.89	739.58
72.6	159	56206.50	774.19	76.80	54301.13	747.95
80.2	180.1	63665.35	793.83	87.24	61676.04	769.03
90.7	198.7	70240.45	774.43	96.69	68362.62	753.72
99.3	217.3	76815.55	773.57	105.87	74851.93	753.80
108	235.8	83355.30	771.81	115.21	81450.28	754.17
113.2	247	87314.50	771.33	120.86	85449.00	754.85
126.9	276.7	97813.45	770.79	135.85	96046.51	756.87
133.9	291.5	103045.25	769.57	143.31	101318.43	756.67
142.6	310.1	109620.35	768.73	152.66	107930.51	756.88
160	354.5	125315.75	783.22	171.64	121352.28	758.45
178.1	391.8	138501.30	777.66	190.97	135012.97	758.07

V. Induced voltage measured (Gain: 47.168) in the voltage injection system for bipolar sensing mode, results from oscilloscope Picotech 5000 (RMS value) and results from signal processing in MATLAB.

Voltage Injection	Measuring System Output	Induced Voltage	Induced Voltage per 1 mV injection	Measuring System Output (50 Hz)	Induced Voltage (50 Hz)	Induced Voltage per 1 mV injection
mVrms	mVrms	uVrms	uV	mVpeak	uVrms	uV
	Oscilloscope			FFT		
36	494.4	3705.27	102.92	243.43	3649	101.35
39.5	559.7	4194.66	106.19	275.50	4130	104.55
47.5	694.9	5207.92	109.64	343.71	5152	108.46
55.8	834.8	6256.40	112.12	412.52	6183	110.81
72.9	1110	8318.88	114.11	549.99	8244	113.08
81.5	1250	9368.11	114.95	618.53	9271	113.76
90.2	1390	10417.34	115.49	687.77	10309	114.29
99	1530	11466.57	115.82	756.80	11344	114.58
107.7	1676	12560.76	116.63	825.20	12369	114.85
113.5	1807	13542.54	119.32	894.00	13400	118.06
127.1	1956	14659.22	115.34	963.02	14435	113.57
133.8	2086	15633.50	116.84	1031.99	15468	115.61
142.7	2216	16607.78	116.38	1100.95	16502	115.64
160.3	2514	18841.14	117.54	1239.20	18574	115.87
162.2	2645	19822.92	122.21	1307.92	19604	120.87
178	2775	20797.20	116.84	1376.42	20631	115.91

Reference

[1] Aquilina, Oscar. “A brief history of cardiac pacing.” Images in paediatric cardiology vol. 8,2 (2006): 17-81.

[2] Writing committee of the report on cardiovascular health and diseases in china. “Report on cardiovascular health and diseases in China 2021: an updated summary.” Biomedical and environmental sciences : BES vol. 35,7 (2022): 573-603. doi:10.3967/bes2022.079

[3] van Hemel, N M, and E E van der Wall. “8 October 1958, D Day for the implantable pacemaker.” Netherlands heart journal : monthly journal of the Netherlands Society of Cardiology and the Netherlands Heart Foundation vol. 16,Suppl 1 (2008): S3-4.

[4] Nordbeck, Peter et al. “Magnetic resonance imaging safety in pacemaker and implantable cardioverter defibrillator patients: how far have we come?” European heart journal vol. 36,24 (2015): 1505-11. doi:10.1093/eurheartj/ehv086

[5] Strom, Jordan B et al. “Safety and utility of magnetic resonance imaging in patients with cardiac implantable electronic devices.” Heart rhythm vol. 14,8 (2017): 1138-1144. doi:10.1016/j.hrthm.2017.03.039

[6] Nazarian, Saman et al. “Clinical utility and safety of a protocol for noncardiac and cardiac magnetic resonance imaging of patients with permanent pacemakers and implantable-cardioverter defibrillators at 1.5 tesla.” Circulation vol. 114,12 (2006): 1277-84. doi:10.1161/CIRCULATIONAHA.105.607655

[7] Directive 2013/35/EU of the European Parliament and of the Council of 26 June 2013 on the Minimum Health and Safety Requirements Regarding the Exposure of Workers to the Risks Arising from Physical Agents (Electromagnetic Fields) (20thIndividual Directive within the meaning of Article 16(1) of Directive 89/391/EEC) and Repealing Directive 2004/40/EC.

[8] Timmis, Adam et al. “European Society of Cardiology: Cardiovascular Disease Statistics 2017.” European heart journal vol. 39,7 (2018): 508-579. doi:10.1093/eurheartj/ehx628

[9] Tsao, Connie W et al. “Heart Disease and Stroke Statistics-2022 Update: A Report From the American Heart Association.” Circulation vol. 145,8 (2022): e153-e639. doi:10.1161/CIR.0000000000001052

[10] Glikson, Michael et al. “2021 ESC Guidelines on cardiac pacing and cardiac resynchronization therapy.” European heart journal vol. 42,35 (2021): 3427-3520. doi:10.1093/eurheartj/ehab364

[11] Timmis, Adam et al. “European Society of Cardiology: cardiovascular disease statistics 2021: Executive Summary.” European heart journal. Quality of care & clinical outcomes vol. 8,4 (2022): 377-382. doi:10.1093/ehjqcco/qcac014

[12] Hopps, John A. "The Development of the Pacemaker." Pacing and Clinical Electrophysiology vol 4 (1981): 106-108. https://doi-org.bases-doc.univ-lorraine.fr/10.1111/j.1540-8159.1981.tb03682.x

[13] Lown, Bernard, and Axelrod, Paul. "Implanted standby defibrillators." Circulation vol. 46,4 (1972): 637-9. doi: 10.1161/01.cir.46.4.637

[14] Gasparini, Maurizio, and Seah Nisam. "Implantable cardioverter defibrillator harm?" Europace vol. 14,8 (2012): 1087-93. doi:10.1093/europace/eus025

[15] Matchett, Melissa et al. "The implantable cardioverter defibrillator: its history, current psychological impact and future." Expert review of medical devices vol. 6,1 (2009): 43-50. doi:10.1586/17434440.6.1.43

[16] Jiang, Meng et al. "Comparison of CRT and CRT-D in heart failure: systematic review of controlled trials." International journal of cardiology vol. 158,1 (2012): 39-45. doi:10.1016/j.ijcard.2010.12.091

[17] Shakibfar, Saeed et al. "Effectiveness of CRT-D Versus ICD on Prevention of Electrical Storm: Big Data from the USA." IEEE Engineering in Medicine and Biology Society. Annual International Conference vol. 2019 (2019): 302-304. doi:10.1109/EMBC.2019.8857530

[18] Martínez-Sande, José Luis et al. "The Micra Leadless Transcatheter Pacemaker. Implantation and Mid-term Follow-up Results in a Single Center." Revista espanola de cardiologia (English ed.) vol. 70,4 (2017): 275-281. doi:10.1016/j.rec.2016.11.027

[19] Ouyang, Han et al. "Symbiotic cardiac pacemaker." Nature communications vol. 10,1 1821. 23 Apr. 2019, doi:10.1038/s41467-019-09851-1

[20] Peskin, Michael et al. An Introduction to Quantum Field Theory. Westview Press. (1995) ISBN 978-0-201-50397-5.

[21] "Electromagnetic Fields 2009 Update." Electromagnetic Fields: 1. Introduction to Electromagnetic Fields, ec.europa.eu/health/scientific_committees/opinions_layman/en/electromagnetic-fields/l-2/1-electromagnetic-fields.htm#0. Accessed 28 June 2023.

[22] The world bank. Access to electricity (% of population), 1990-2020. https://data.worldbank.org/indicator/EG.ELC.ACCS.ZS

[23] The National Institute for Occupational Safety and Health (NIOSH) EMFs in the Workplace. [(accessed on 29 January 2021)]; Available online: https://www.cdc.gov/niosh/docs/96-129/default.html

[24] Migault, Lucile et al. "Development of a Job-Exposure Matrix for Assessment of Occupational Exposure to High-Frequency Electromagnetic Fields (3 kHz-300 GHz)." Annals of work exposures and health vol. 63,9 (2019): 1013-1028. doi:10.1093/annweh/wxz067

[25] Furman, Syemour et al. “The influence of electromagnetic environment on the performance of artificial cardiac pacemakers.” The Annals of thoracic surgery vol. 6,1 (1968): 90-5. doi:10.1016/s0003-4975(10)65997-8

[26] Daubert, James P et al. “Inappropriate implantable cardioverter-defibrillator shocks in MADIT II: frequency, mechanisms, predictors, and survival impact.” Journal of the American College of Cardiology vol. 51,14 (2008): 1357-65. doi:10.1016/j.jacc.2007.09.073

[27] Zink, Matthias Daniel et al. “In Vivo Study of Electromagnetic Interference With Cardiac Contractility Modulation Devices at Power Frequency.” Journal of the American Heart Association vol. 10,17 (2021): e019171. doi:10.1161/JAHA.120.019171

[28] Kursawe, Michael et al. “Human detection thresholds of DC, AC, and hybrid electric fields: a double-blind study.” Environmental health : a global access science source vol. 20,1 92. 21 Aug. 2021, doi:10.1186/s12940-021-00781-4

[29] Stunder, Dominik et al. “In Vivo Study of Electromagnetic Interference With Pacemakers Caused by Everyday Electric and Magnetic Fields.” Circulation vol. 135,9 (2017): 907-909. doi:10.1161/CIRCULATIONAHA.116.024558

[30] Seidman, Seth J et al. “In vitro tests reveal sample radiofrequency identification readers inducing clinically significant electromagnetic interference to implantable pacemakers and implantable cardioverter-defibrillators.” Heart rhythm vol. 7,1 (2010): 99-107. doi:10.1016/j.hrthm.2009.09.071

[31] Napp, Andreas et al. “Electromagnetic interference with implantable cardioverter-defibrillators at power frequency: an in vivo study.” Circulation vol. 129,4 (2014): 441-50. doi:10.1161/CIRCULATIONAHA.113.003081

[32] Korpinen, Leena et al. “Implantable cardioverter defibrillators in electric and magnetic fields of 400 kV power lines.” Pacing and clinical electrophysiology : PACE vol. 37,3 (2014): 297-303. doi:10.1111/pace.12270

[33] Korpinen, Leena et al. “Implantable Cardioverter Defibrillators in Magnetic Fields of A 400 kV Substation.” Progress in Electromagnetics Research M vol 40 (2014) : pp.205-213.

[34] Korpinen, Leena et al. “Cardiac pacemakers in electric and magnetic fields of 400-kV power lines.” Pacing and clinical electrophysiology : PACE vol. 35,4 (2012): 422-30. doi:10.1111/j.1540-8159.2011.03327.x

[35] Seidman, Seth J et al. “In vitro tests reveal sample radiofrequency identification readers inducing clinically significant electromagnetic interference to implantable pacemakers and implantable cardioverter-defibrillators.” Heart rhythm vol. 7,1 (2010): 99-107. doi:10.1016/j.hrthm.2009.09.071

[36] Seidman, Seth J et al. “Static magnetic field measurements of smart phones and watches and applicability to triggering magnet modes in implantable pacemakers and implantable

cardioverter-defibrillators." Heart rhythm vol. 18,10 (2021): 1741-1744. doi:10.1016/j.hrthm.2021.06.1203

[37] Seidman, Seth J, and Howard I Bassen. "Determining EMC Test Levels for Implantable Devices in Bipolar Lead Configuration." Biomedical instrumentation & technology vol. 55,3 (2021): 91-95. doi:10.2345/0899-8205-55.3.91

[38] Sher, Neal A et al. "An in vitro evaluation of electromagnetic interference between implantable cardiac devices and ophthalmic laser systems." Europace vol. 13,4 (2011): 583-8. doi:10.1093/europace/euq495

[39] Huang, Jing et al. "An in vitro Evaluation of the Effect of Transient Electromagnetic Fields on Pacemakers and Clinical Mitigation Measures." Frontiers in cardiovascular medicine vol. 7 607604. 23 Dec. 2020, doi:10.3389/fcvm.2020.607604

[40] Mattei, Eugenio et al. "An optically coupled sensor for the measurement of currents induced by MRI gradient fields into endocardial leads." Magma (New York, N.Y.) vol. 28,3 (2015): 291-303. doi:10.1007/s10334-014-0463-2

[41] Gustrau, Frank et al. "Active medical implants and occupational safety--measurement and numerical calculation of interference voltage." Biomedizinische Technik. Biomedical engineering vol. 47 Suppl 1 Pt 2 (2002): 656-9. doi:10.1515/bmte.2002.47.s1b.656

[42] Kersschot, Ivo. Unipolar versus bipolar leads. Cardiac Pacing and Electrophysiology (1994). Springer, Dordrecht. https://doi.org/10.1007/978-94-011-0872-0_20

[43] Xu, Xie George. "An exponential growth of computational phantom research in radiation protection, imaging, and radiotherapy: a review of the fifty-year history." Physics in medicine and biology vol. 59,18 (2014): R233-302. doi:10.1088/0031-9155/59/18/R233

[44] Makarov, Sergey N et al. "Virtual Human Models for Electromagnetic Studies and Their Applications." IEEE reviews in biomedical engineering vol. 10 (2017): 95-121. doi:10.1109/RBME.2017.2722420

[45] Dimbylow, Peter. "Development of the female voxel phantom, NAOMI, and its application to calculations of induced current densities and electric fields from applied low frequency magnetic and electric fields." Physics in medicine and biology vol. 50,6 (2005): 1047-70. doi:10.1088/0031-9155/50/6/002

[46] Christ, Andreas et al. "The Virtual Family--development of surface-based anatomical models of two adults and two children for dosimetric simulations." Physics in medicine and biology vol. 55,2 (2010): N23-38. doi:10.1088/0031-9155/55/2/N01

[47] Gosselin, Marie-Christine et al. "Development of a new generation of high-resolution anatomical models for medical device evaluation: the Virtual Population 3.0." Physics in medicine and biology vol. 59,18 (2014): 5287-303. doi:10.1088/0031-9155/59/18/5287

[48] Jagielski, Kai et al. “Interference of cardiovascular implantable electronic devices by static electric and magnetic fields.” Expert review of medical devices vol. 18,4 (2021): 395-405. doi:10.1080/17434440.2021.1902802

[49] Hasgall, Philippe et al. “IT’IS Database for thermal and electromagnetic parameters of biological tissues,” Version 4.1, Feb 22, 2022, DOI: 10.13099/VIP21000-04-1. itis.swiss/database

[50] Gabriel, Sami et al. “The dielectric properties of biological tissues: II. Measurements in the frequency range 10 Hz to 20 GHz.” Physics in medicine and biology vol. 41,11 (1996): 2251-69. doi:10.1088/0031-9155/41/11/002

[51] De Santis, Valerio et al. “An equivalent skin conductivity model for low-frequency magnetic field dosimetry.” Biomedical Physics and Engineering Express vol 1 (2015). https://doi.org/10.1088/2057-1976/1/1/015201

[52] Schmid, Gernot et al. “The role of skin conductivity in a low frequency exposure assessment for peripheral nerve tissue according to the ICNIRP 2010 guidelines.” Physics in medicine and biology vol. 58,13 (2013): 4703-16. doi:10.1088/0031-9155/58/13/4703

[53] Thomas Weiland, “A discretization method for the solution of Maxwell’s equations for six-component fields,” Electronics and Communications AEU, vol. 31, 3 (1977): 116–120

[54] Katrib, Juliano. Etude théorique et expérimentale des implants médicaux actifs en environnement électromagnétique : application aux défibrillateurs implantables en champ magnétique basse fréquence dans la bande 50Hz - 50kHz. Lorraine University Repository (2011). http://docnum.univ-lorraine.fr/public/SCD_T_2011_0134_KATRIB.pdf

[55] Potter, Michael E. et al. Low Frequency Finite Difference Time Domain (FDTD) for Modeling of Induced Fields in Humans Close to Line Sources. Journal of Computational Physics vol 162, 1 (2000): 82–103. https://doi.org/10.1006/jcph.2000.6523

[56] Kavet, Robert et al. “Evaluation of biological effects, dosimetric models, and exposure assessment related to ELF electric- and magnetic-field guidelines.” Applied occupational and environmental hygiene vol. 16,12 (2001): 1118-38. doi:10.1080/10473220127412

[57] Tarao, Hiroo et al. “Numerical evaluation of currents induced in a worker by ELF non-uniform electric fields in high voltage substations and comparison with experimental results.” Bioelectromagnetics vol. 34,1 (2013): 61-73. doi:10.1002/bem.21738

[58] Findlay, Richard. “Induced electric fields in the MAXWEL surface-based human model from exposure to external low frequency electric fields.” Radiation protection dosimetry vol. 162,3 (2014): 244-53. doi:10.1093/rpd/nct281

[59] Zhou, Mengxi et al. “Interference thresholds for active implantable cardiovascular devices in occupational low-frequency electric and magnetic fields: a numerical and in vitro study.” Medical engineering & physics vol. 104 (2022): 103799. doi:10.1016/j.medengphy.2022.103799

[60] Gercek, Cihan et al. “Computation of Pacemakers Immunity to 50 Hz Electric Field: Induced Voltages 10 Times Greater in Unipolar Than in Bipolar Detection Mode.” Bioengineering (Basel, Switzerland) vol. 4,1(2017): 19. doi:10.3390/bioengineering4010019

[61] Joosten, Stephan et al. “The influence of anatomical and physiological parameters on the interference voltage at the input of unipolar cardiac pacemakers in low frequency electric fields.” Physics in medicine and biology vol. 54,3 (2009): 591-609. doi:10.1088/0031-9155/54/3/008

[62] Marchal, Christian et al. “Dielectric properties of gelatine phantoms used for simulations of biological tissues between 10 and 50 MHz.” International journal of hyperthermia : the official journal of European Society for Hyperthermic Oncology, North American Hyperthermia Group vol. 5,6 (1989): 725-32. doi:10.3109/02656738909140497

[63] Katrib, Juliano et al. “In vitro assessment of the immunity of implantable cardioverter-defibrillators to magnetic fields of 50/60 Hz.” Physiological measurement vol. 34,10 (2013): 1281-92. doi:10.1088/0967-3334/34/10/1281

[64] International Electrotechnical Commission, “Standard IEC 62226-3-1 Exposure to electric or magnetic fields in the low and intermediate frequency range - Methods for calculating the current density and internal electric field induced in the human body - Part 3-1: Exposure to electric fields - Analytical and 2D numerical models”, Jun. 2007 +AMD1:2016 CSV.

[65] Bernstein, Alan D et al. “The NASPE/BPEG generic pacemaker code for antibradyarrhythmia and adaptive-rate pacing and antitachyarrhythmia devices.” Pacing and clinical electrophysiology : PACE vol. 10,4 Pt 1 (1987): 794-9. doi:10.1111/j.1540-8159.1987.tb06035.x

[66] Reade, Michael C. “Temporary epicardial pacing after cardiac surgery: a practical review. Part 2: Selection of epicardial pacing modes and troubleshooting.” Anaesthesia vol. 62,4 (2007): 364-73. doi:10.1111/j.1365-2044.2007.04951.x

[67] Levy, Terry et al. “A comparison between passive and active fixation leads in the coronary sinus for biatrial pacing: initial experience.” Europace : European pacing, arrhythmias, and cardiac electrophysiology : journal of the working groups on cardiac pacing, arrhythmias, and cardiac cellular electrophysiology of the European Society of Cardiology vol. 2,3 (2000): 228-32. doi:10.1053/eupc.2000.0105

[68] Liu, Lie et al. “A long-term, prospective, cohort study on the performance of right ventricular pacing leads: comparison of active-fixation with passive-fixation leads.” Scientific reports vol. 5 (2015): 7662. doi:10.1038/srep07662

[69] “EN 50527 Procédure pour l'évaluation de l'exposition des travailleurs porteurs de dispositifs médicaux implantables actifs aux champs électromagnétiques”, janvier 2017.